Contrasting mixed siliciclastic-carbonate shelf-derived gravity-driven systems in compressional intra-slope basins (southern Hikurangi margin, New Zealand)

Claussmann B.[1,2,*], Bailleul J.[1], Chanier F.[3], Caron V.[4], McArthur A. D.[5], Mahieux G.[4], Chaptal C.[1], Vendeville B. C.[3]

1. U2R 7511, Basins-Reservoirs-Resources (B2R), Geosciences department, UniLaSalle - University of Picardie Jules Verne, 60026, Beauvais, France
2. Schlumberger, Software Integrated Solutions, London, SW1E 6AJ, United Kingdom
3. University of Lille, CNRS, ULCO, UMR 8187, Laboratory of Oceanology and Geosciences (LOG), Lille, France
4. U2R 7511, Basins-Reservoirs-Resources (B2R), University of Picardie Jules Verne - UniLaSalle, 80039 Amiens, France
5. School of Earth and Environment, University of Leeds, Leeds, LS2 9JT, United Kingdom

Accepted Manuscript version (unedited PDF accepted for publication).

Published Journal Article version available online, 30 July 2021:

https://doi.org/10.1016/j.marpetgeo.2021.105252

Published by Elsevier in Marine and Petroleum Geology Journal.

*Correspondence: bclaussmann@slb.com

1. ABSTRACT

Along active margins, the combination of predominant tectonic activity and shallow-marine mixed siliciclastic-carbonate source systems developing upon and around actively growing structures challenges traditional source-to-sink models. This study aims to investigate the implications of mixed siliciclastic-carbonate shelfal domains located in contrasting geotectonic settings (thrust forelimb and backlimb) for the development of the concomitant gravity-driven systems beyond the shelf edges. Here, we document the vertical and lateral stratigraphic variabilities of the shelf-derived turbidites and mass-transport deposits (MTDs) at outcrop-scale through the integrated interpretation of photogrammetry, field and taphonomic data from the emerged southern portion of the Hikurangi subduction margin. Results highlight the role and importance of varying structural setting of the sediment source, whereby the different morphologies of the source regions (continent-attached forelimb, continent-detached backlimb) control the development of highly varied shelf-derived gravity-driven depositional systems that interact with the structures across the same confined intra-slope basin. The deposits are tens to a few hundred of meters in thickness and have a lateral extent of several kilometers. The depositional systems are characterized by durations of 1 to 2 Ma and were primarily controlled by the geometries and tectonic motion of the underlying structures at the shelf edges. Shelf-derived mass-wasting systems occurred on both sides of the actively growing thrust structures and were sourced from both shelfal domains that were attached or detached from the continental domain. When sourced from the backlimbs however, the subsequent MTDs exhibit more complex internal architectures, ultimately recording the dynamic changes in slope gradient, and can therefore be used as proxies for unraveling the tectonic activity of an individual structure. Our study provides new insights to better predict mixed siliciclastic-carbonate depositional settings along active margins, sourced from thrust forelimb and backlimb. These results may be important for deep-marine exploration and tectonostratigraphic reconstruction of fold-and-thrust belts.

Keywords: active margin, confined slope channel system, mass-wasting system, mixed siliciclastic-carbonate systems, confined basins, trench-slope basins, thrust forelimb, thrust backlimb

2. INTRODUCTION

Understanding sediment transfer and distribution beyond the shelf edge and in the outboard part of continental margins has been at the heart of numerous studies in the past 60 years (*e.g.,* Bouma 1962; Posamentier and Vail 1988; Richards et al. 1998; Posamentier and Kolla 2003; Sømme et al. 2009;

Paumard et al. 2020). Commonly, the pathways taken by sediments across the shelf margins are believed to some extent control different types of sediment gravity flows and related depositional systems (Prather 2003; Gong et al. 2016; Paumard et al. 2020). Submarine canyons and slope channels are more likely to funnel turbidity currents (Peakall and Sumner 2015), transferring continental and or shelf-derived material downslope (Kuenen 1964; Mulder et al. 2017) and normally ending their course as weakly confined to unconfined lobe systems (*e.g.,* Brunt et al. 2013), whereas unconfined shelf edge failures typically generate shelf-derived debris flows that are either captured on the slope or deposited on the basin floor (*e.g.,* Moscardelli and Wood 2008).

Along active margins, the combination of predominant tectonic activity and mixed siliciclastic-carbonate source systems developing upon and around actively growing structures challenges traditional source-to-sink models (Chiarella et al. 2012; Chiarella et al. 2019). Resulting deep marine sedimentation styles are highly variable, intricate and not readily predictable (McArthur et al. 2019). Whilst the underlying structural styles and motions fundamentally impact the morphology of continental shelves and their margins, they also induce dynamic changes in slope gradient, confinement and connection to sediment sources (Sømme et al. 2009). Shallow marine, mixed shelfal systems are common in active tectonic settings (Puigdefàbregas et al. 1986; Chiarella et al. 2012). Typified by repeated terrigenous sediment input (Chiarella et al. 2017), the shallow marine, mixed shelfal systems commonly result in intricate shelf sedimentation and sediment routing systems (Chiarella et al. 2019; Moscardelli et al. 2019; Cumberpatch et al. 2021). All these parameters control the dynamics of the flows from the shelf to the basin floor and can be expected to have a significant impact on the development of the coeval deep-marine systems, influencing (1) the types of sediment gravity flow, (2) the patterns of sediment dispersal, (3) the morphologies (size, extent) of the systems and (4) the related sedimentary facies (*e.g.,* Fisher 1983; Pirmez et al. 2000; Mulder and Alexander 2001; Sprague et al. 2005; Sømme et al. 2009; Mulder et al. 2012; Moscardelli et al. 2019; Paumard et al. 2020).

Although previous studies looked at the depositional frameworks of shallow-marine mixed siliciclastic-carbonate systems along tectonically active margins (*e.g.,* Caron et al. 2004; Ćosović et al. 2018; Chiarella et al. 2019), the stratigraphic implications for the subsequent shelf-derived gravity-driven systems remain unclear. Few studies have proposed generic depositional models linking mixed shallow systems with their potential coeval deep-marine counterparts. However, they mostly rely on subsurface data (*e.g.*, Moscardelli et al. 2019) and only rarely discuss the impact of changes in structural setting of the sediment source (*e.g.,* thrust forelimb and backlimb settings) on the deposits (*e.g.,* Ćosović et al. 2018).

Here, we investigate the type and distribution of shelf-derived sediments, sourced from mixed siliciclastic-carbonate systems (*i.e.,* compositional systems (*sensu* Chiarella et al. (2017)) that developed above the asymmetrical basin-bounding structures (*e.g.* thrusts and or fault-growing folds) of an actively deforming, confined intra-slope basin. We examine the vertical and lateral stratigraphic variability of the shelf-derived gravity-driven deposits, at outcrop-scale, from the Whareama trench-slope basin, in the emerged southern portion of the Hikurangi subduction margin, North Island of New Zealand. The deposits are of Middle Miocene age and incorporate similar material (nature and size of the clasts), albeit transported through a variety of sediment gravity flows, thereby suggesting different source, delivery and geotectonic settings across the same confined intra-slope basin.

Our study aims to determine how variations in the structural style (thrust forelimb and backlimb) and tectonic activity (renewal or quiescence) influence the generation of contrasting mixed siliciclastic-carbonate shelf-derived gravity-driven systems and deposits across a confined, intra-slope basin (*e.g.,* trench-slope basin).

Specific objectives are to:

- Document the nature, architecture, and size of the different styles of shelf-derived sedimentation that can occur in a confined intra-slope basin, through an integrated interpretation of photogrammetry, fieldwork and taphonomic data.
- Gain new understandings on the controls on sediment transfer and distribution beyond the edges of mixed siliciclastic-carbonate shelves located upon and around the forelimb and backlimb of actively growing asymmetrical structures.
- Develop generic depositional models of the distribution and styles of shelf-derived systems and subsequent deposits in tectonically active settings.
- Determine the implications for the stratigraphic prediction of deep-marine, shelf-derived gravity-driven systems and, of shelf-derived mass-wasting systems along active margins.

3. GEOLOGICAL SETTING

3.1. Regional setting

The study area is located on the eastern North Island of New Zealand, on the tectonically active Hikurangi Margin (Figure 1). The Hikurangi subduction wedge (*sensu* Bailleul et al. 2013) formed in response to the Uppermost Oligocene-to-Recent westward subduction of the Pacific Plate beneath the Australian

Plate (Ballance 1976; Spörli 1980; Pettinga 1982; Chanier and Ferrière 1991; Field et al. 1997; Nicol et al. 2007). Bounded by the Hikurangi Trench to the east and the Forearc Basin to the west, the Hikurangi subduction wedge comprises a succession of elongated trench-parallel sedimentary basins (*i.e.,* trench-slope basins) separated by tectonically active structural ridges (Chanier and Ferrière 1991; Lewis and Pettinga 1993; Bailleul et al. 2013; McArthur et al. 2019).

Since the onset of subduction, the Hikurangi subduction wedge underwent a polyphase tectonic history, comprising three main tectonic periods (Figure 2 and references within). Complex stratigraphic architectures and geometries, such as diachronous sedimentation patterns, syn-sedimentary deformations and discontinuities, are characteristic of the Miocene-to-Recent trench-slope basin fills and attest of the close interplay between tectonics and sedimentation (Neef 1992; Neef 1999; Bailleul et al. 2007; Bailleul et al. 2013; Burgreen and Graham 2014; McArthur et al. 2019; McArthur et al. 2021). Deep-marine sedimentation dominates their fill and includes mass-transport deposits (MTDs), turbidites and extensive hemipelagic mudstones; yet carbonate, biogenic and shallow-marine fringe deposits can also be found sporadically (Figure 2) (Field et al. 1997; Lee and Begg 2002; Bailleul et al. 2007; Bland et al. 2015; McArthur and McCaffrey 2019). These basin fills either conformably or unconformably overlie the Cretaceous to Paleogene pre-subduction basement, mainly composed of the Lower Cretaceous Torlesse greywackes and the Upper Cretaceous to Oligocene detrital to pelagic series (Spörli 1980; Bradshaw 1989; Chanier and Ferrière 1991; Field et al. 1997; Lee and Begg 2002).

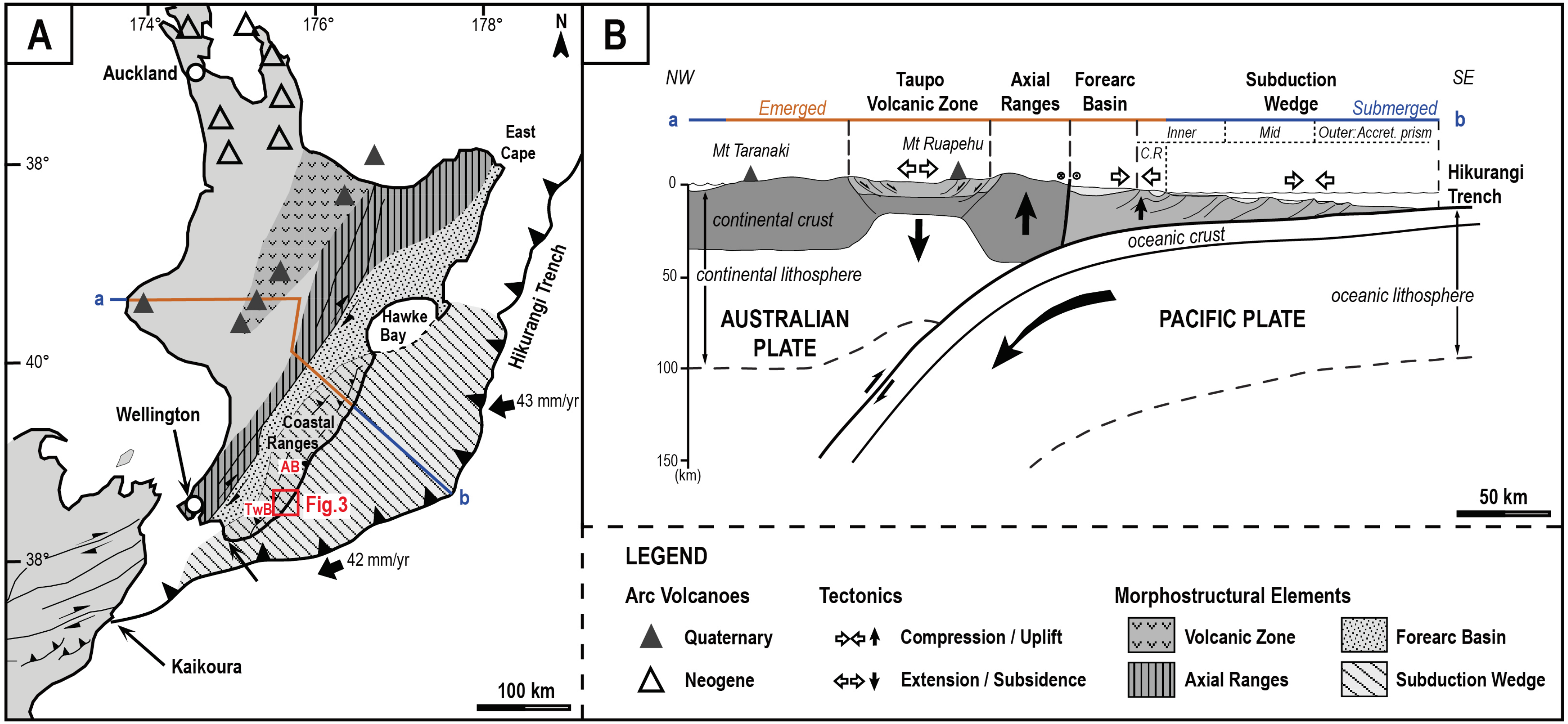

Figure 1: (A): Major subduction-related morphostructural features of the active Hikurangi Margin, north Island of New Zealand. Black arrows show present-day relative plate motion between Pacific and Australian Plates from Beavan et al. (2002). (AB – Akitio Basin; TwB – Te Wharau Basin). See (B) for the a – b general cross-section of the Hikurangi subduction complex (C.R – Coastal Ranges). Modified after Chanier et al. (1999), Bailleul et al. (2007) and Bailleul et al. (2013).

3.2. Southern Coastal Ranges

The study area lies within the exhumed inner portion of the subduction wedge (*e.g.,* emergent trench-slope break) that forms the southern Coastal Ranges of the eastern North Island of New Zealand. Here, we focus on the tectonic settings at the end of the first compressional phase (Figure 2; Middle Miocene, Clifdenian – Lillburnian (Langhian to early Serravallian, 15.9 – 13.05 Ma)), where both the inception and development of the trench-slope basins occurred (Chanier and Ferrière 1991; Bailleul et al. 2013; Malie et al. 2017).

During this time period, compressional tectonics resulted in uplift of some of the fold and thrust basin-bounding structures and more generally of the margin (Crundwell 1987; Bailleul et al. 2013). The induced changes in depositional environments (*e.g.,* neritic conditions) atop the structures controlled the development of shelfal environments, and, in particular, mixed siliciclastic-carbonate systems (*i.e.,* compositional systems (*sensu* Chiarella et al. (2017)) at shallower waters whilst gravity-systems dominated elsewhere at deeper waters (Crundwell 1987; Chanier and Ferrière 1991; Neef 1992; Lee and Begg 2002; Bailleul et al. 2007; Bailleul et al. 2013; McArthur et al. 2019; McArthur and McCaffrey 2019; Crisóstomo-Figueroa et al. 2020; McArthur et al. 2021).

Numerous mixed siliciclastic-carbonate systems co-existing during this period formed a regional shelf domain throughout the south-western portion of Hikurangi Margin (Crundwell 1987; Chanier 1991; Bailleul et al. 2007; Bailleul et al. 2013; Bailleul et al. 2015; Claussmann et al. 2021). The shelves developed above substantially different substrata inherited from local tectonics, and they either unconformably overlie Lower to Middle Miocene syn-subduction sedimentary rocks or Cretaceous to Paleogene pre-subduction basement. Their depositional settings preferentially suggest narrow, continent-attached shelfal systems receiving regular terrigenous inputs from the hinterland (Bailleul et al. 2015; Claussmann et al. 2021). However, isolated, continent-detached platform systems may also have locally occurred on some of the actively growing structures (see (Caron et al. 2004; Caron et al. 2021) for examples along the same margin, yet at different geological times).

Claussmann et al. (2021) previously demonstrated that short-lived periods (ca. 1 to 2 Ma) of sustained (with or without phases of quiescence) compressional tectonics favor the propagation of the folds and thrusts, and thus the expansion of abrupt, unstable areas close to these structurally-controlled shelf-margins. Repeated uplift and slope oversteepening of these areas eventually lead to recurrent shelf collapses, sourcing shelf-derived sediments (*e.g.,* mass-wasting products) into deep water. The associated deposits result from sediment gravity flows, such as cohesive debris flows or mudflows, and

Accepted Manuscript version. Published Journal Article version available online, published by Elsevier in Marine and Petroleum Geology Journal: https://doi.org/10.1016/j.marpetgeo.2021.105252

rework a substantial amount of shelf-derived material, incorporating sediments and fossils from neritic shelfal environments. Several occurrences of such shelf-derived mass-wasting events and related deposits of Middle Miocene age were identified in the southern Coastal Ranges cropping out across several trench-slope basins (*i.e.,* Whareama, Te Wharau and Akitio Basins) (Figure 1; Figure 2; Figure 3).

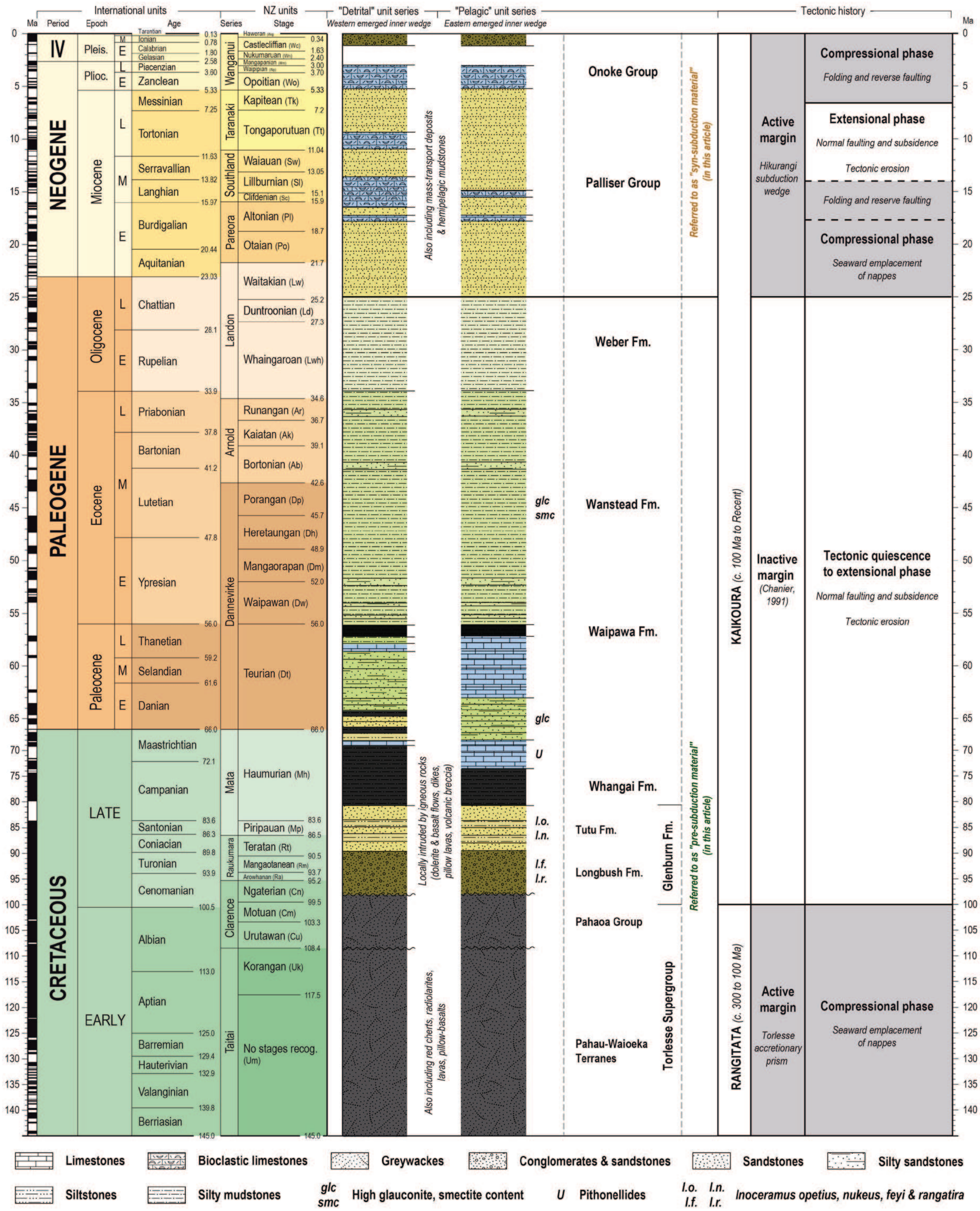

Accepted Manuscript version. Published Journal Article version available online, published by Elsevier in Marine and Petroleum Geology Journal: https://doi.org/10.1016/j.marpetgeo.2021.105252

Figure 2: Chronostratigraphic chart for the southern, emerged portion of the Hikurangi subduction wedge adapted from Claussmann et al. (2021). Lithostratigraphy details adapted from Chanier et al. (1990), Chanier (1991), Chanier and Ferrière (1991), Field et al. (1997), Lee and Begg (2002) and Bland et al. (2015) and detailing the pre- and syn-Hikurangi subduction series. Regional tectonism adapted from Chanier et al. (1999), Bailleul et al. (2013) and Malie et al. (2017). New Zealand stages after Raine et al. (2015) showing the equivalence with the international stages.

3.3. The Whareama Basin

The Whareama Basin is narrow (two to six kilometers wide), elongated (50 kilometers long) and trench-parallel (NE-SW) (Johnston 1980; Chanier 1991). It is bounded by pre-Miocene basement ridges that are controlled by the Adams-Tinui Fault complex and Pukeroro Fault to the west (*i.e,* landward basin margins, Figure 3) and the Flat Point-Whakataki Fault complex to the east (*i.e,* seaward basin margin, Figure 3). The basin's development began at the onset of subduction and thus records gravity-driven deposits dating from the earlymost Miocene. It formed on the back of the Glenburn Nappe, a trenchward-advancing thrust sheet composed of Cretaceous to Eocene pre-subduction series that are either unconformably or conformably overlain by syn-subduction deposits (Chanier 1991; Chanier and Ferrière 1991).

The study area is located on the eastern limb of the Whareama Basin, with beds strongly dipping towards the west (ca. 40°). Nearby, well-exposed Middle Miocene shelf-derived MTDs were previously described and attributed to result from the collapses of coevally developing narrow, continent-attached shelf-margins located to the north-west (Figure 3; Sefton Hills s-1 and s-2 sections) (Claussmann et al. 2021).

4. DATA AND METHODS

This outcrop-based study integrates traditional and digital field data acquired during three field campaigns (2018, 2019, 2020) in the southern portion of the Hikurangi subduction wedge (Coastal Ranges, eastern North Island of New Zealand), and focuses on the shelf-derived gravity-driven deposits of the Waikaraka and Homewood localities (Figure 3; wk and hw sections).

Fieldwork consisted of logging sedimentological profiles (total of 312 meters at 1:50 bed-scale), measuring structural (*e.g.,* ductile deformation analysis) and stratigraphic features (*e.g.,* bedding, paleocurrent) as well as describing each shelf-derived flow deposit in a standardized manner (facies and geometries).

Owing to the abundant macrofossils contained in the deposits, occurring both as whole skeletons and fragmented remains, five taphonomic analyses were performed on approximately one square meter areas for both the outcrops (*i.e.,* four at Waikaraka and one at Homewood). These analyses were restricted to the coarsest fraction (larger than five millimeters) of death assemblages contained in the deposits. Three categories of skeleton damages, namely fragmentation, abrasion and bioerosion, were described visually using the graded classification scale presented in Appendix 1, complemented by Caron (2011) and Caron et al. (2019).

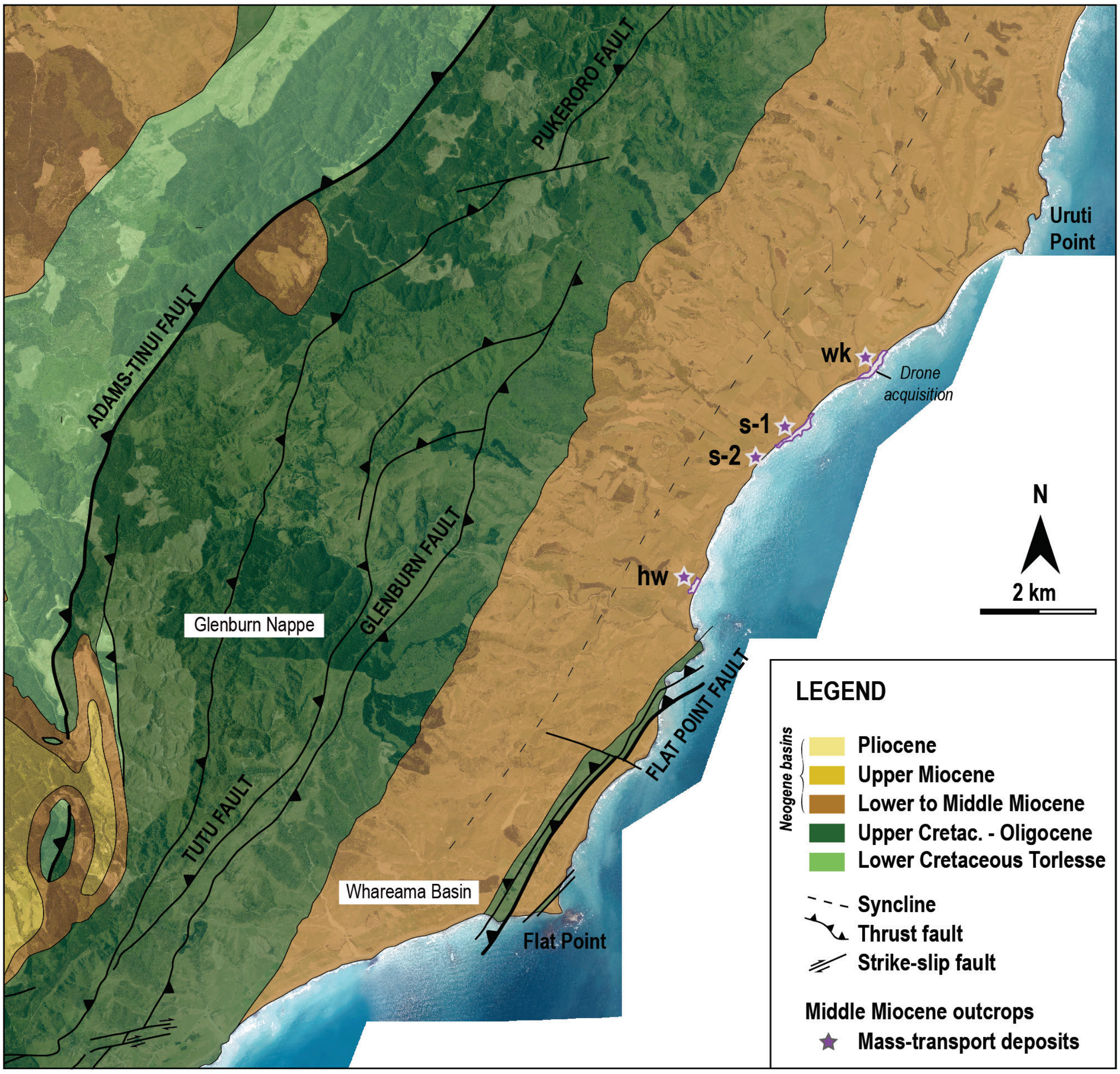

Figure 3: Satellite map from World Imagery (ESRI), and onshore geological map from Chanier (1991) of the Whareama Basin. Location of the drone acquisition and related 3D outcrop models presented in this study = wk = Waikaraka section and hw = Homewood section. See Claussmann et al. (2021) for the s-1 and s-2: Sefton Hills section and 3D outcrop model.

Seven samples were collected to supplement the Fossil Record Electronic Database (https://fred.org.nz/) since both areas are currently mapped as Quaternary beach deposits on the 1:250 000 Geological Map of New Zealand (QMAP) of Wairarapa (https://www.gns.cri.nz/). The micro- and macropaleontological analyses were conducted by GNS New Zealand and allowed to determine the age of the sedimentary units and related depositional paleobathymetries (Appendix 2; Appendix 3).

Digital fieldwork involved the acquisition of high-resolution aerial images (1,900 at Waikaraka and 690 at Homewood) using a DJI Phantom 4 Pro drone, supplemented by a number of Ground Control Points (GCP) collected with a Trimble GeoExplorer 2008 differential global positioning system tool (DGPS) and a Trimble Tempest antenna positioned at two meters above the measured point. Two georeferenced 3D outcrop models were then created in the form of high-resolution triangulated mesh textured with the photographs.

5. FACIES AND ARCHITECTURAL ELEMENTS

5.1. Facies and architectural schemes

Integration of the data allowed an analysis and comparison of the stratigraphic architectures and facies organization within both outcrops.

A total of 14 lithofacies were recognized across the two outcrops (summarized in Table 1 and illustrated in Figure 4, Figure 5, Figure 6 and Figure 7) and classified according to their dominant lithology, primary sedimentary features and interpreted in terms of flow processes using models from (Bouma 1962; Nardin et al. 1979; Lowe 1982; Postma 1986; Kneller 1995; Mulder and Alexander 2001).

These comprise massive silty mudstones (**MDST**); tabular, very thin- to medium-bedded (**LDTC-a**) or medium- to thick-bedded (**LDTC-b**) sandstones with mudstone caps; lenticular, medium to very-thick bedded sandstones (**HDTC**); structured (**SST-a**) or structureless (**SST-b**) sandstones; pebbly sandstones (**sHDTC-a**); bioclastic grits (**sHDTC-b**); lenticular, medium to very-thick bedded gravel sandstones with mudstone caps (**gsHDTC**); organized to disorganized clast-supported (respectively **gHDTC, CF**) and matrix-support (**DF**) conglomerates; as well as deformed (**SL-a**) or undeformed (**SL-b**) mass of sediments.

Accepted Manuscript version. Published Journal Article version available online, published by Elsevier in Marine and Petroleum Geology Journal: https://doi.org/10.1016/j.marpetgeo.2021.105252

Deposit	Dominant lithology	Lithofacies code	Thickness (cm)	Lithofacies description	Classification and process interpretation	
Turbidite	Mudstone	**MDST** Massive, siltstone to silty mudstone	1 to 60 (HMD) nul (WKS)	Siltstone to silty mudstone. Mainly massive, rare parallel lamination visible. Ungraded to (normally) graded. Variable degree of bioturbation, tends to be highly bioturbated.	(Td)-Te	Low-density turbidity currents and hemipelagic suspension settling
	Sandstone to Mudstone	**LDTC-a** Tabular, very thin-to medium-bedded sandstone with mudstone cap	1 to 20 (HMD) 2 to 20 (WKS)	Fine- to medium-grained. Parallel laminations (Tb), passing into climbing ripples (Tc) with sometimes dewatering or soft sedimentation deformation structures installed above. Sometimes only developping the parallel laminations or sometimes directly developping the climbing ripples. Laminations can be highlighted by organic-rich, carbonaceous debris and shell ashes. Common bioturbation.	Tb-e Tb-Te Tc-Te	Low-density turbidity currents
		LDTC-b Tabular, medium to thick-bedded sandstone with mudstone cap	5 to 100 (HMD) 10 to 100 (WKS)	Fine- to coarse-grained. If present, medium- to very coarse-grained Ta at the base of the thicker beds, commonly massive and structureless, with sand- to granule-(up to pebble-) grade clasts (lithoclasts, bioclasts and rip-up mudstone clasts), sometimes displaying sole marks such as flute casts. Fine- to medium-grained, well-developped parallel laminations (Tb), climbing ripples (Tc) with often dewatering or soft sedimentation deformation structures installed above. Common amalgamation. Lamination often highlighted by organic-rich, carbonaceous debris and shell ashes. Common bioturbation.	Ta-e	Low-density turbidity currents
		HDTC Lenticular, medium to very thick-bedded sandstone with mudstone cap	5 to 20 (HMD) 5 to 200 (WKS)	Fine- to coarse-grained. Lenticular, medium- to very-coarse-grained base, commonly massive and structureless, with sand- to granule-(up to pebble-) grade clasts (lithoclasts, bioclasts and (elongated) rip-up mudstone clasts), overlain by well-developed parallel or cross-laminations in the same material, overall normally grading. Followed by fine- to medium-grained, well-developped parallel laminations (Tb), climbing ripples (Tc) with often dewatering or soft sedimentation deformation structures installed above. Lamination often highlighted by organic-rich, carbonaceous debris and shell ashes. Common bioturbation. HMD only presents the bottom part.	S-Ta-e	Sandy high- to low-density turbidity currents
	Sandstone	**SST-a** Structured sandstone, above gHDTC, CF, DF or MF	5 to 20 (HMD) 15 to 100 (WKS)	Fine- to medium-grained. Parallel, sometimes passing into faint climbing ripples and or dewatering or soft sedimentation deformation structures, usually normally graded. Common scattered shell ashes; organic-rich, carbonaceous debris, and or granule- (to pebble-) grade lithoclasts. Mudstone cap commonly absent.	Tb-Tc	Turbulent cloud, deposition from traction/traction-plus-fallout
		SST-b Structureless sandstone, above gHDTC, CF, DF or MF	5 to 30 (HMD) 15 to 100 (WKS)	Fine- to coarse-grained. Structureless, sometimes dewatering structures. Ungraded or (normally) graded. Common scattered shell ashes; organic-rich, carbonaceous debris, and or granule- (to pebble-) grade lithoclasts. Mudstone cap commonly absent.	S	Turbulent cloud, rapid suspension fall-out
	Conglomerate to Sandstone	**sHDTC-a** Pebbly sandstone	5 to 30 (HMD) nul (WKS)	Fine- to coarse-grained. Structureless, or crude parallel laminations, commonly normally graded. Presenting extraformational clasts and rip-up mudstone clasts scattered or organized. Common mudstone cap.	S-Te	Sandy high-density turbidity currents
		sHDTC-b Dis- to organized clast-supported, bioclastic	1 to 20 (HMD) nul (WKS)	Clast-supported, siltstones to silty mudstones with ≤90% of granule- to pebble-grade, extra- and intraformational clasts. Ungraded, sometimes normally graded laterally. Highly bioclastic with possible shell ashes organization. Frequent rip-up mudstone clasts in the normally graded sections. Often overlying sand with parallel laminations and common load structures, and either overlain by structureless sand and or mudstone cap, rarely bioturbated.	R?-S/Ta?-Te	Cohesionless debris flow or bed-load transport underneath gravelly to sandy high-density turbidity currents
		gsHDTC Organized gravel to fine-grained sandstone with mudstone cap	nul (HMD) 50 to 300 (WKS)	Combination of facies gHDTC (sometimes even facies CF) at the base, overlain by facies HDTC. Clast-supported interval particularly rich in shell ashes and debris content, mostly composing the binding link between the lithoclasts; frequent rip-up mudstone clasts; very frequent boulder-graded clasts marking R2-R3 transition; low-angle, lenticular, slightly erosive base. Common amalgamation in HDTC interval.	(R2)-R3-S/Ta-e	Gravelly to sandy (bipartite) high-density turbidity currents: bed-load transport underneath high-density turbidity currents
	Conglomerate	**gHDTC** Organized clast supported	10 to 100 (HMD) 10 to 200 (WKS)	Clast-supported, siltstone to silty mudstone with ≤90% of granule- to boulder-grade, extra- and intraformational clasts. Highly bioclastic when of average granule-grade clast size, with possible shell ashes organization. Graded (inverse to normally graded, or only normally graded). Occasional clast imbrication / organization and load structures. Rare to locally frequent rip-up mudstone clasts.	R2-R3 R3	Gravelly (bipartite) high-density turbidity currents: bed-load transport underneath high-density turbidity currents
Debrite		**CF** Disorganized clast-supported	10 to 200 (HMD) 20 to 400 (WKS)	Clast-supported, siltstone to silty mudstone with ≤90% of granule- to boulder-grade extra- and intraformational clasts. Highly bioclastic when of average granule-grade clast size. Ungraded, disorganized. Common load structures.	R1	Cohesionless debris flow or bed-load transport underneath gravelly high-density turbidity currents
		DF Disorganized matrix-supported	150 to 400 (HMD) 100 to 400 (WKS)	Matrix-supported, siltstone to silty mudstone with varying quantity of granule- to boulder-grade extra- and intraformational clasts. Ungraded, disorganized. Common recumbent folds, shear and load structures. Traction carpet possible.	/	Cohesive debris flow to cohesionless, sheared debris flow when comprising facies CF at base, top or edges
Slide-Slump	Alternating conglomerate, sandstone and or mudstone	**SL-a** Deformed mass of sediments	100 to 2000 (HMD) nul (WKS)	Contorted, remobilized facies characterized by recumbent folds. Commonly sandy to silty mudstone background sediments.	/	Slump: coherent mass of sediment that moves along a glide plane, resulting in significant internal deformation
		SL-b Undeformed mass of sediments	100 to 2000 (HMD) 100 to 200 (WKS)	Coherent, remobilized facies displaying sharp truncations, slightly concave-up geometries with downlap.	/	Slide scar / scour: initiation of movement of a coherent mass of sediment along a glide plane, no internal deformation

Table 1: Lithofacies encountered at the Waikaraka (WKS) and Homewood (HMD) outcrops. See Figure 4 and Figure 5for representative photographs of each lithofacies at Waikaraka; and Figure 6 and Figure 7at Homewood. Note that the 'Classification' column refers to (Bouma 1962) and (Lowe 1982), and that extraformational clasts include pre- and syn-subduction lithoclasts, and syn-subduction bioclasts. Intraformational clasts include syn-subduction lithoclasts.

Accepted Manuscript version. Published Journal Article version available online, published by Elsevier in Marine and Petroleum Geology Journal: https://doi.org/10.1016/j.marpetgeo.2021.105252

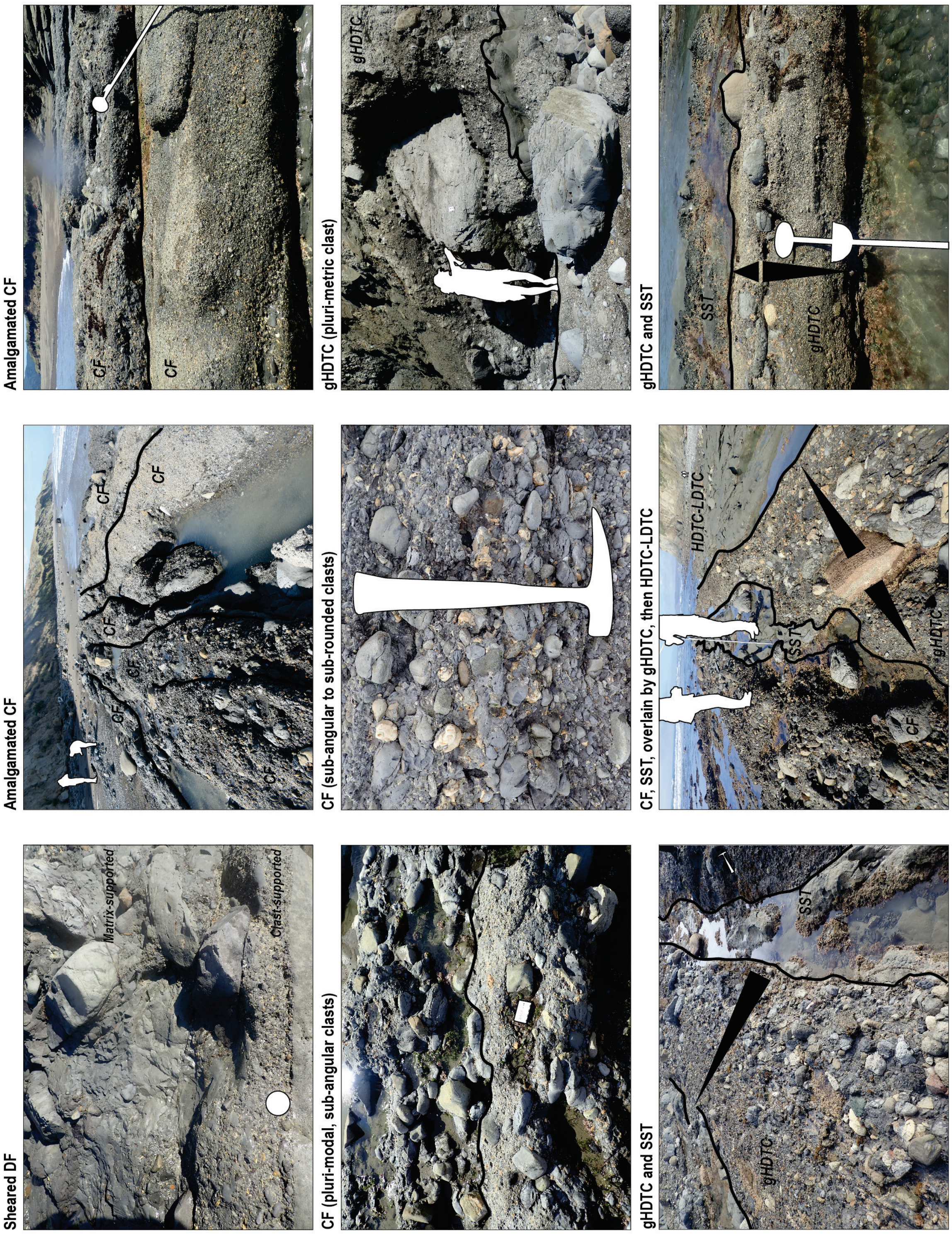

Figure 4: Representative photographs of the lithofacies summarized in Table 1 and recognized at Waikaraka. Scales: human size (~1.70-1.75 meters); Jacob's staff (1.5 meter); hammer (33 centimeters); card (8.5 centimeters long); coin (2.3 centimeters).

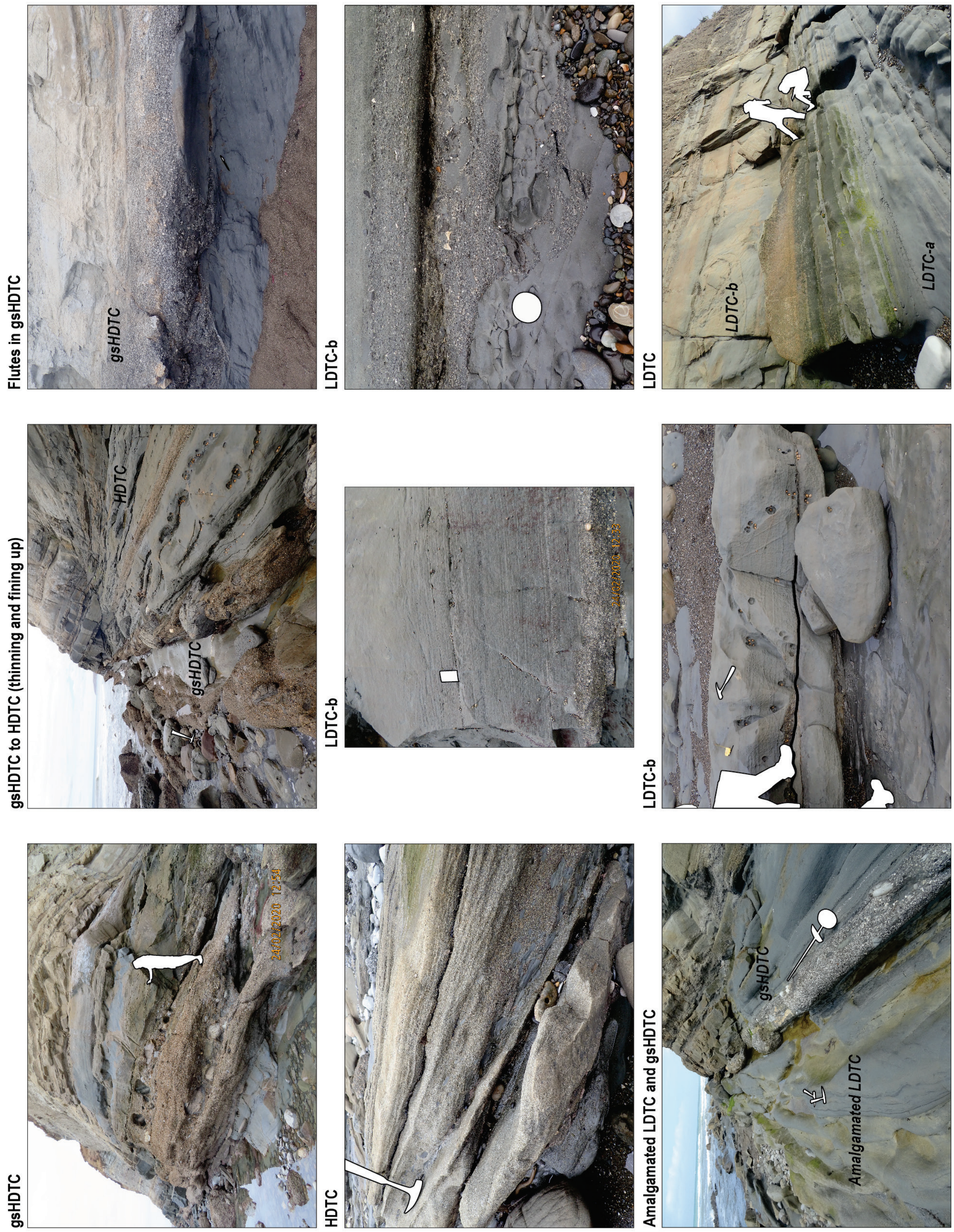

Figure 5: Representative photographs of the lithofacies summarized in Table 1 and recognized at Waikaraka. Scales: human size (~1.70 meters); Jacob's staff (1.5 meter); hammer (33 centimeters); card (8.5 centimeters long); coin (2.5 centimeters).

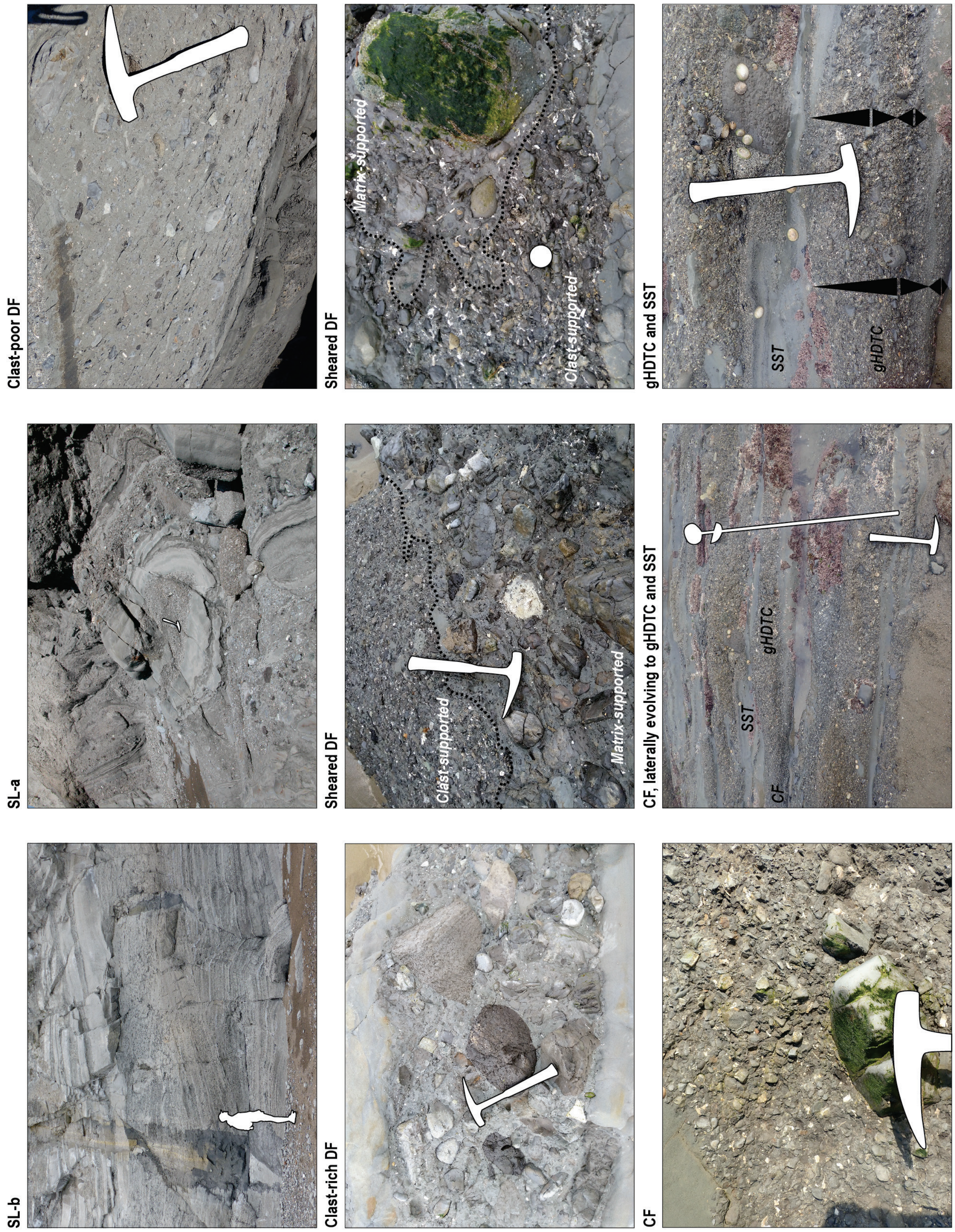

Figure 6: Representative photographs of the lithofacies summarized in Table 1 and recognized at Homewood. Scales: human size (~1.70 meters); Jacob's staff (1.5 meter); hammer (33 centimeters); card (8.5 centimeters long); coin (2.3 centimeters).

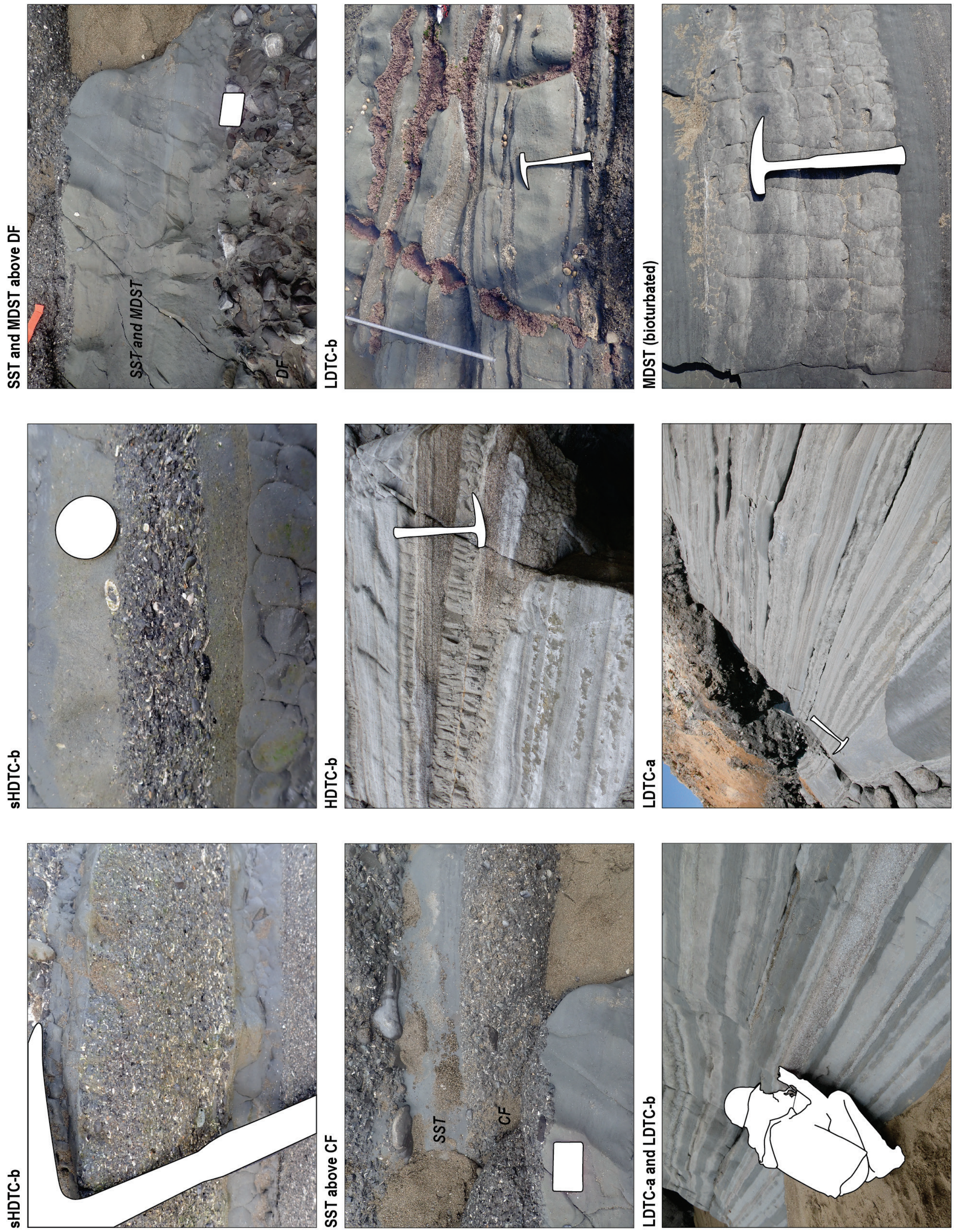

Figure 7: Representative photographs of the lithofacies summarized in Table 1 and recognized at Homewood. Scales: human size (~1.70 meters); Jacob's staff (1.5 meter); hammer (33 centimeters); card (8.5 centimeters long); coin (2.3 centimeters).

They were then grouped into three main facies associations, which are related to main depositional systems (**Fa1g, Fa2c, Fa3p**) (Figure 8; Figure 9). The nomenclature we adopted follows the one defined by Bailleul et al. (2007), Bailleul et al. (2013) and Claussmann et al. (2021), in which **Fa1g** refers to depositional lobe settings, **Fa2c** to confined slope channel settings and **Fa3p** to shelf-derived mass-wasting systems.

Each facies association is described and interpreted in sequence below, directly in context of the outcrop where they were recorded. Figure 10, Figure 11 and Figure 12 illustrate the geometric relationships that exist between the different lithofacies and their associations as well as some of the sedimentary structures at different scales. The nature of the extra- and intraformational clasts reworked in the conglomeratic and coarse sandstone intervals is described separately (see Section 6) and summarized in Figure 13 and Figure 14.

5.2. Confined slope system

The Waikaraka section crops out five kilometers south of the Uruti Point and extends across one kilometer along the coast (Figure 3). Deposition occurred in the Middle Miocene, Lillburnian to Waiauan (Late Langhian to Serravallian, 15.1 – 11.63 Ma, Appendix 2) and features the **Fa2c** depositional system, which can be divided into two main depositional units (**Fa2c-e, Fa2c-l**), hereafter described and interpreted in sequence. These units are bounded by major erosion surfaces. These prominent surfaces can laterally be traced over several hundreds of meters (>600 meters), exhibit a relief of up to two meters, and characteristically separate contrasting depositional facies (Figure 8).

5.2.1. Confined slope channel: axis to off-axis, early-stage fills (Fa2c-e)

Observations

Fa2c-e is characterized by crude fining- and thinning-upward series, dominated by coarse-grained facies. Here, this association crops out over more than 600 meters laterally and is generally between 10 to 50 meters in thickness (Figure 8).

Fa2c-e mostly comprises amalgamated, very thick-bedded (one to >two meters), disorganized (**CF**) to organized (**gHDTC**), polymict and clast-supported conglomerates (Figure 4; Figure 10l; Figure 11; Table 1). The conglomerates commonly form continuous, broadly lenticular and fairly symmetrical bodies with low-relief erosional bases, thereby indicating a cross-sectional, rather than longitudinal, view of them. Their upper topographies are uneven and they are occasionally overlain by thin- to thick-bedded, structured or structureless sandstones (**SST**), themselves often incised by the overlying conglomerates, thus forming composite conglomeratic bodies (Figure 4; Figure 8; Figure 11; Table 1). The conglomerates essentially evolve from (1) being internally disorganized (**CF**), only comprising local internal stratifications,

Accepted Manuscript version. Published Journal Article version available online, published by Elsevier in Marine and Petroleum Geology Journal: https://doi.org/10.1016/j.marpetgeo.2021.105252

marked by subtle variations in clast grade and alignment, or in matrix concentration (**DF**) to (2) being internally organized, displaying inverse- to normally- or only normally-graded patterns (**gHDTC**) (Figure 4; Figure 8; Figure 11; Table 1).

The conglomerates are generally overlain by series of laterally continuous, mostly medium- to fine-grained, thin- to very thick-bedded sandstones, which are either amalgamated or capped by bioturbated mudstones (**HDTC to LDTC**) (Figure 5; Figure 8; Figure 11j; Table 1). The thicker beds show frequent grain-size breaks, indicating bed amalgamation (**HDTC** to **LDTC-b**). Their basal, coarser intervals are discontinuous, erosive and typically composed of gravel material similar to that of the conglomerates, which occasionally includes aligned mud clasts, plant debris and some shell fragments (Figure 5, LDTC-b). The sandstones frequently contain soft-sediment deformation features (*e.g.,* flame, load) in their structured intervals (Figure 10k), whereas, the mudstone caps, where present, commonly include *Phycosiphon* sp. and *Chondrites* sp. bioturbations.

Four occurrences of **Fa2c-e** were observed at Waikaraka (Figure 8; Figure 11).

The first occurrence is exposed at the base of the outcrop. Its basal surface is not visible as it lies below the sea level. The conglomerates are disorganized (**CF**) (Figure 8; Figure 4; Figure 11) with an average clast size ranging from granule- and pebble-grades, to pebble- and cobble-grades toward the southward wavecut platform. Boulders and outsized clasts (deci- to decametric) are frequent (Figure 10l), particularly to the south and in the disorganized intervals (**CF**). Sub-rounded clasts dominate, but, sub-angular clasts are common and sometimes restricted to specific intervals (Figure 4; see Section 6). The overlying sandstone-rich series generally fine and thin-upward, evolving from thick- to medium-bedded, concave-up sandstones pinching out to the north into nearly-flat bottomed, thinner-bedded sandstones with very thin- to thin-bedded mudstone caps (**HDTC** to **LDTC**) (Figure 8; Figure 10j, k; Figure 11). To the south, amalgamation dominates throughout (Figure 10i; Figure 11). This first occurrence ends with a couple of laterally continuous, very thick- to medium-bedded sandstones (**LDTC-b**) that are overlain by few thinner-bedded intervals (**LDTC-a**) and characteristically comprise large-scale fluid escape and soft-sediment deformation features (Figure 10j, k).

The second occurrence directly overlies the first, separated by a basal surface that varies from being sharp to erosional (> two meters incision) to the south (Figure 8; Figure 10i; Figure 11). The associated conglomerates are organized (**gHDTC**), mostly showing normally-graded patterns, amalgamated (*i.e.,* no capping sandstone) and smaller (~one to one and a half meters thick) (Figure 8; Figure 4; Figure 11).

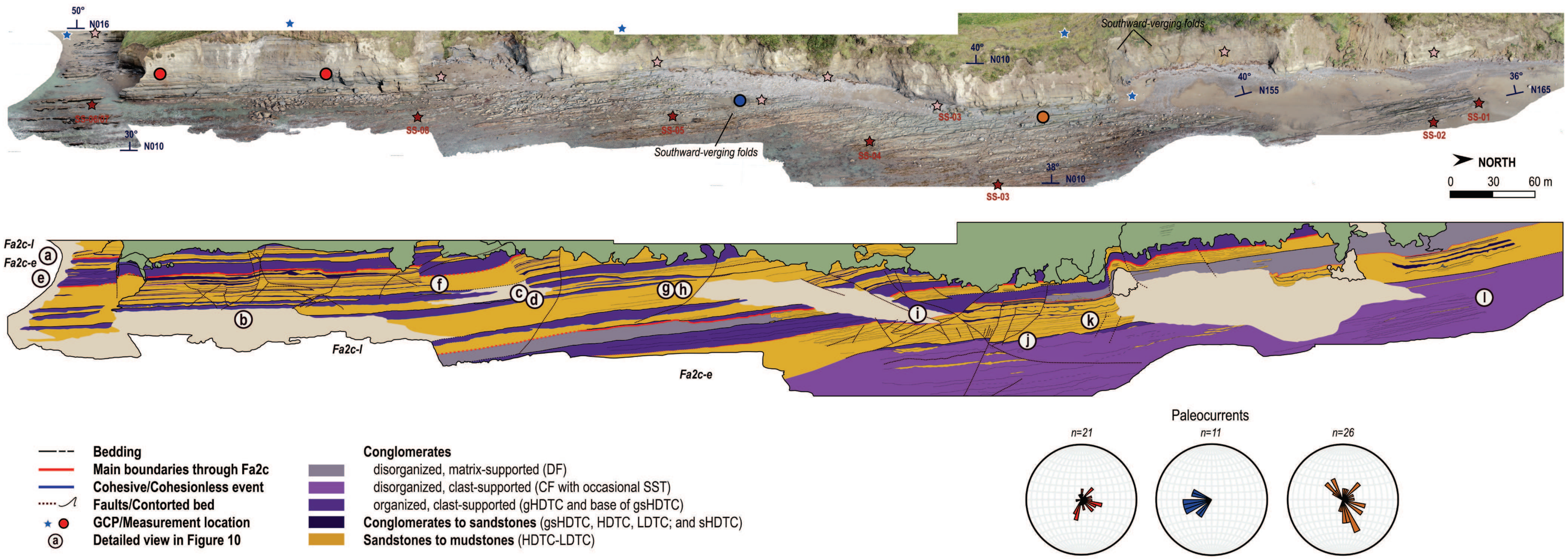

Figure 8: 3D outcrop model (top) and interpretation (bottom) of the Waikaraka coastal outcrop that exposes a confined slope channel system (Fa2c). This system comprises two distinct channel complexes, essentially divided into early-stage confined channel fills (Fa2c-e) and late-stage confined channel fills (Fa2c-l). The letters refer to remarkable architectural elements that characterize the Waikaraka system: a detailed view and explanation of each of them is available in Figure 10. The colors used in the stereoplots correspond to the location circles presented on the outcrop model (top). Stereoplots (Schmidt, lower hemisphere) highlight the paleocurrents taken in the turbidite system after back-tilting of bedding planes to initial horizontal position (assuming cylindrical folding).

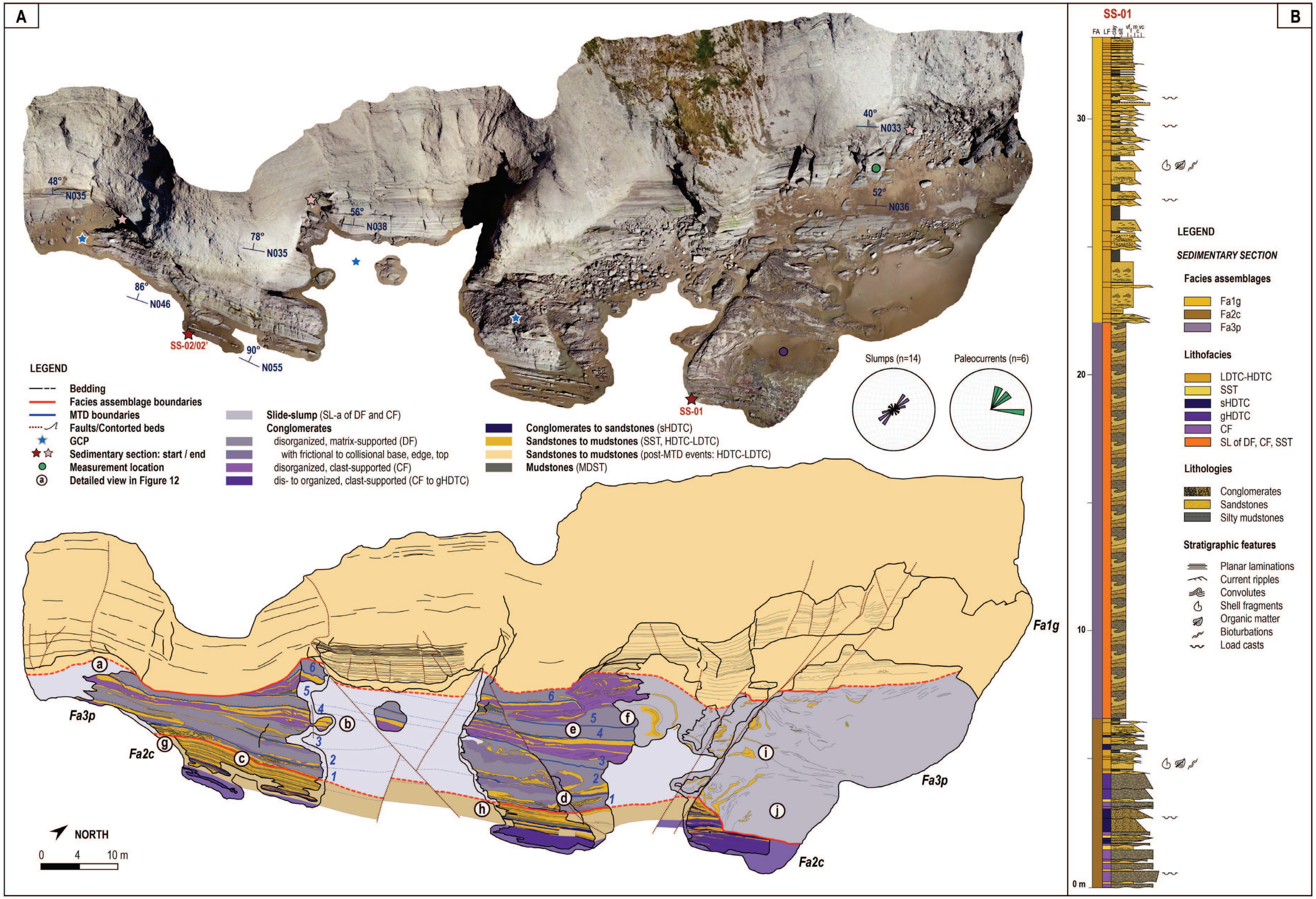

319

320 Figure 9: (A): 3D outcrop model (top) and interpretation (bottom) of the Homewood coastal outcrop. This outcrop exposes three distinct gravity-driven systems, from the bottom to the top, a slope channel system (Fa2c), a shelf-derived mass-wasting system (Fa3p) and a distal depositional
321 lobe system (Fa1g). The letters refer to remarkable architectural elements that characterize the Homewood system: a detailed view and explanation of each of them is available in Figure 12. The colors used in the stereoplots correspond to the location circles presented in the outcrop model
322 (top). Stereoplots (Schmidt, lower hemisphere) highlight the paleocurrents taken in the turbidite system (Fa1g, in green) and the fold axis of the slump-related folds taken in the mass-wasting system (Fa3p, in purple) after back-tilting of bedding planes to initial horizontal position (assuming
323 cylindrical folding). The blue numbers U1 to U6 highlights six units, corresponding to six distinct episodes of mass wasting. (B): Sedimentary section 01 (SS-01) recorded at Homewood. This section provides an overview of the three facies associations encountered.

Accepted Manuscript version. Published Journal Article version available online, published by Elsevier in Marine and Petroleum Geology Journal: https://doi.org/10.1016/j.marpetgeo.2021.105252

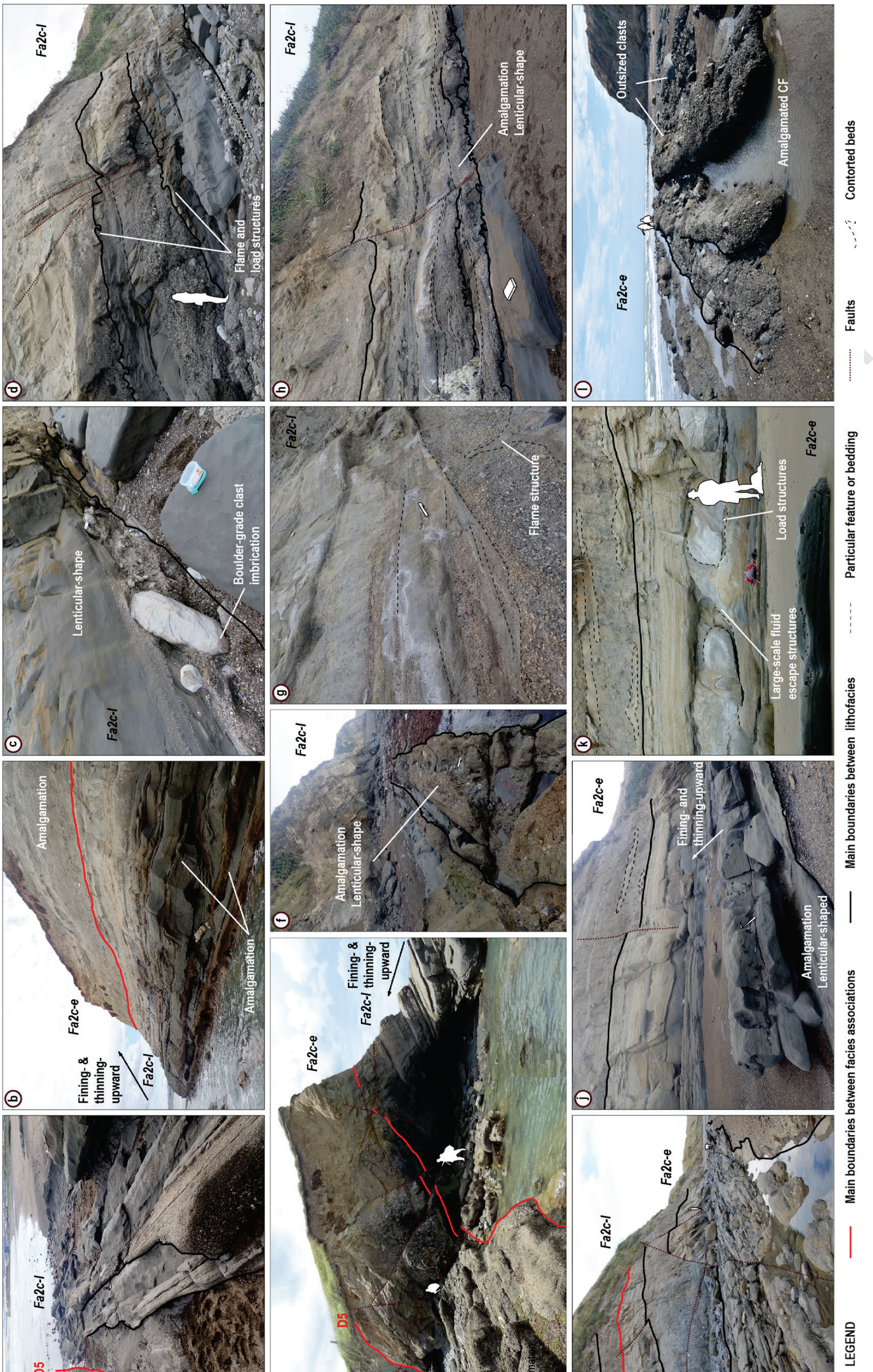
a
Fa2c-e
D5
Fa2c-l
b
Fining- & thinning-upward
Fa2c-l
Fa2c-e
Amalgamation
Amalgamation
c
Fa2c-l
Lenticular-shape
Boulder-grade clast imbrication
d
Fa2c-l
Flame and load structures
e
Fa2c-l
D5
Fa2c-e
Amalgamation
Fining- & thinning-upward
Fa2c-l
f
Fa2c-l
Amalgamation
Lenticular-shape
g
Fa2c-l
Flame structure
h
Fa2c-l
Amalgamation
Lenticular-shape
i
Fa2c-l
Fa2c-e
j
Fa2c-e
Fining- and thinning-upward
Amalgamation
Lenticular-shaped
k
Fa2c-e
Large-scale fluid escape structures
Load structures
l
Fa2c-e
Outsized clasts
Amalgamated CF
LEGEND
Main boundaries between facies associations
Main boundaries between lithofacies
Particular feature or bedding
Faults
Contorted beds

324

Figure 10: [previous page] Detailed views of the shelf-derived gravity-driven deposit main architectural and sedimentary elements supporting the interpretation of the Waikaraka 3D outcrop model (Figure 8). Fa2c corresponds to the confined slope channel system facies association, whereby Fa2c-e means early-stage fills and Fa2c-l late-stage fills. CF, DF, gHDTC, gsHDTC, SST, HDTC, LDTC correspond to the lithofacies summarized in Table 1. (a): Discontinuity *D5* from Bailleul et al. (2007) and Bailleul et al. (2013) marking the transition from Fa2c-e to the uppermost sand-rich deposits; (b, e): Fa2c-l fining- and thinning-upward conglomerate (gHDTC, gsHDTC) to sandstone series (HDTC, LDTC) overlain by Fa2c-e amalgamated conglomerates (CF and gHDTC) then followed by sandstones (HDTC, LDTC); (c): Fa2c-l boulder-grade clast imbrication (base of gsHDTC); (d): Fa2c-l three successive channel storey fills characterized by conglomerate-rich bases (gsDHTC) with upward (*e.g.,* flame) and downward (*e.g.,* load) soft-sediment features, overlain by sandstone-rich lithofacies (HDTC to LDTC); (f, h): Fa2c-l amalgamated, broadly lenticular channel storey fills (gsHDTC, HDTC, LDTC) ; (g): Fa2c-l upward (*e.g.,* flame) soft-sediment features and trough cross stratifications; (i): Fa2c-e transitioning to Fa2c-l; (j): Fa2c-e amalgamated sandstones (HDTC) pinching out to the north overlaid by the Fa2c-e conglomerates (DF, CF); (k): large-scale fluid escape structures and downward (*e.g.,* load) soft-sediment features in the Fa2c-e sandstones series (HDTC, LDTC) that underlies the next Fa2c-e conglomerate events (DF, CF); (l): Fa2c-e amalgamated conglomerates with outsized clasts (CF).

The deposits are moderately-sorted and in average comprise sub-rounded granule- to pebble-grade clasts with a few scattered boulders and outsized clasts (Figure 4; see Section 6). To the north, these conglomerates are matrix-supported (Figure 8) and locally include a very thin, clast-supported basal layer (**sheared DF**) (Figure 4). The overlying sandstones characteristically present well-developed, southward-oriented soft-sediment deformation features in their structured intervals and their beds are frequently contorted, presenting apparent southward-verging recumbent folds (Figure 8). To the south, these folds appear to eventually evolve into matrix-supported conglomerates containing both folded sandstones and extraformational pebble-grade clasts (**SL-a** to **DF**) (Figure 8; Figure 11).

Finally, the third occurrence is present toward the top of the Waikaraka outcrop and alternatively comprises disorganized (**CF**) and organized (**gHDTC**) conglomerates, sometimes overlain by structured to structureless sandstones (**SST**) (Figure 8; Figure 10e; Figure 11). The deposits are generally moderately sorted and, on average, comprise sub-rounded pebble- to cobble-grade clasts (Figure 4; see Section 6), although some occurrences carry boulders and outsized clasts (Figure 10e). The overlying sandstone series is only a few meters thick, interrupted by another couple of meter-thick conglomeratic episode (fourth occurrence), itself characterized by a sharp upper surface (Figure 10a).

<u>*Interpretations*</u>

Fa2c-e is interpreted to characterize the axis to off-axis, early-stage (Stage I of Kneller et al. (2020)) fills of confined slope channel complexes (*sensu* Sprague et al. 2005).

Accepted Manuscript version. Published Journal Article version available online, published by Elsevier in Marine and Petroleum Geology Journal: https://doi.org/10.1016/j.marpetgeo.2021.105252

The laterally extensive, coarse-grained and clast-supported conglomerates at its base represent deposition from gravelly gravity flows (Lowe 1982, R1, R2, R3 divisions). Upslope failures may have triggered all or part of these flows, which then began to transform from cohesive to cohesionless debris flows downslope (Lowe 1982; Postma 1986; Sohn et al. 2002). Their abundant amalgamation surfaces, clast-supported textures (*e.g.,* disorganized, inverse, normal) and very coarse grain sizes indicate significant bed load transport and rapid deposition of the gravels underneath gravelly high-density turbidity currents in an environment dominated by high-energy flows, erosion and bypass (Lowe 1982). The abundant scoured bases, combined with the other textural and sedimentary features suggest that these flows were funneled through low sinuosity, braid-like channels, as recurrently found in base of confined slope channel complexes *(e.g.,* Galloway 1998; Di Celma et al. 2010; Gamberi et al. 2013; Li et al. 2018; McArthur and McCaffrey 2019; Kneller et al. 2020). The southward increase in clast size observed in the first occurrence suggests a southward evolution from off-axis to axis settings (Campion et al. 2000).

The general upward internal organization observed in the conglomerates and the overlying sandstone series likely resulted from gravelly to sandy high- to low-density turbidity currents from multiple, rather than single flows (Lowe 1982), with flows initiating from a shallow marine environment connected to a vegetated hinterland sourcing the abundant terrigenous material (Kuenen 1964). The resulting deposits suggest lower energy environments leading to both the progressive abandonment of the channel system and passive infilling of the relief (Galloway 1998; McHargue et al. 2011). Axis to off-axis abandonment facies are typically sand-rich, fairly thick (*e.g.,* medium-bedded) and highly to moderately amalgamated (Campion et al. 2000; McHargue et al. 2011; Hubbard et al. 2014).

As previously described, four distinct occurrences of these axis to off-axis, early-stage fills were observed at Waikaraka, thereby indicating the presence of several slope channel complexes infilling one larger channel conduit (*sensu* Sprague et al. 2005). However, **Fa2c-e** only provides information on the deposits that form the lower part of these channel complexes.

The textural changes observed in the second occurrence here suggest transformation from cohesive to cohesionless flows, resulting from progressive dilution of a parental debris flow (**DF**) evolving into a high-concentration gravelly dispersion overlain by a lower-concentrated and turbulent suspension (**gHDTC**) (Sohn et al. 2002, *i.e.,* bipartite or stratified flows). When taken in consideration with the recurrent soft-sediment deformations, these elements suggest that this second occurrence may originate from several, small-scale failure events, either at or near the shelf break, or directly from the channel walls (Di Celma et al. 2010; Janocko et al. 2013; Janocko and Basilici 2021). The resulting mass-wasting products

Accepted Manuscript version. Published Journal Article version available online, published by Elsevier in Marine and Petroleum Geology Journal: https://doi.org/10.1016/j.marpetgeo.2021.105252

deposited in the channel conduit and the southward component observed in the above features indicate a potential northward location of the source region. Whether it is regional or local is here a matter of speculation. The large-scale fluid escape structures present in the underlying sandstones would result from sudden loading of the mass-wasting products onto the sandstone strata, increasing pore pressure and promoting dewatering (Figure 10k) (Browne et al. 2020).

Despite the changes observed in the second occurrence's texture and clasts (see Section 6.3), the absence of shutdown mud drape, the only weakly erosional basal surface separating the first and second occurrences, and their general crude fining- and thinning-upward trend all suggest that these two occurrences belonged to the same channel complex, rather than two distinct complexes (Kneller et al. 2020). The same reasoning applied to the third and fourth occurrences allows considering that these two belonged to another confined channel complex.

Overall, the lateral and vertical facies evolution observed throughout **Fa2c-e** suggests a general evolution from off-axis to axis settings towards the south. Notwithstanding the overall outcrop conditions (no 3D control) and or the orientation of the outcrop to withhold their exposures, the absence of recognizable lateral-accretion packages (LAPs) (*sensu* Abreu et al. 2003) may also inform that the slope channel system (**Fa2c**) was likely low to moderately sinuous and generally erosional. Such channel belts usually occur in the upper- to middle-parts of the continental slope (Janocko et al. 2013). Finally, the micropaleontological analyses suggest that deposition took place at outer bathyal paleodepths (Appendix 2).

5.2.2. Confined slope channel: axis to off-axis, late-stage fills (Fa2c-l)

Observations

Fa2c-l presents contrasting sedimentary facies and architectural styles to those of the underlying **Fa2c-e**, characteristically comprising fining- and thinning-upward series, dominated by fine-grained facies, only punctuated by coarser intervals. This association is traceable across the entire outcrop laterally (>900 meters) and can hold over 40 meters in thickness.

Accepted Manuscript version. Published Journal Article version available online, published by Elsevier in Marine and Petroleum Geology Journal: https://doi.org/10.1016/j.marpetgeo.2021.105252

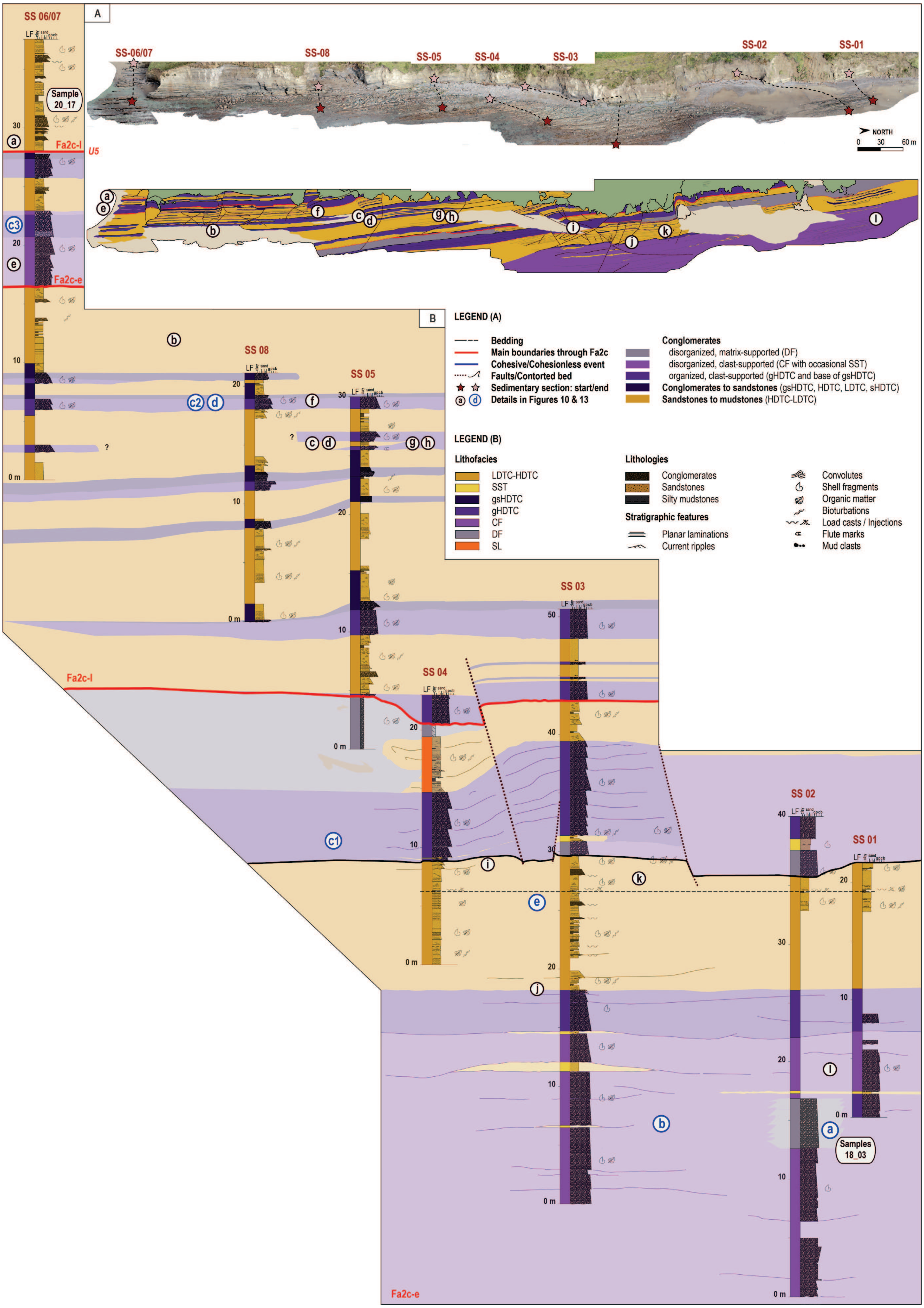

Figure 11: Sedimentary sections recorded at the Waikaraka outcrop. This system comprises two distinct channel complexes, respectively divided into the early-stage confined channel fills (Fa2c-e) and late-stage confined channel fills (Fa2c-l). The letters in dark red refer to remarkable architectural elements that characterize the Waikaraka system: a detailed view and explanation of each of them is available in Figure 10. The letters and numbers in blue give the location of the clast analyses summarized in Figure 13. Details on the sample data are available in Appendix 2. The red surface named *D5* at the top of the Waikaraka fill corresponds to the discontinuity *D5* from (Bailleul et al. (2007) and Bailleul et al. (2013), which marks the transition to the period of generalized subsidence that affected the Hikurangi Margin during the Middle Miocene, Waiauan.

Accepted Manuscript version. Published Journal Article version available online, published by Elsevier in Marine and Petroleum Geology Journal: https://doi.org/10.1016/j.marpetgeo.2021.105252

Fa2c-I comprises eight successive channel storey fills (*sensu* Sprague et al. 2005) (Figure 8; Figure 11). Each storey commonly starts with amalgamated, thick- to very thick-bedded (one to one and a half meters), organized, polymict and clast-supported conglomerates (**gHDTC**) deposited above a broadly erosional, concave-up base (Figure 4; Figure 11). These are overlain by a fining- and thinning-upward conglomerate to sandstone series, capped by bioturbated mudstones (**gsHDTC**), which is, in turn, overlain by another fining- and thinning-upward series of nearly-flat bottomed, thick- to thin-bedded sandstones and mudstones (**HDTC** to **LDTC**) (Figure 5; Figure 10b, h; Figure 11). The basal conglomerate to sandstone series shows repeated bed amalgamation, thus forming composite stratigraphic infills (Figure 10f; Figure 11). Conglomerates are concentrated within the basal intervals; sandstones quickly become dominant, generally representing a third of the channel storey fill (Figure 8; Figure 11). The conglomeratic intervals are broadly lenticular, laterally pinching out, amalgamated and often include clast imbrications and subtle cross-stratifications (Figure 10c, f, h). Interestingly, their matrix seems primarily made of bioclast content (*e.g.,* shell fragments) toward the top of **Fa2c-I**.

The bases of the conglomerates commonly display centi- to decametric soft-sediment deformation structures (*e.g.,* flames) and large sole marks (*e.g.,* flutes) (Figure 5; Figure 10d, g). Boulders and outsized clasts usually mark the transition from the inverse- to normally-graded patterns, and their proportion generally increases toward the south (Figure 5, gsHDTC to HDTC). Clasts are sometimes of larger size than the conglomerate bed itself, thus protruding into the overlying sandstones (Figure 5, gsHDTC to HDTC). On average, sub-rounded pebble-grade clasts dominate. In **Fa2c-I**, the **HDTC** sandstones that directly overlie the conglomerates are commonly coarse-grained in their traction intervals, show trough cross-stratifications and include plant debris, numerous shell fragments (Figure 10g) and abundant aligned mud clasts at their base. These sandstones form broadly lenticular bodies, with locally erosive bases characterized by very coarse- to coarse-grained material (Figure 10a, f). They eventually reach medium- to fine-grain sizes in the remaining intervals and in the subsequent fining- and thinning-upward series (**HDTC** to **LDTC**). The paleocurrents measured in the sandstone intervals indicate a general southward trend (Figure 8), which is consistent with measurements from imbrications within the coarse-grained basal fills.

Two occurrences of **Fa2c-I** were observed at Waikaraka (Figure 8; Figure 11).

The first occurrence corresponds to the above description. It is about 40 meters thick and comprises eight channel storeys (*sensu* Sprague et al. 2005). Its basal surface is sharp, concave-up and broadly incises **Fa2c-e** with up to 2 meters relief (Figure 8). The second occurrence is observed at the top of the Waikaraka outcrop and only crops out for about 15 meters laterally and vertically, being covered by quaternary beach deposits after that. Its basal surface is sharp above the underlying **Fa2c-e** occurrence and it is only comprised of sandstones (**HDTC to LDTC**) (Figure 10a, e; Figure 11).

Interpretations

Fa2c-I is interpreted to represent the axis to off-axis, late-stage (Stage II of Kneller et al. (2020)) fills of confined slope channel complexes (*sensu* Sprague et al. 2005). Characterized by multiple episodes of erosional bypass and sedimentation, these form the middle fills of channel complexes.

The conglomerate- to sandstone-dominated basal successions (**gHDTC** and **gsHDTC**) that broadly fill the erosion surface result from stratified gravelly gravity flows that are confined within channels (Lowe 1982; Campion et al. 2000; Sohn et al. 2002). The basal dewatering features suggest rapid deposition and loading of the channel fills, whereas the frequent amalgamation observed in both the conglomerates and sandstones implies that erosion and bypass were dominant in the basal interval (Lowe 1982). Transport of large (*e.g.,* outsized) clasts can be explained by flow confinements such as the ones found in confined slope channels, where the flow size, velocity and carrying capacity are maximized (Postma et al. 1988). The high degree of preservation of mud clasts in both the conglomerates and overlying sandstones, scattered as lag material indicates high fall-out rates (Postma 1986), whereas the increase in content of coarse and fine skeletal fraction toward the top of the series rather suggest deposition of calciturbidites (*e.g.,* Haak and Schlager 1989; Reijmer et al. 2015). The gravelly gravity flows then decelerated and became less confined. The overlying tabular, fining- and thinning-upward series of sandstones and mudstones (**HDTC to LDTC**) mark the transition to lower energy depositional environments, resulting in passive filling and progressive abandonment of the channel system (Galloway 1998; McHargue et al. 2011). As in **Fa2c-e**, such sand-rich abandonment facies here suggest axis to off-axis settings (Campion et al. 2000). Overall, these broadly lenticular and laterally extensive channel storey fills are dominated by sandy high- to low-density turbidites, scouring a mud-rich substrate during downslope transport and or at hydraulic jumps (*i.e.,* abundant mud clasts) (Fonnesu et al. 2016). The vertically aggrading, semi-amalgamated style of the channel storey fills confirms a generally confined slope channel complex settings (Sprague et al. 2005), but less steep and confined to those of the previously described **Fa2c-e**.

Although most likely belonging to the same slope channel system, the uppermost occurrence characteristics and micropaleontological analyses both suggest contrasting depositional settings. Not only the micropaleontological study indicates lower paleodepths of deposition (*i.e.,* lower bathyal), it also indicates that this latter series was restricted to the Middle Miocene, Waiauan (Serravallian, 13.05 – 11.63 Ma) (Figure 11; Appendix 2).

Overall, we interpret the Waikaraka outcrop to represent the axis to off-axis stratigraphic infills of two distinct channel complexes, essentially capturing the early- to late-stage fills of a larger, yet confined slope channel system (*sensu* Sprague et al. 2005). We further discuss the controls on such a system and the implications of its uppermost deposits in Section 7.

5.3. Weakly confined slope and depositional lobe systems

The Homewood section crops out one kilometer north of the Kaiwhata river mouth and extends over 110 meters along the coast (Figure 3). It features three distinct Middle Miocene, Lillburnian (Late Langhian to Serravallian, 15.1 – 13.05 Ma, Appendix 2) gravity-driven systems described and interpreted below as three separate facies associations (**Fa2c, Fa3p, Fa1g**) (Figure 9).

5.3.1. Slope channel (Fa2c)

<u>*Observations*</u>

At Homewood, **Fa2c** is characterized by crude fining- and thinning-upward series, evolving from coarse- to fine-grained facies. Owing to outcrop conditions, it is intermittently exposed for about 80 meters laterally and only represents a ten of meter-thick succession of sub-vertical beds. Its basal surface does not crop out and it is overlain by the erosive **Fa3p** (Figure 9).

Here, **Fa2c** is characterized by a series of tabular, continuous (1) medium- to thick-bedded (10 to 50 centimeters), disorganized (**CF**) to organized (**gHDTC**) clast-supported conglomerates with sandstone caps (**SST**), followed by (2) thin- to medium-bedded (3 to 15 centimeters) pebbly sandstones (**sHDTC-a**) or bioclastic grits (**sHDTC-b**), either interbedded with mudstones (**MDST**) or structureless sandstones (**SST-b**) and mudstones (**MDST**), finally overlain by (3) medium- to thick-bedded bedded (10 to 50 centimeters) sandstones with mudstone caps (**LDTC-b**) (Figure 6; Figure 7; Figure 9; Figure 12g, h).

Overall, a greater internal organization is observed in **Fa2c** to the north-east of the outcrop. Conglomerates are generally ungraded (**CF**) to the south-west of the outcrop, whereas they gradually show internal organization (**gHDTC**), displaying inverse- to normally- or only normally-graded patterns to the north-east (Figure 6). The conglomerates mostly consist of sub-angular to sub-rounded granule- to pebble-grade clasts (see Section 6). Cobbles and boulders are locally observed. Similarly, the bioclastic grits (**sHDTC-b**) become normally-graded, and include mud clasts and or bioclastic fractions aligned along horizons towards the north-east of the outcrop (Figure 7). In both cases, the basal surfaces of the conglomerates and bioclastic grits are slightly erosive and commonly display load structures.

Finally, the sandstones (**LDTC-b**) to the south-west present rare, discontinuous, centimeter-thick, very coarse basal intervals (Ta), whereas to the north-east, these basal intervals are well-developed, fairly continuous and include frequent mud clasts and bioclastic fractions aligned along horizons, as well as load structures (Figure 7). The related sandstones also commonly show distinct grain-size breaks, indicating amalgamation of beds.

Interpretations

We interpret this basal succession to result from both flow processes and depositional environments (**Fa2c**) similar to those described at Waikaraka. While outcrop exposure hinders recognition of specific architectural elements, such as channels, and of particular depositional units (**Fa2c-e, Fa2c-l**), the stratigraphic infill outlines comparable crude fining- and thinning-upward conglomerate to sandstone series, resulting from gravelly to sandy high- to low-density turbidity currents (Lowe 1982). The main difference resides in the scale of the individual beds, being significantly smaller at Homewood, which could either point towards (1) smaller source region or slope-channel system, and or (2) contrasting locations along the slope or laterally within the channel.

5.3.2. Mixed shelf-derived mass-transport deposits (Fa3p)

Observations

Fa3p mostly comprises interbedded coarse-grained facies, here exposed across more than 120 meters laterally and about 15 meters thick (Figure 9).

Fa3p is characterized by a succession of thick- to very thick-bedded (<one to >two meters), disorganized, polymict, matrix- (**DF**) and clast-supported (**CF**) conglomerates, that laterally becomes entirely deformed and contorted (**SL-a**) to the north-east of the outcrop (Table 1; Figure 6; Figure 7; Figure 9). The conglomerates are recurrently capped by thin- to thick-bedded, either structureless or structured sandstones (**SST**) (Table 1; Figure 6; Figure 7; Figure 9; Figure 12), the latter of which can sometimes evolve to a few interbedded structured, very thin- to medium-bedded sandstones with mudstone caps, commonly bioturbated (**LDTC-a**) (Table 1; Figure 7; Figure 9; Figure 12b, e).

Accepted Manuscript version. Published Journal Article version available online, published by Elsevier in Marine and Petroleum Geology Journal: https://doi.org/10.1016/j.marpetgeo.2021.105252

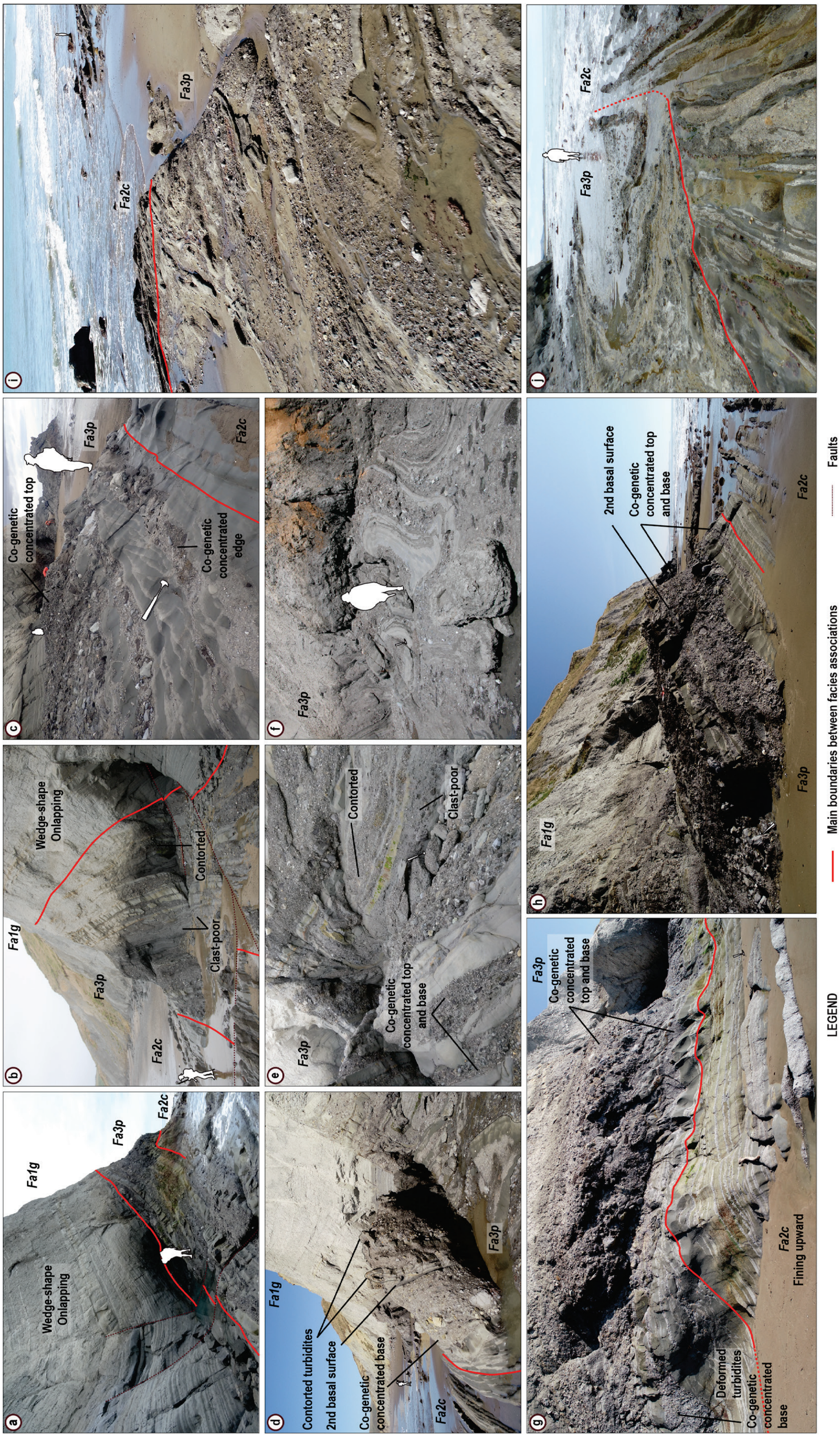

Accepted Manuscript version. Published Journal Article version available online, published by Elsevier in Marine and Petroleum Geology Journal: https://doi.org/10.1016/j.marpetgeo.2021.105252

Figure 12: [previous page] Detailed views of the shelf-derived gravity-driven deposit main architectural and sedimentary elements supporting the interpretation of the Homewood 3D outcrop model (Figure 9). Fa2c corresponds to the confined slope channel system facies association, Fa3p to the shelf-derived mass-wasting system and Fa1g to the distal depositional lobe system. SL, CF, DF, gHDTC, SST, sHDTC, HDTC, LDTC correspond to the lithofacies summarized in Table 1. (a, b): Fa3p succession of interbedded conglomerates (DF, CF) recurrently capped by sandstones (SST) and overlain by the onlapping Fa1g sandstones (HDTC, LDTC); (b): Fa3p varying bed dips and upper contorted unit; (c, d, e, g, h): Fa3p conglomerates showing local variation in clast concentrations at their base, edge and or top (sheared DF), (d, h): Fa3p sharp surface at the base of the succeeding conglomerate, which holds contorted sandstones; (e): Fa3p occurrence of clast-poor conglomerate (DF) and upper contorted unit; (f, i, j): Fa3p contorted conglomerates (SL-a, made of DF, CF and SST); (g, h): Fa2c crude fining- and thinning-upward conglomerate to sandstones (gHDTC, sHDTC, LDTC), overlain by Fa3p, which is characterized by erosion as well as local substrate entrainment and deformation at its base; (i, j): Fa3p basal eroded through Fa2c towards the north-east.

The basal surface is highly erosive (>8 meters) towards the north-east (Figure 9, red surface at the base of Fa3p; Figure 12g, i, j), and both local entrainment and deformation (*i.e.,* apparent northward-verging contorted sandstones) of the substrate are observed (Figure 9; Figure 12g). In contrast, the upper surface is highly irregular, with overlying beds onlapping on a deci- to decametric scale (Figure 9; Figure 12a, b). Laterally, the upper surface can appear rather flat and overlain by relatively tabular sandstones. The first overlying sandstone beds are generally internally chaotic; they sometimes incorporate material from **Fa3p** (*e.g.,* pebbles and cobbles) and can form well-developed, decametric-scale soft-sedimentation deformation structures.

Five additional internal surfaces were also identified, which allows division of **Fa3p** into six units (Figure 9, blue surfaces within Fa3p). Commonly observed at the top of the structureless or structured beds (**SST**), these surfaces are sharp and characterized by thin- to medium-bedded silty mudstones (**MDST**) that can be traced across the outcrop (Figure 9, blue surfaces; Figure 12d, h).

In the southern and central parts of the outcrop, **Fa3p** comprises fairly tabular beds. Their thicknesses tend to increase north-eastward, thus generally forming lens-like shapes opening towards the north-east (Figure 9). The beds' orientation changes from N055 to N035 and the dip measurements show an abrupt evolution from 90° (sub-vertical) to ~60° towards the west in only 15 meters. The dip of the first four units (separated by the internal surfaces described above) changes from 90° to 78°, whereas the remaining two directly onlap onto the preceding ones with a dip starting around 70° and evolving towards 60°. To the north-east, **Fa3p** is completely disorganized and shows SW-NE oriented recumbent folds (Figure 9, slump measurements; Figure 12j).

Three different scales of internal contortion are observed in **Fa3p**, evolving both vertically and laterally: (1) at clast-scale; (2) at unit-scale and (3) at the scale of several units. First, the entrained sandstones display both apparent NE-verging (Figure 9) and NE-SW-oriented recumbent folds (Figure 12f). Second, the fifth unit, previously observed to onlap on the underlying beds, appears to be severely folded, with a NE-SW main axis (Figure 9, unit 5; Figure 12b, e). Third, the upper **Fa3p** units become remobilized laterally, folding following an apparent NE-verging trend (Figure 12f). To the north-east of the outcrop, this remobilization involves the entire facies association (*i.e.,* interbedded **DF**, **CF** and **SST**) (Table 1; Figure 9; Figure 6; Figure 12f, i, j).

The matrix of the interbedded polymict conglomerates generally represents 40 to 70% of the **DF** deposits with two occurrences comprising up to 80% of matrix (Figure 6; Figure 12b, e; Figure 13), and <5 to 15% in **CF**. **DF** can display slight upward increase in matrix content. Alternatively, **DF** commonly shows vertical and or lateral variations in both clast concentration and size at its base, top and or edges that appear akin to the clast-supported lithofacies (**CF**) (Figure 9; Figure 6; Figure 12c, d, e, g, h). These concentrated intervals are characterized by clasts of smaller grades (*i.e.,* granule- to pebble-grade) than those of the general matrix-supported intervals (*i.e.,* pebble- to cobble-grade) (Figure 6). Overall, the average clast size is of pebble- to cobble-grade in **DF**, whereas granule- to pebble-grade dominates **CF**. In **DF**, larger clasts are frequent and can be outsized (deci- to decametric); conversely, they are rare and of cobble-grade in **CF**. In both **DF** and **CF**, clast edges typically vary between sub-angular to sub-rounded shapes. The highest proportions of sub-angular clasts are found in the largest clasts (*e.g.,* boulders). Sub-rounded to rounded clasts are mostly present in the concentrated granule- to pebble-grade intervals of **DF** or in some rare occurrences of **CF**.

<u>*Interpretations*</u>

We interpret **Fa3p** to represent deposition (*i.e.,* mass-transport deposits [MTDs]) from successive mass-wasting events that triggered recurrent debris flows (**DF** and **CF**) (Postma 1986; Mulder and Cochonat 1996). The clast-supported debris flows (**CF**) are inferred to result from cohesionless flows (Postma 1986). Even if matrix strength dominates in **DF**, thereby suggesting cohesive flows (Nardin et al. 1979; Lowe 1982), Nemec and Steel (1984) demonstrated that the predominance of matrix in conglomerates was not always a criterion to discriminate cohesive and cohesionless debris flows. Although the ungraded, disorganized and matrix-rich occurrences of **DF** result from cohesive flows (Johnson 1984; Postma 1986), the 2-to-3 phase occurrences (**sheared DF**) show internal organization that indicates fully sheared flows with additional support mechanisms, such as grain collisions and dispersive pressure, characteristic of cohesionless debris flows (Lowe 1982; Nemec and Steel 1984; Postma 1986).

Multiphase debris flows require steep slopes (Postma 1986). The lens-like shapes observed in some of their deposits may suggest channelization, characteristic of steep slope settings (Ortiz-Karpf et al. 2017;

Accepted Manuscript version. Published Journal Article version available online, published by Elsevier in Marine and Petroleum Geology Journal: https://doi.org/10.1016/j.marpetgeo.2021.105252

Calhoun and Clague 2018). The high-amplitude variations recorded in the dip of beds (~40°) indicates that they were syn-kinematic with the rise of a structure to the east, *i.e.,* growth strata. Changes in slope gradient chiefly impact flow behavior (*e.g.,* velocity) and may promote flow transformations (*e.g.,* dilution, shearing) (Fisher 1983), which in turn control the nature and geometry of the resultant deposits. Hence, slope angle changes could partly explain the variety of debris flow deposits recorded in **Fa3p**. Also, the considerable amounts of granule- and pebble-grade clasts (Sohn et al. 2002) as well as the recurrent presence of mudstone layers and fine sandstones (**SST**), respectively under- and overlying the conglomerates, all point toward fast-moving debris flows that hydroplane (*sensu* Mohrig et al., 1998). The multiphase debris flows described here would thus result from efficient dilution of cohesive, hydroplaning debris flows (Mohrig et al., 1998); dilution which can arise only a few kilometers from the source areas (Sohn et al. 2002) and which can lead to the generation of slower-moving suspended sediment clouds eventually depositing above them (**SST**) (Mohrig et al. 1998; Sohn et al. 2002; Mohrig and Marr 2003; Talling et al. 2004). The first debris flow, however strongly erosional, suggests both an abrupt change in the depositional settings to that of the underlying **Fa2c** deposits and an initially different mechanism (*i.e.,* substrate erosion) responsible for flow mobility (Sobiesiak et al. 2018).

The internal surfaces allow to distinguish at least six mass-wasting events. The different scales of internal contortion and deformation observed in the **Fa3p** deposits however complicates their depositional history, thereby questioning the hypothesis of simple deposition of one mass flow on top of another. Basal deformation of the substrate linked to the passage of an overriding flow is common, however the flow mobility mechanisms proposed here (*i.e.,* hydroplaning) diverges from such a scenario, promoting little to no interaction between the moving flow and underlying deposits for five of the units (Sobiesiak et al. 2018). Notwithstanding the possibility for the contorted strata to shear and deform in the direction of the flow and thus capture the paleoslope direction at the clast-scale (Fonnesu et al. 2016), we here suggest a different mechanism to explain the deformation recorded at the unit-scale and propose that a change in slope gradient can both trigger development of a mass flow upslope and coeval remobilization (translation and deformation) of the previously deposited and only poorly lithified mass-flow deposits downslope. When combined with bed dips, the analysis of the fold hinges and axial planes at both clast- and unit-scales consistently indicates a NW-dipping paleoslope and transport direction (Alsop et al. 2019; Alsop and Weinberger 2020), coherent with a rising structure to the east.

The larger-scale remobilization observed to the north-east that involves the entire facies association **Fa3p** could also be associated with this growing structure. As such, we interpret it to result from local failure of the entire series due to the recurrent loading of sediments onto this rising slope, two mechanisms known

Accepted Manuscript version. Published Journal Article version available online, published by Elsevier in Marine and Petroleum Geology Journal: https://doi.org/10.1016/j.marpetgeo.2021.105252

to greatly affect slope stability and encourage its failure (Hein and Gorsline 1981). Finally, the micropaleontological studies imply an upper- to mid-bathyal depositional environment (Appendix 2).

5.3.3. Distal depositional lobe system (Fa1g)

Observations

Fa1g is characterized by laterally continuous, on average medium-bedded (~14 centimeters) and fine-grained sandstones that show decreasing bed dips upward (56° to 32°). This association is exposed along ~one kilometer of coastline and is over 200 meters in thickness (Appendix 4). Only the lowermost part of this system is described in context of the outcrop model presented in this study (Figure 9; Fa1g).

Fa1g mostly comprises interbedded tabular, medium- to thick-bedded, frequently amalgamated sandstones (**LDTC-b**) and very thin- to medium-bedded (**LDTC-a**), often dewatered, argillaceous sandstones (Table 1; Figure 7). Most beds include shell fragments and plant debris in the structured intervals, and are capped by silty mudstones that regularly include bioturbations (Figure 7) such as *Phycosiphon* sp., *Zoophycos* sp., *Skolithos* sp. and *Scolicia* sp. Episodes of thin-bedded bioclastic grits (**sHDTC-b**) are recurrent (Figure 7). Very-thick sandstone beds punctually occur; they tend to have sole marks, several grain-size breaks, and sometimes show decametric soft-sedimentation deformation structures. A few lenticular, medium- to very thick-bedded sandstones (**HDTC**) are also observed. Their incision rarely exceeds 50 centimeters and can comprise coarse bioclastic material (Figure 7). Paleocurrent measurements from sole marks and traction structures generally indicate a north-eastward direction at the base of this system (Figure 9). Finally, disorganized, contorted strata (**SL-a**) and coherent, remobilized strata displaying sharp internal truncations in the same lithofacies (**SL-b**) recurrently interrupt the strata (Table 1; Figure 6).

Interpretations

Fa1g is interpreted to record the emplacement and sustained development of a distal depositional lobe system (Bailleul et al. 2007; Prélat et al. 2009; McArthur et al. 2021) installed above and subsequently pinned at its base within the rugose topography left by the underlying MTDs (*e.g.,* Bull et al. 2009; Armitage et al. 2009) (Figure 9; Figure 12a, b). These laterally extensive, tabular, sandstone-rich deposits are interpreted as the deposits of dominantly low-density turbidity currents (**LDTC**) (Bouma 1962), commonly deposited in off-axis to fringe positions (Prélat et al. 2009). The punctual bioclastic grits as well as the locally erosive, amalgamated and very thick occurrences, are however attributed to higher-density turbidity currents (Lowe 1982) resulting from larger flow events. The onlapping and growth strata geometries as well as the recurrent yet localized remobilization of strata both suggest an unstable depositional environment, likely due to a continued rise of the eastern structure. The paleocurrent directions to the NE indicate that the flow at the start of this depositional system was parallel to the rising NE-SW oriented structure to the east and thus both point towards a different sourcing system to the underlying MTDs (see Section 5.3.2) and an axial routing of the turbidity currents (Burgreen and Graham 2014). The abundance of land-derived material suggest that these turbidity currents likely initiated from a shallow marine environment connected to a hinterland (Kuenen 1964), while the micropaleontology analyses indicate that deposition of the turbidites occurred at mid bathyal depths or deeper (> 800 meters) (Appendix 2).

6. SOURCE REGIONS

Despite lithofacies similarities, the sediment gravity flows observed at Waikaraka and Homewood are lithologically different (Figure 13) and thus indicate different sediment sources. Here, we use the nature of the reworked material in the conglomerates (**DF, CF, gHDTC, gsHDTC**), pebbly sandstones (**sHDTC-a**), bioclastic grits (**sHDTC-b**) and coarser intervals of the sandstones (**HDTC**) as a tool for better understanding and characterizing their provenance and source areas as well as deciphering local paleotransport directions (*e.g.,* Nemec and Steel, 1984).

6.1. Extrabasinal sources

Clast observations

Across both Waikaraka and Homewood, the conglomeratic units (**DF**, **CF**, **gHDTC**, **gsHDTC**, **sHDTC**, **HDTC**) essentially rework extraformational clasts from pre- and syn-subduction strata (>95%) (Figure 13). Pre-subduction material dominates (> 80%) and comprises lithoclasts from the Early Cretaceous up to the Paleocene at Waikaraka and from the Late Cretaceous up to the Eocene at Homewood. The syn-subduction material is divided into Miocene lithoclasts and bioclasts.

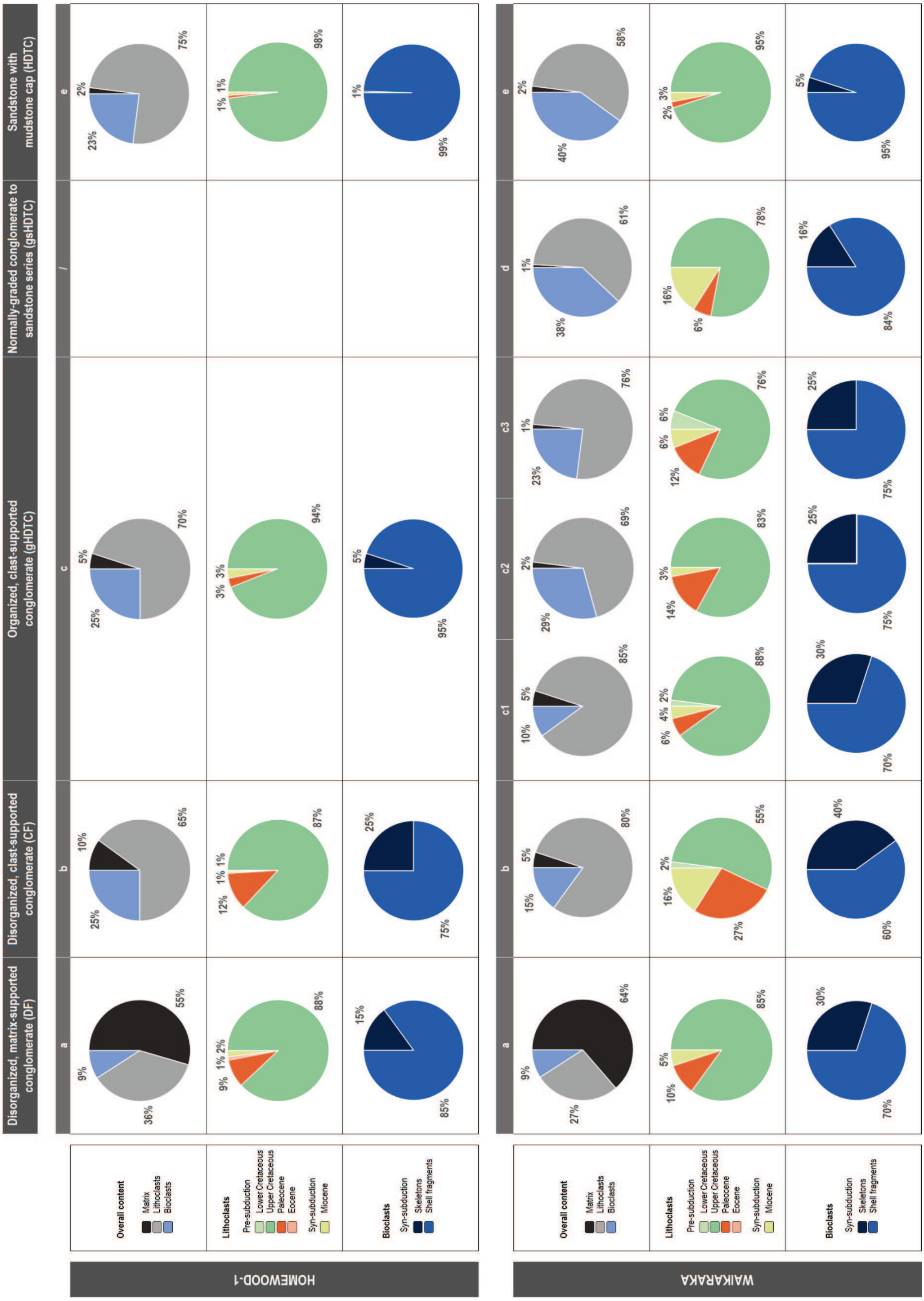

Figure 13: Quantitative analyses of the clast content recognized at Waikaraka and Homewood outcrops. The analyses looked at both the lithoclast and bioclast content. The lithoclasts were classified according to the tectonostratigraphic unit they

belonged to and the bioclasts were subdivided into two main types, *i.e.,* the preserved skeletons and the shell fragments. DF, CF, gHDTC, gsHDTC and HDTC correspond to the lithofacies summarized in Table 1.

Intraformational clasts are virtually absent (<1%) in **CF**, but are more frequent in the conglomerates deposits resulting from matrix strength (**DF**; *e.g.,* poorly lithified turbidites) and fluid turbulence (**gHDTC**, **gsHDTC**, **sHDTC**, **HDTC**; *e.g.,* mud clasts).

Clast interpretations

The dominance of extraformational clasts implies that the flows responsible for these conglomeratic units initiated outside of their final depositional environment and incorporated material belonging to structural units and or paleogeographic domains different to that of the intrabasinal sediments (*i.e.,* extrabasinal) (*e.g.,* Ogata et al. 2019). The abundance of pre-subduction material indicates that during the Middle Miocene, the exposed extrabasinal paleogeography was dominated by Cretaceous to Eocene strata. In compressional settings, uplift of thrust-related structures is known to develop bathymetric highs and or steep slopes, which can in turn, expose rocks from the older substratum (*i.e.,* pre-subduction), ready to be reworked and incorporated into the subsequent flows and MTDs (*e.g.,* Ogata et al. 2019).

6.2. Mixed siliciclastic-carbonate shelves

Bioclast observations

A substantial amount (~10 to 40%) of syn-subduction bioclasts is present in all the deposits, either as shell fragments or as well- to partly-preserved skeletons (Figure 13). Molluscan species (*e.g.,* bivalves and gastropods) dominates; yet, corals (solitary and colonial) and red algae are also locally present (Appendix 3). At Homewood, the preserved forms of macrofossils reach between 15 and 25% of the bioclasts contained in the debris flow deposits (**DF** and **CF**) whereas they are virtually absent in the turbidites (**gHDTC and HDTC**), which are dominated by shell fragments. At Waikaraka however, the preserved forms represent a considerably larger proportion of the bioclasts, mostly oscillating between 25 and 40%, even at the base of the turbidites (**gHDTC and HDTC**). Although the content in both the coarse (macrofossils) and fine (shell fragments) skeletal fractions gradually increases toward the top of the Waikaraka deposits, this upward evolution is particularly remarkable in the late-stage fill deposits (**Fa2c-I**) (Figure 13, cf. c2, c3, d, e).

Overall, the taphonomic analyses shows that destructive processes dominate the taphonomic record of the deposits, constructive taphonomic processes such as encrustation being virtually absent (Figure 14). At Homewood, the deposits are characterized by bioclasts being: (1) moderately to highly fragmented,

Accepted Manuscript version. Published Journal Article version available online, published by Elsevier in Marine and Petroleum Geology Journal: https://doi.org/10.1016/j.marpetgeo.2021.105252

(2) moderately abraded and, (3) poorly bioeroded. At Waikaraka, the finer bioclastic fractions compare markedly in both debris flows (**DF**, **CF**) and high-density turbidite flows (**gHDTC**, **gsHDTC**). By contrast, the coarser skeletal material in the former exhibit higher degrees of abrasion and bioerosion than in the latter (Figure 14).

Bioclast interpretations

The nature and amount of reworked molluscan species indicate that the sediment gravity flows originated from shallow marine middle- to inner-shelf neritic environments before being transported to deep-marine outer to mid bathyal depths (Appendix 2; Appendix 3).

The contemporaneously developing mixed siliciclastic-carbonate environments (*i.e.,* compositional systems (*sensu* Chiarella et al. (2017)) previously identified and described in the Coastal Ranges present markedly similar faunal assemblages (Crundwell 1987; Chanier 1991; Bailleul et al. 2007; Bailleul et al. 2013; Bailleul et al. 2015) and are thus great candidates for providing both the preserved skeletons and shell fragments. The depositional system envisaged for those sources is one of a regional, continent-attached shelf domain, recurrently supplied with terrigenous sediments from the exposed Cretaceous basement located to the west (Crundwell 1987; Chanier 1991; Bailleul et al. 2007; Bailleul et al. 2013; Bailleul et al. 2015; Claussmann et al. 2021).

The substantial amount of gravels transported beyond the shelf and captured within the deposits (see Sections 5 and 6.3) requires narrow shelf settings to easily connect to the slope beyond (Nemec and Steel 1984), which typify the shelfal systems along active margins (Sømme et al. 2009). No lateral continuity has yet been proven between the mixed siliciclastic-carbonate environments and therefore, isolated, continent-detached shelfal systems likely also developed locally (*e.g.,* (Bailleul et al. 2013), Fingerpost shelf) upon and around actively growing folds and faults (Caron et al. 2004) (see Section 6.3 and 7).

In fact, at Waikaraka, the fairly constant proportion of shelfal macrofossils found throughout the 90 meter-thick succession points to paleophysiographies allowing for molluscan communities to thrive above storm-wave base (Pomar 2001). At Homewood however, the macrofossils are mostly found in the conglomerates (**DF, CF**) of the mass-wasting system (**Fa3p**) and their quantity tends to be generally smaller to that of Waikaraka. This could indifferently indicate a smaller-sized source area, slightly different paleoenvironmental conditions at the source as well as different transport processes and distances. The paleotransport directions recorded in the mass-wasting system (**Fa3p**) of Homewood also inform that the

Accepted Manuscript version. Published Journal Article version available online, published by Elsevier in Marine and Petroleum Geology Journal: https://doi.org/10.1016/j.marpetgeo.2021.105252

shelfal source was located to the east and thus was most-likely detached from the main regional shelf domain located to the west.

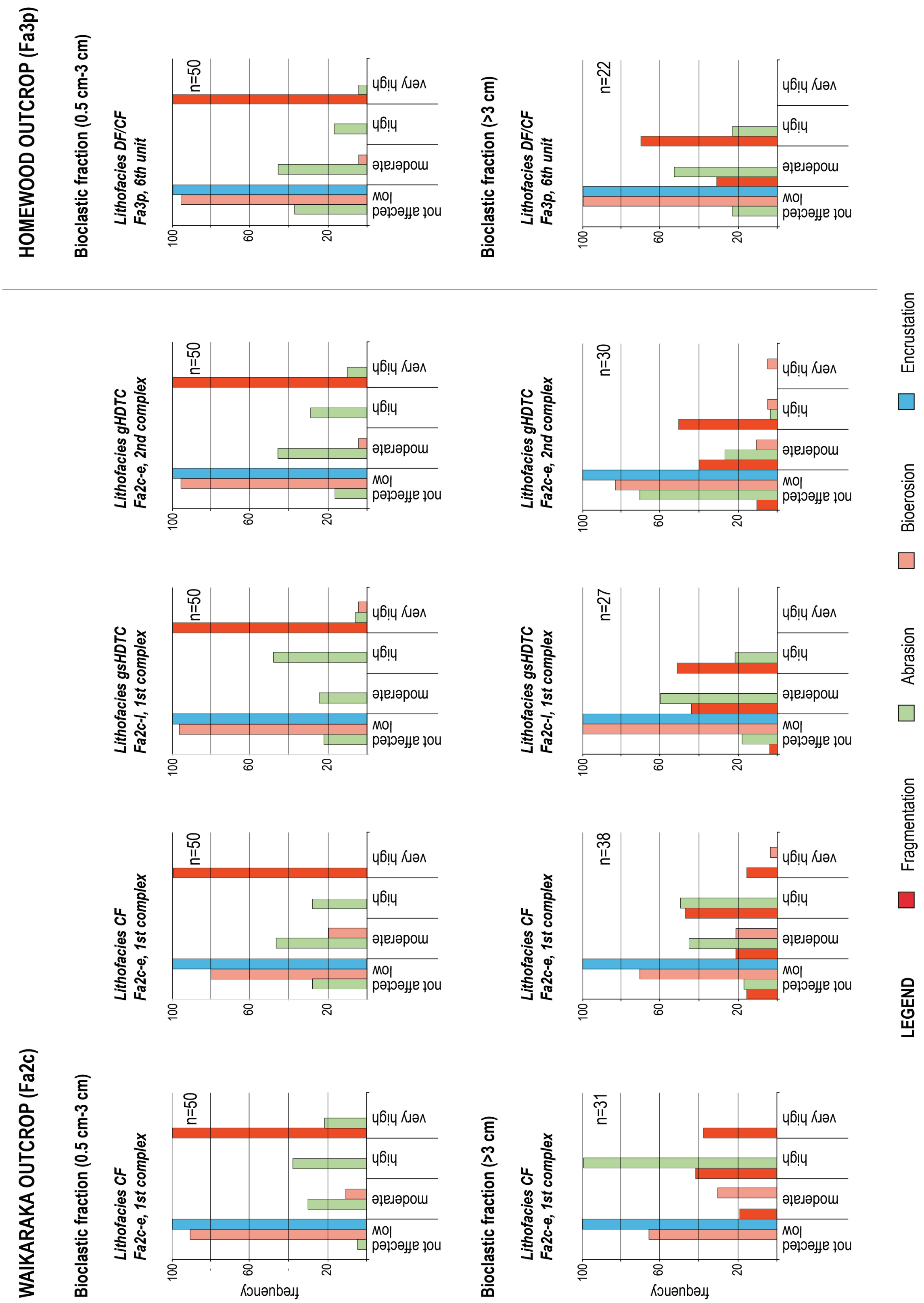

Figure 14: Taphonomic characterization of fossil remains described from one square meter area of outcrop at Waikaraka and Homewood, using frequency histograms of the degree of alteration (*e.g.,* low, moderate, high, very high) for each category of skeleton damage (*i.e.,* fragmentation, abrasion, bioerosion) and encrustation. Lithofacies CF, DF, gHDTC and gsHDTC are described in details in Table 1 and facies associations Fa2c and Fa3p in Section 5.

Conversely, the profuse shell fragments found in the overlying, well-developed, north-eastward prograding turbidite system (**Fa1g**) indicate a change of source region, likely belonging to the main westward continent-attached shelf domain.

The regular detrital sand and pebble supply (see Sections 5 and 6.3) likely restricted the development of carbonate factories dominated by suspension-feeding organisms (Caron et al. 2004), thereby promoting molluscan communities (Bimol assemblage of Hayton et al. (1995)) often associated with relatively turbid waters due to fine material in suspension. The occurrence in the deposits of occasional coralline red algal branches and small-sized-rhodoliths indicate sources within the photic zone (Pomar 2001; Nebelsick et al. 2005).

Differences in the degrees of taphonomic alteration observed in skeletal remains relate to their residence time in the taphonomic active zone (TAZ; (Davies et al. 1989)). Typically, taphonomic alteration consistently increases with increasing residence time in the TAZ where skeletons are affected by destructive processes, such as disarticulation, fragmentation, abrasion and bioerosion. For example, low net sedimentation rates and repeated exhumation of buried skeletal remains by waves and currents, and by seafloor burrowers favor mechanical destruction and bioinfestation. By contrast, rapid and definite burial prevents such alterations (*e.g.,* Best and Kidwell 2000; Best et al. 2007). Fragmentation of skeletal remains over three centimeters in size is moderate to high, both at Waikaraka and Homewood in debris flows and turbidite flows (Figure 14). Although it cannot be ruled out that skeletons were partly fragmented in their source area through hydraulic and biological processes (Zuschin et al. 2003), it should be expected that fragmentation also occurred, as a result of mechanical crushing, once they were integrated in their host clast-supported gravity-driven flows. Abrasion of the coarser skeletal fraction, translating in the loss of ornamentation and rounding of bioclast edges, is: (1) higher in debris flows than in turbidite flows, and (2) overall higher than fragmentation in debris flows compared to turbidite flows. Abrasion is caused by physical erosion, through friction and at a lesser degree through waterborne collision, and reworking leading to mobilization and redeposition of bioclasts. Moderate to high degrees of abrasion, along with the abundance of small-sized skeletal debris, are indicative of frequently destabilized substrates by wave action, storms and, potentially here, gravity-driven flows (*e.g.,* Kowalewski 1996). Further, such unstable substrates may have inhibited colonization of dead shells by encrusters, and their infestation by borers, thereby explaining the low degrees of taphonomic alteration for these processes

(Figure 14). However, possible causes for the observed differences in biogenic alteration (slightly higher in Waikaraka debris flow deposits for example) are multifarious, including high-sedimentation rates leading to rapid burial, unsuitable shell substrates and/or ecological conditions for infester communities (Caron et al. 2019).

Results of the taphonomic evaluation suggest that the alteration state of skeletal remains in the studied deposits not only reflects depositional and ecological conditions at the site of carbonate production on the shelf, but has also potential to record conditions of transport during their remobilization in gravity-driven systems. In particular, the taphonomy of skeletal contents, as a complementary tool to other analytical approaches, may provide clues on the laminar (*i.e.,* debris flows) versus turbulent (*i.e.,* turbidites) character of flow, and whether deposition by traction sedimentation prevailed over suspension sedimentation (Lowe 1982).

6.3. Distinct substratum and continental connection

Lithoclast observations

At Homewood, the extra- and intraformational lithoclasts tend to oscillate between sub-angular to sub-rounded shapes and are in average of granule- to pebble-grades in the confined channel fills (**Fa2c**) and granule- to cobble-grades in the mass-wasting system (**Fa3p**). Conversely, at Waikaraka, sub-rounded clasts dominate and sub-angular shapes only preferentially occur in the early-stages confined channel fills (**Fa2c-e**). At Waikaraka, the clast grades also largely depend on the style of channel fills, and are preferentially of pebble- to outsized-grades in the early-stages fills (**Fa2c-e**) and of pebble-grades in the late-stage fills (**Fa2c-l**) (see Section 5).

Pre-subduction extraformational clasts largely dominate representing 95 to 99% of the overall lithoclast content at Homewood and 84% to 97% at Waikaraka (Figure 13). They mostly rework (>80%) Upper Cretaceous strata (*e.g.,* mainly siliceous and calcareous mudstones, rare lavas) and frequently include (~4 to 10%) Paleocene clasts (*e.g.,* limestones). Conversely, Lower Cretaceous clasts (*e.g.,* Torlesse greywackes) are only observed, sporadically (~2%), at Waikaraka, whereas Eocene clasts (*e.g.,* smectitic mudstones) are virtually absent and only rarely found (~1%) at Homewood (Figure 13).

At Waikaraka, the early-stage fills of the first channel complex (**Fa2c-e**) deviate from this model, remobilizing sub-angular to sub-rounded, pebbles to outsized clasts (deci- to decametric) from the entire Lower Cretaceous to Paleocene pre-subduction series at their base. Interestingly, sub-rounded to rounded, granule- to pebble-grade Lower Cretaceous clasts are also occasionally observed throughout

Accepted Manuscript version. Published Journal Article version available online, published by Elsevier in Marine and Petroleum Geology Journal: https://doi.org/10.1016/j.marpetgeo.2021.105252

the confined slope channel system (**Fa2c**) (Figure 13). They are preferentially restricted to particular conglomerate intervals (**CF**, **gHDTC**) of the confined channel fills, generally located at the top of the early-stage fills (**Fa2c-e**).

The syn-subduction extraformational lithoclasts most commonly include pebble- to boulder-grade clasts of lithified shell beds. They are frequent in the confined slope channel system of Waikaraka. There, eight distinct varieties of shell bed clasts are observed (Appendix 5), which are often of cobble- to boulder-grades in the early-stage fills (**Fa2c-e**). Thick-shelled Molluscan remains are frequent in the shell bed clasts (Appendix 5, A-F, H), along with well-rounded lithic pebbles commonly bearing the trace fossil Gastrochaenolites (Appendix 5, B-D). The overall faunal assemblages, including *Struthiolaria* sp., *Polinices* sp., Oysters, Turritellids, Serpulids and zooxanthellate corals (Appendix 5), and moderate degrees of pre-burial taphonomic alteration collectively point to rapid deposition in high-energy proximal inner-shelf to middle-shelf environments. Conversely, shell bed clasts are only punctually found (<0.5%) in the confined slope channel (**Fa2c**) and mass-wasting system (**Fa3p**) of Homewood. They however only comprise pebble- to cobble-grade skeletal and bioclastic fine-grained sandstones dominated by turritellid gastropods (cf. facies Fa6c from Bailleul et al. (2007)).

The remaining syn-subduction extraformational lithoclasts comprise pebble-grade wood fragments and disseminated plant debris. A few cobble- to boulder-grade clasts of fossil tubular concretions (Malie et al. 2017) were also observed in the early-stage fills (**Fa2c-e**) at Waikaraka.

Finally, the syn-subduction intraformational lithoclasts are characterized by outsized, contorted sandstones and pebble- to boulder-grade mudstone clasts. The outsized, contorted sandstones are generally restricted to **DF**, particularly at Homewood; whereas the mudstone clasts, although present in some of the conglomerates, are dominantly found in the coarse-grained basal intervals of the sandstones at both Waikaraka and Homewood.

Lithoclast interpretations

As previously observed elsewhere in the Coastal Ranges (Neef 1992; Bailleul et al. 2013; Claussmann et al. 2021), the nature of the extraformational lithoclasts informs that the mixed siliciclastic-carbonate shelfal domain sourcing the Waikaraka deposits developed above a pre- (*e.g.,* Cretaceous to Paleogene series) and syn-subduction (*e.g.,* Miocene sediments) substratum, whereas the paucity of extraformational syn-subduction clasts (*e.g.,* a couple of shell bed clasts) at Homewood suggests a pre-subduction-dominated substratum.

At Waikaraka, the variety encountered in both the proportion and nature of pre-subduction material informs that the basal deposits of the confined slope channel system (**Fa2c**) remobilized the entire pre-subduction series down to the Lower Cretaceous, whereas the remainder mostly captured remobilized Upper Cretaceous strata (Figure 13). The absence of Lower Cretaceous greywackes and predominance of Upper Cretaceous strata at Homewood both suggest a slightly different substratum and or exhumed paleobathymetric high sourcing the deposits. The implications for both these localities are discussed in Section 7.

At Waikaraka, the syn-subduction material, mostly comprising shell bed clasts, likely results from destabilization of previously deposited and lithified strata (*i.e.,* substratum) rather than contemporaneous sediments. Their diversity captures different mixed siliciclastic-carbonate shelfal environments, which either (1) belonged to the same shelfal system, thus suggesting different phases of shelf development or local variations in depositional settings (Bailleul et al. 2015), and or (2) resulted from distinct shelfal systems that formed in the area since the onset of subduction (Bailleul et al. 2007; Bailleul et al. 2013; Caron et al. 2021). Conversely, at Homewood, the occasional sandy shell beds could be contemporaneous with the development of the shelfal environment. Early lithification of the deposits at or near the seafloor may have been triggered by increased saturation of seawaters with respect to $CaCO_3$, following partial dissolution of aragonitic turritellid shells, though such process has been documented to predominantly result from burial diagenesis (*i.e.,* mesodiagenesis) (Nicolaides 1995; Haywick 2004; Caron and Nelson 2009).

The abundant pebble-grade to outsized sub-angular clasts found in the confined slope channel (**Fa2c**) and mass-wasting system (**Fa3p**) of Homewood, and more sporadically in the early-stage confined channel fills (**Fa2c-e**) of Waikaraka, both indicate that despite clast interactions, not only the sediment sources were nearby but also that the material was “freshly” eroded to allow preservation of such features (Postma et al. 1988).

Notwithstanding partial remobilization of the shelf and slope substratum through submarine destabilization (*e.g.,* mass-wasting failure) and or erosional processes (*e.g.,* channel cutting through the slope substratum) to provide for most of the lithoclast content (*e.g.,* Sømme et al. 2009; Janocko et al. 2013; Paumard et al. 2020), dismantlement and erosion of exhumed paleobathymetric highs probably contributed as well (*e.g.,* Ogata et al. 2019). In fact, the presence of wood fragments and plant debris in both settings informs that the source areas were connected to a terrestrial ecosystem (Kuenen 1964), which indicate the nearby presence and connection with exhumed land. Also, the occurrence of sub-rounded lithoclasts can suggest a fluvial and or shallow-marine origin with extraformational clasts that

Accepted Manuscript version. Published Journal Article version available online, published by Elsevier in Marine and Petroleum Geology Journal: https://doi.org/10.1016/j.marpetgeo.2021.105252

resided for at least some time in a littoral zone, before being transferred to bathyal depths (Di Celma et al. 2010). Where grain collision is inferred as a dominant grain-support mechanism (*e.g.,* in most of the **Fa2c** and **Fa3p** deposits), it can also be expected to have favored the quick abrasion and rounding of the harder, coarse-grained clasts.

The large volume of wood fragments and plant debris recorded throughout the confined slope channel deposits of Waikaraka (**Fa2c**) and the well-developed turbidite system of Homewood (**Fa1g**) both support source connections to mature hinterlands (*e.g.,* Stanley 1986; McArthur et al. 2016b). The discrete occurrences observed in the mass-wasting system of Homewood (**Fa3p**) rather points toward a small and or isolated source system, such as an island developed above tectonically-controlled topography (McArthur et al. 2016a), hence reinforcing the hypothesis of a source system detached from the main shelf domain.

Finally, the nature of intraformational clasts, such as mud clasts, informs that these gravity flows were erosive and ploughed through mud-prone substrates as they moved downslope or at hydraulic jumps (Posamentier and Martinsen 2011). At Homewood, the contorted sandstones also indicate of the varying nature of the ploughed substrate, locally supported by the underlying sandier deposits (**Fa2c**).

7. DISCUSSION

7.1. Gravity-driven systems from forelimb, continent-attached shelfal source

The depositional system proposed for Waikaraka is one of a confined slope channel system (CSCS) (*sensu* Campion et al. 2000) distributing land-derived, shallow- and deep-marine bedrock-derived sediments to the trench-slope basin.

As interpreted (see Sections 5 and 6), this system was likely sourced from the regional, narrow and continent-attached mixed siliciclastic-carbonate shelfal domain, which was contemporaneously developing to the west during the Middle Miocene, atop seaward-verging thrust-cored anticlines (Figure 15A; Figure 16) (Crundwell 1987; Chanier 1991; Bailleul et al. 2007; Bailleul et al. 2013; Bailleul et al. 2015; Claussmann et al. 2021).

Precise geometry of the slope upon which the CSCS developed is here a matter of speculation; yet, the forelimb settings rather suggest a steep, probably irregular, tectonically-controlled gradient close to the shelf edge and across the slope (Figure 15A; Figure 16) (*e.g.,* Naranjo-Vesga et al. 2020). The large volume of terrigenous material as well as the nature of the reworked clasts (*e.g.,* well-preserved bioclasts, shell fragments, pre-subduction strata) recorded throughout the CSCS deposits (**Fa2c**) both indicate persistent connection with a shelfal domain, recurrently supplied by the mature, vegetated hinterland to the west, exhumed since the onset of the Hikurangi subduction and mostly exposing Cretaceous strata (Figure 16) (Chanier and Ferrière 1991).

Along active margins, CSCS commonly represents long-lived transport routes for sediments across the shelf and slope that are typically insusceptible to sea-level changes and directly connect the hinterland (Type I, shelf-incising and river-associated system of Harris and Whiteway (2011)) and or shoreface depositional systems (Type II, shelf-incising system of Harris and Whiteway (2011)) to the deep sea (Sømme et al. 2009). Here however, although regional tectonics (*i.e.,* margin uplift) largely governed the initial emplacement of this mixed siliciclastic-carbonate shelfal domain installed atop thrust-cored anticlines (Bailleul et al. 2013), eustatic processes appear to then chiefly control their development and stratigraphic architecture (Bailleul et al. 2015). Notwithstanding the reworking of Upper Cretaceous conglomerates characteristically rich in already-reworked Lower Cretaceous Torlesse greywackes (Chanier and Ferrière 1991) as a potential source for providing gravels readily available to be transferred across the narrow shelf, the punctual input of well-rounded pebbles of Torlesse greywackes observed at the top of the early-stages fills of the CSCS (see Section 6) could also be attributed to an intermittent connection of the shelf with river(s). The successive T-R sequences that characterize these shelfal environments (Bailleul et al. 2015) could explain such periodic communication with the exhumed Cretaceous hinterland and would in turn suggest some eustatic control here, eventually captured in the CSCS infill.

The broad fining- and thinning-upwards trends observed in the CSCS (**Fa2c**) are common in many other slope channel systems, indicating channel bypass and backfilling processes (*e.g.,* Mutti 1985; Deptuck et al. 2003; Beaubouef 2004; Sylvester et al. 2011; Kneller et al. 2020). The repeating series of architecture and facies associations inform that this CSCS system likely behaved in a cyclic manner through time that may well have been in phase with the sea-level changes, yet likely also resulted from external forcing factors, such as pulses of thrust fault activity (*e.g.,* uplift and or related seismicity) at the edge of the shelf, known to periodically renew erosion and active sediment transport into CSCS along active margins (*e.g.,* Mountjoy et al. 2009; Mountjoy et al. 2018; Watson et al. 2020).

Interestingly, the reworked material contradicts the traditional unroofing model, incorporating clasts from the entire Lower Cretaceous to Paleogene pre-subduction strata only within its lowermost record and being otherwise dominated by Upper Cretaceous strata (see Section 6.3). Although direct erosion of the exhumed Cretaceous basement likely acted as an additional source, we attribute the former clast content to chiefly result from CSCS forming processes, such as initial slope failure (*e.g.,* Janocko et al. 2013) and or slope erosion (*e.g.,* Sømme et al. 2009). These processes exposed the underlying submarine bedrock of the thrust-cored anticline (*i.e.,* forelimb setting) upon which the shelfal domain developed, making it ready to be included into the subsequent gravity flows (Figure 15A; Figure 16) (*e.g.,* Ogata et al. 2019). For the latter contrasting clast content, we here infer the autogenic evolution of this shelf-incising CSCS (Type I, shelf-incising and river-associated system of Harris and Whiteway (2011)) during late low-stand conditions, whereby retrogressive erosion at the head of the system (*sensu* Daly 1936) would have favored the failure, storage and reworking of the marginal siliciclastic-carbonate sediments, contemporaneously (*e.g.,* living or freshly deceased macrofauna, terrigenous debris) and previously deposited (*e.g.,* shell bed lithoclasts), along with their underlying substratum, here dominated by Upper Cretaceous strata (Figure 15B; Figure 16). The upward increase of bioclastic material recorded in the channel fill may also partially illustrate such progressive upslope variation in source region, whereas the dominance of skeletal grains (over non-skeletal, *e.g.,* ooids, pellets) typically occur during such sea-level low-stands (Reijmer et al. 2015).

Here, regional tectonics appear to have chiefly governed both the birth (emplacement) and death (drowning) of (1) the continent-attached mixed siliciclastic-carbonate shelfal domain installed atop thrust-cored anticlines (Bailleul et al. 2013; Bailleul et al. 2015) and of (2) its related shelf-derived, deep-marine systems. Whilst the shelfal domain development then became largely eustatically-controlled (Bailleul et al. 2015), the combination of steep slope gradient, high sediment supply and narrow shelf width resulted in the development of a CSCS (**Fa2c**) that efficiently transferred the shelf-derived sediments to the deep-marine environments (*e.g.,* Naranjo-Vesga et al. 2020). Although punctually capturing the sea-level changes, the overall evolution and geometry infill of the CSCS seemed essentially controlled by local tectonic activity at the mixed siliciclastic-carbonate shelf edge, which, in turn, determined its stratigraphic infill (sediment distribution and architecture) (Figure 15; Figure 16).

The abrupt changes in sedimentation styles (*i.e.,* sand-dominated) and paleodepth of deposition (*i.e.,* lower bathyal) recorded in the uppermost CSCS deposits (see Section 5; Appendix 2) could be attributed to the major change in tectonic regime (*i.e.,* generalized subsidence) that was recorded along the Hikurangi margin at the time, which in turn resulted in rapid bathymetric deepening of the area (*i.e.,* high-stand conditions) (Chanier et al. 1999; *D5* discontinuity and *U5* unit of Bailleul et al. 2013) (Figure 10a, e). Direct coarse-grained sediment supply stopped; yet, some high-stand activity was maintained along the CSCS (*e.g.,* Mountjoy et al. 2009).

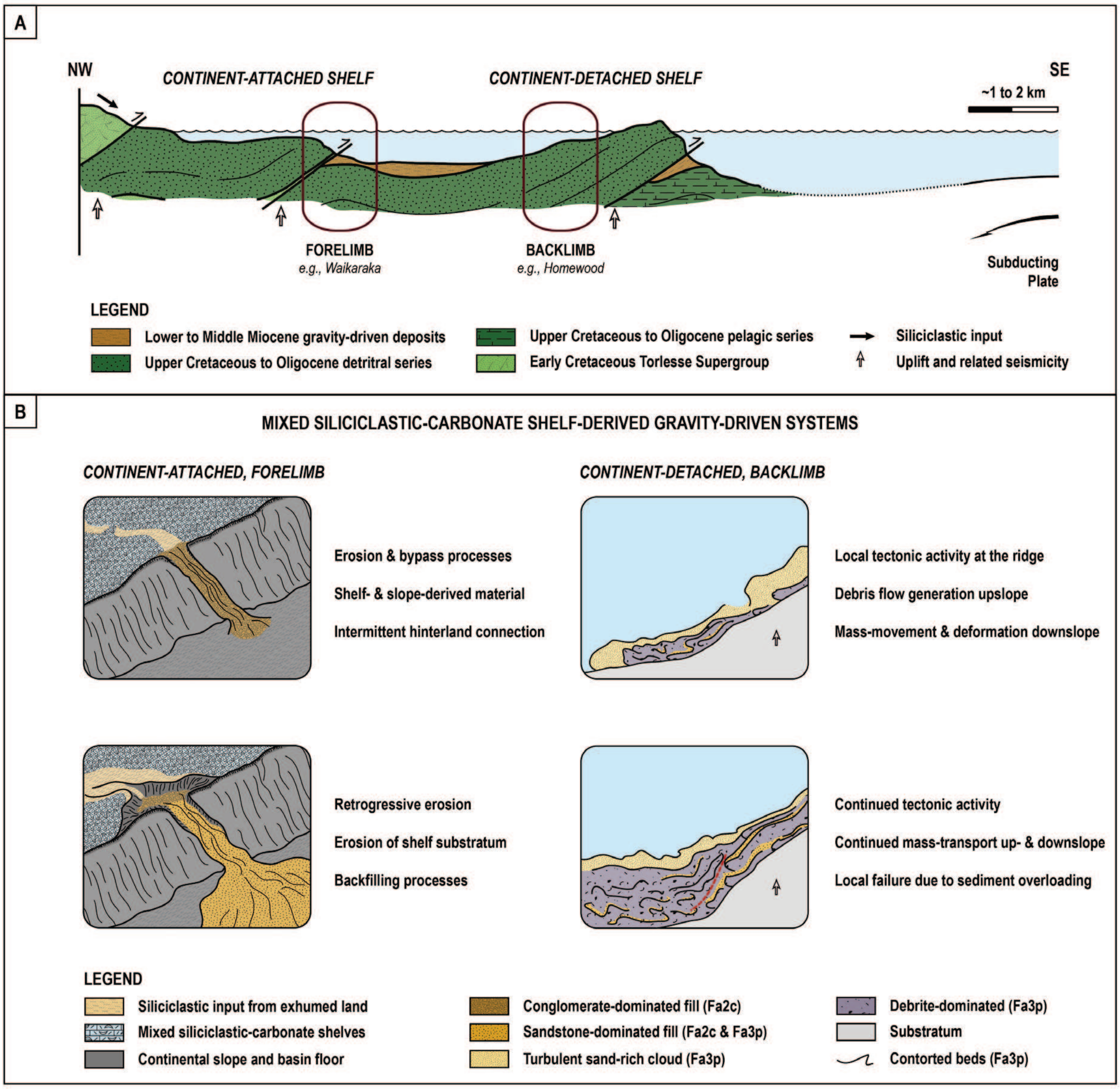

Figure 15: (A): Schematic NW-SE cross-section through the subduction-related, compressive Whareama intra-slope basin (*i.e.,* trench-slope basin) during the Middle Miocene. The depositional settings for the forelimb and backlimb settings of actively growing thrust-cored structures are highlighted. (B): Schematic representation of the inferred shelf-derived gravity-driven systems and processes related to the forelimb and backlimb settings.

7.2. Gravity-driven systems from backlimb, continent-detached shelfal source

The source and depositional system envisaged at Homewood contrast with the coeval continent-attached shelfal environment and slope channel delivery system of Waikaraka. As previously described (see Sections 5 and 6), the nature of the deposits (**Fa2c** and **Fa3p**) indicates a shelfal environment that developed upon and around a structurally-controlled ridge located to the east of Homewood, which was detached from the regional shelf and hinterland (Figure 15A).

Isolated platforms may develop above fault-growing folds and favor biogenic carbonate production as they lack continent-derived siliciclastic inputs (Caron et al. 2004; Ćosović et al. 2018; Caron et al. 2021). At Homewood however, analyses of the reworked material (see Section 6) inform that mixed siliciclastic-carbonate sediments dominated, thereby suggesting both emergence and subsequent erosion of the uplifted ridge (Figure 15A; Figure 16). Previous work highlighted that islands developed above tectonically-controlled topography can supply terrigenous material (*e.g.,* McArthur et al. 2016a) and result in mixed siliciclastic-carbonate sedimentation (*e.g.,* Chiarella et al. 2012; Chiarella and Longhitano 2012; Ćosović et al. 2018).

More particularly, the nature of the deposits (*i.e.,* **Fa2c** and **Fa3p** slope deposits) and their clasts (see Part 5) suggests that the ridge was nearby and exhumed for some time to allow (1) the dismantlement of the pre-subduction series down to the Upper Cretaceous strata, (2) their subsequent reworking in the littoral domain and (3) the formation of sandy shell beds. Notwithstanding submarine erosion, the abundance of sub-rounded clasts of Upper Cretaceous strata implies that these strata likely outcropped at the time (*e.g.,* Di Celma et al. 2010), thereby inferring initial rise and emergence of the ridge prior to the Middle Miocene, Upper Clifdenian to Lower Lillburnian (Langhian, 15.9 – 14 Ma, Appendix 2).

When combined, the pre-subduction Paleogene cover, about 600 meters thick in the study area (Van den Heuvel 1960; Chanier 1991; Chanier and Ferrière 1991), and the general exhumation rate of up to 0.3 kilometer/million year calculated by Jiao et al. (2014) along the eastern North Island of New Zealand indicate that the ridge emergence (*i.e.,* island setting) and subsequent erosion started at least ca. 2 Ma prior to that time. This ridge likely corresponded to the seaward margin of the Whareama Basin, structurally controlled by the underlying seaward-verging Flat Point-Whakataki Fault complex and located to the east of Homewood (*i.e.,* Glenburn Nappe) (*e.g.,* Chanier 1991) (Figure 3; Figure 15A). The set of morphometric relationship equations calculated by Moscardelli and Wood (2015) predicts a length of about two kilometers for the MTDs (Appendix 6), which may or may not include the evacuation area (*sensu* Moscardelli and Wood 2015) yet provides a broad insight as to the potential distance to the ridge at the time (less than two kilometers).

The envisaged shelfal system was narrow and located on the western side of the island, upon the backlimb of the underlying asymmetrical thrust (Figure 15A; Figure 16). Similarly, the mixed siliciclastic-carbonate Fingerpost shelf developed further north during the Early to Middle Miocene; it was also positioned to the west of an emergent landmass (*i.e.,* the Cape Turnagain Structural High), itself

Accepted Manuscript version. Published Journal Article version available online, published by Elsevier in Marine and Petroleum Geology Journal: https://doi.org/10.1016/j.marpetgeo.2021.105252

controlled by an underlying seaward-verging thrust (*i.e.,* backlimb setting) (Bailleul et al. 2013, their figure 12).

At Homewood, the shelf was likely cut by a network of small slope channels connecting the island through the shelf to the Whareama Basin (**Fa2c**) (Figure 16). The transition from slope channel (**Fa2c**) to shelf-derived mass-wasting (**Fa3p**) systems is attributed to a period of tectonic activity (*e.g.,* uplift) at the basin-bounding structure, resulting in growth strata deposition on the eastward-margin of the basin (see Section 5.3) (*e.g.,* Moore and Karig 1976; Stevens and Moore 1985) and typically lasting 1 to 2 Ma in these settings (Nicol et al. 2002; Bailleul et al. 2013).

Structure growth both (1) promoted the repeated destabilization of the isolated shelf and generation of the **Fa3p** mass-wasting flows as well as (2) controlled the axial routing and syn-kinematic development of the overlying **Fa1g** turbidite lobe system sourced from the mature hinterland to the west (Figure 16). The associated MTDs (**Fa3p**), only ~15 meters thick, recorded a difference of ~40° in bed dips (*i.e.,* growth strata), thereby indicating complex interplay between the growing structure and sediment deposition. The slope gradient acted as a dynamic control triggering (1) mass-wasting processes upslope, as well as, down the slope, (2a) rapid flow transformation and efficient dilution (*e.g.,* Fisher 1983; Strachan 2008) resulting into fast-moving multiphase debris flows (*e.g.,* Postma 1986; Mohrig et al. 1998; Sohn et al. 2002) and (2b) coeval remobilization (soft-sediment translation and deformation) of the previously deposited, unlithified mass-flow deposits (*e.g.,* Maltman 1994) (Figure 15B; Figure 16).

The MTDs' succession and the variations in slope gradient recorded throughout can therefore be used as a proxy for the tectonic activity of an individual structure. Here, they inform that at least six main tectonic pulses with uplift affected the structurally-controlled shelf-margin(s), each respectively generating one to several coalescing debris flows. Towards the top of the MTDs' succession, the high amount of sheared debris flow deposits, contorted strata, and the increasing bed dip variations (Figure 9) suggest both steep slope gradients (*e.g.,* Postma 1986) and an acceleration of the ridge activity. Steep, rising slopes, recurrently loaded with sediments, are unstable (Hein and Gorsline 1981) and thus likely provided the right settings for locally triggering the failure of the entire MTDs' series as previously observed at Homewood (Figure 9; Figure 15).

7.3. Generic implications

7.3.1. For shelf-derived gravity-driven systems sourced from thrust forelimb and backlimb

In this study, the high variability encountered within one intra-slope basin in terms of sediment delivery systems as well as transport and depositional processes highlights the role and importance of varying structural settings of the sediment source for controlling the subsequent deep-marine depositional settings. Despite similar source environments (*i.e.,* mixed siliciclastic-carbonate shelves) developed atop the basin-bounding structures (*i.e.,* thrust) along with comparable sediment delivery systems (*i.e.,* slope channel and remobilization) and nature of flow processes (*i.e.,* gravity-driven), the resulting shelf-derived deposits downslope are characterized by contrasting lithofacies assemblages, sizes and geometries.

Notwithstanding the size and extent of the catchment area or continental connection (attached or detached) as critical controls (Sømme et al. 2009), we here suggest that along active margins, the geometry and activity of the underlying structures (thrust forelimb and backlimb settings) at the shelf edges also greatly influence the resulting sediment distribution and architecture.

The shelf-edges on the forelimbs of underlying thrusts are abrupt, generally associated with steep, irregular and tectonically-controlled slope profiles (Naranjo-Vesga et al. 2020). Erosion and transport capacities proportionally increase with slope gradient and thus favor significant sediment bypass to the deeper settings (Sømme et al. 2009; Crisóstomo-Figueroa et al. 2020). Here, the tectonic activity at the shelf edges generally favored the development of systems that dynamically interact and rejuvenate the slopes (*e.g.,* Waikaraka retrogressive system or Sefton Hills repeated collapse events (Claussmann et al. 2021)) and the resulting gravity-driven systems are generally hundreds of meters thick and several kilometers wide, preferentially transporting sediments through sediment gravity flows.

Conversely, thrust backlimb commonly provide longer and gentler slope gradients upon which a more gradual shelf edge transition may be expected and may facilitate the development of less efficient depositional systems (Sømme et al. 2009). In this study however, these settings were connected to limited catchment areas (*e.g.,* isolated island), thereby preventing the development of particularly large systems that typically occur on gentler slopes. Therefore, despite similar delivery systems to those associated to forelimb-related slopes (*e.g.,* slope channels and destabilization), their sizes were largely smaller (tens of meters thick).

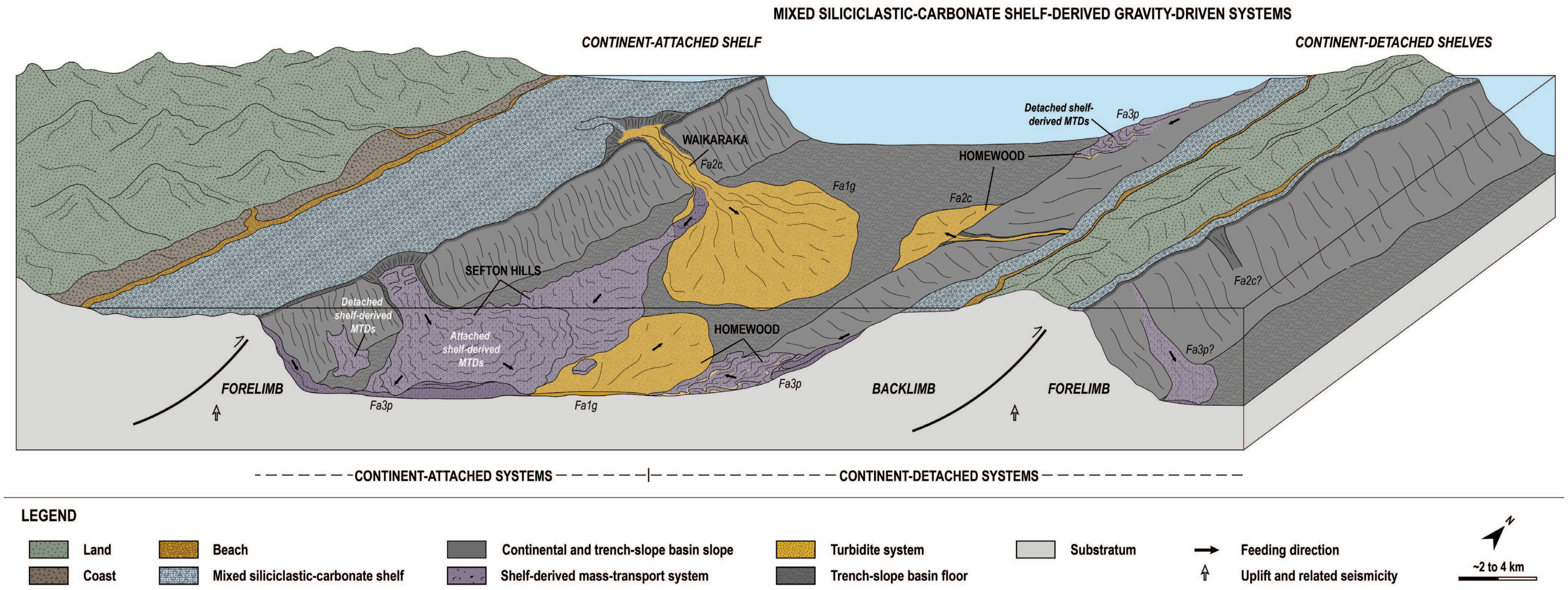

Figure 16: Contrasting depositional systems for mixed siliciclastic-carbonate shelf-derived gravity-driven flows along tectonically active margins, using the southern portion of the Hikurangi subduction margin as an example (Whareama trench-slope basin). Fa1g – refers to depositional lobe system; Fa2c – to confined slope channel system; Fa3p – to shelf-derived mass-wasting systems. Depositional settings from the Sefton Hills localities were adapted from Claussmann et al. (2021).

Destabilization and collapses of the mixed siliciclastic-carbonate shelfal sources occurred on both sides of the basin-bounding structures and thus indicate that any of these shelves, either attached to the main continental domain or detached from it (*e.g.,* isolated island) can be subjected to shelf-derived sediment mass movement and mobilization (*sensu* Iverson 1997).

When sourced from the backlimb of an actively growing structure (*i.e.,* thrust) however, the mass-wasting deposits exhibit more complex internal architectures, clearly recording the slope gradient variations and resulting in intricate interactions between mass movements and mass flows, such as the ones observed at Homewood. The changes in slope gradient will dynamically control both (1) the generation of mass movements and flows upslope, and (2) the coeval remobilization (*e.g.,* sliding) and soft-deformation (*e.g.,* slumping) of the previously deposited, poorly-lithified sediments (*e.g.,* debrites) downslope. Conversely, although mass movement (*e.g.,* slide, slump) can undoubtedly occur as well, the MTDs sourced from the forelimb of an actively growing structure (*i.e.,* thrust) seem primarily characterized by a series of coalescing mass-flow deposits (*e.g.,* debris flows) (*e.g.,* Festa et al. 2010 and references therein). Mass movements either seem preferentially recorded close to the source region or at the base of the MTDs' sequence, where they often result from soft-sediment deformations (*e.g.,* slide, slump) of the unlithified sediments that were previously deposited at the front of the rising structure (*e.g.,* Festa et al. 2010; Lackey et al. 2020).

Overall, the shelf morphology (*i.e.,* narrow), extent (*e.g.,* regional or isolated), continental connection (*e.g.,* attached or detached), sediment type (*i.e.,* mixed siliciclastic-carbonate sedimentation) as well as the respective geotectonic settings (*e.g.,* upon and around the forelimb or backlimb of the underlying thrusts and fault-growing folds) all chiefly controlled the architecture and subsequent shelf-derived deposits. However, along tectonically-active margins, when sourced from mixed siliciclastic-carbonate systems, the deep-marine, shelf-derived deposits seem characterized by tens to a few hundred of meters of thickness and several kilometers of lateral extent. The durations of the associated depositional systems are from 1 to 2 Ma, being controlled by the structural styles and local tectonic activity at the source rather than regional-scale variations.

7.3.2. For mass-transport deposit nomenclature

Moscardelli and Wood (2015) have proposed differentiating mass-wasting products into *attached* and *detached* systems, respectively sitting in a proximal and a distal position from any shelf break, and either sourced from this regional area (*e.g.,* shelf) or local structures. *Attached* MTDs commonly represent the largest occurrences, being regionally extensive, and are essentially triggered by sea-level variations and or high sedimentation rates (Moscardelli and Wood 2008; Posamentier and Martinsen 2011; Moscardelli and Wood 2015). As discussed here however, along active margins, shelfal environments not only develop in the submerged prolongation of the main hinterland, constituting continent-attached shelves, which can source large-scale shelf-derived mass-wasting products (*e.g.,* Claussmann et al. 2021). Shelfal environments can also form episodically upon and around structurally controlled and active ridges, resulting in shelves that are detached from the main shelf domain (*e.g.,* Ćosović et al. 2018). These isolated settings, with a virtually absent to limited catchment area (whether underwater or emerged), feature reduced shelfal source systems, which will, in turn, produce significantly smaller shelf-derived mass-wasting products such as the ones described at Homewood. The size of the resulting deposits best compares to those commonly found in *detached* MTDs (*sensu* Moscardelli and Wood 2015) (Appendix 6) whereas their internal characteristics inform that tectonic acted as the main triggering mechanism and that the source was nearby.

Notwithstanding sea-level changes and high sedimentation rates as causal mechanisms for shelf-derived mass-wasting events (Posamentier and Walker 2006; Moscardelli and Wood 2008; Moscardelli and Wood 2015; and references within), Bailleul et al. (2013) and Claussmann et al. (2021) previously demonstrated that along active margins, periods of tectonic activity (ca. 1 to 2 Ma) constitute another mechanism to consider for both the development and subsequent shelf failures. The MTDs described in this study not only provide another example of such shelf-derived mass-wasting products, whereby tectonic activity controlled the repeated destabilization and collapses of the shelfal source (see also Romero-Otero et al. 2010; Ortiz-Karpf et al. 2018), but also indicate that shelf-derived mass-wasting events do not always result in large-scale systems (Appendix 6) (see also Claussmann et al. 2021). Similarly, Naranjo-Vesga et al. (2020) observed that owing to the complex relationships that exist between the shelf width, slope profile and sediment supply in an analogous convergent setting (*i.e.,* southern Caribbean fold-and-thrust belt), both *attached* and *detached* MTDs could be sourced from the regional shelf and slope regions.

Therefore, we here propose to slightly amend the MTD nomenclature from Moscardelli and Wood (2008) and Moscardelli and Wood (2015) by using the related '*attached*' and '*detached*' morphometry characteristics independently from the type (*e.g.,* shelf, slope, local bathymetric highs) and distance from source areas to better account for the variety of geotectonic settings (*e.g.,* convergent).

As a result, we introduce the term '*shelf-derived* systems' which refers to all the MTDs that result from the destabilization and collapses of shelfal environments, whether induced by regional and or local causal mechanisms (sea-level changes, high sedimentation rates, periods of repeated tectonic activity, etc.),

Accepted Manuscript version. Published Journal Article version available online, published by Elsevier in Marine and Petroleum Geology Journal: https://doi.org/10.1016/j.marpetgeo.2021.105252

and which can either source large-scale *'attached shelf-derived systems'* or smaller *'detached shelf-derived systems'* (*sensu* Moscardelli and Wood 2008; Moscardelli and Wood 2015) (Figure 16). Similar reasoning can be applied to the MTDs that result from failures of the regional slope (*i.e.,* '*slope-derived* systems').

Notwithstanding the slope profile, here inherently linked to the geometry of the underlying structural styles at the source (*e.g.,* forelimb or backlimb) and the sediment supply as other critical parameters (*e.g.,* Naranjo-Vesga et al. 2020), the present study demonstrates that the geomorphology of source area, and more particularly its connection to the continent (*i.e.,* catchment area) is also critical. Here, the narrow shelves appear to source both '*attached* and *detached shelf-derived systems'* when connected to the main hinterland (narrow continent-attached shelf) and '*detached shelf-derived systems'* when isolated and disconnected from it (narrow continent-detached shelf) (Figure 16). Further work is however required to generalize such an observation; and more particularly, the impact of the forelimb settings on the resulting *shelf-* and *slope-derived* mass-wasting systems (*e.g.,* size, internal characteristics, causal mechanisms) sourced from continent-detached mixed siliciclastic-carbonate shelfal domains remains to be investigated.

Accepted Manuscript version. Published Journal Article version available online, published by Elsevier in Marine and Petroleum Geology Journal: https://doi.org/10.1016/j.marpetgeo.2021.105252

8. CONCLUSIONS

In this study, we used high-resolution outcrop data to investigate the implications of mixed siliciclastic-carbonate source systems developed upon and around the forelimbs and backlimbs of actively growing asymmetrical structures for the development of the subsequent gravity-driven systems beyond the shelf edges. Particularly, this study highlights the role and importance of varying structural setting of the sediment source in controlling the morphologies of the delivery systems, the patterns of sediment dispersal, and the related sedimentary facies along active margins.

First, we demonstrated that during the Middle Miocene, the paleogeography of the southern, inner portion of the Hikurangi Margin was diversified, comprising a mature hinterland to the west as well as isolated islands to the east, developing atop the actively growing seaward-verging thrusts of the subduction wedge. Mixed compositional siliciclastic-carbonate sedimentation dominated at shallow depths and the different morphologies of the source regions (continent-attached, forelimb and continent-detached, backlimb) resulted in the development of highly varied shelf-derived gravity-driven systems downslope within very short distances (less than five kilometers) that interacted with the structures and were eventually captured both on their margins and within the trench-slope basins.

Then, we showed that mixed siliciclastic-carbonate gravity-driven systems in active settings appear preferentially characterized by deposition of tens to a few hundred of meters of thick units, displaying several kilometers of lateral extent, for duration of ca. 1 to 2 Ma. Such systems are primarily controlled by the geometries and tectonic motion of the underlying structures at the shelf edges. Different morphologies of the source regions (*i.e.,* the aforementioned continent-attached forelimb and continent-detached backlimb of thrust settings) result in the development of distinct paleoenvironmental conditions at the shelf and contrasting shelf-derived gravity-driven systems along and downslope. The shelf-edges on the forelimbs of actively growing thrusts are abrupt and commonly associated with irregular steep slopes. Here, they appear to have favored the development of systems that dynamically rejuvenate the slopes (*e.g.,* Waikaraka retrogressive systems). On the backlimbs however, the shelf-edges are generally associated to gentler slopes; yet, pulses in tectonic activity will increase slope gradient variations, thus promoting the development of sedimentary systems that directly interact with the slope (*e.g.,* Homewood mass-wasting system).

Finally, this study highlights that, whether they are caused by regional and or local triggering mechanisms, the destabilization and collapses of shelfal environments source 's*helf-derived* mass-wasting systems', characterized by two types: (1) large-scale, regional '*attached shelf-derived systems*' and (2) small-scale, localized '*detached shelf-derived systems'*. Along active margins, and particularly the Hikurangi Margin, the 's*helf-derived* mass-wasting systems' are sourced from shelves that are either attached to the main continental domain or detached from it (*e.g.,* isolated islands). The associated s*helf-derived* mass-wasting deposits can be found on both sides of actively growing asymmetrical thrusts. When sourced from the backlimbs however, the subsequent shelf-derived MTDs exhibit more complex internal architectures, ultimately recording the dynamic changes in slope gradient, which can both trigger the generation of mass failures and mass flows upslope as well as the coeval remobilization (translation and deformation) of the previously deposited MTDs downslope. As a result, the MTDs from thrust backlimbs can be used as proxies for unraveling the tectonic activity of an individual structure.

9. ACKNOWLEDGEMENTS

This research was funded by Schlumberger. We are grateful to Karen and John Barbour for their warm welcome during our stays at Homewood and for access to the studied areas. Special thanks to Pierre Malié and Andréa Barrier for their support during the fieldwork missions, as well as to Romain Armand, François-Xavier Joanny and Pierre Saulet from UniLaSalle (France) for their technical assistance on the GIS and outcrop modelling workflows. We also thank our colleagues from the Basins-Reservoirs-Resources B2R research unit (University of UniLaSalle, France) for their lasting support and Hugh Morgans and Henry Gard from GNS Science (Lower Hutt, New Zealand) for the paleontological analyses. Finally, we thank the Editor Roberto Tinterri and the reviewers, Bradford Prather and Domenico Chiarella for their helpful and constructive comments and suggestions.

Abreu V, Sullivan M, Pirmez C, Mohrig D. 2003. Lateral accretion packages (LAPs): an important reservoir element in deep water sinuous channels. Marine and Petroleum Geology. 20(6):631–648. https://doi.org/10.1016/j.marpetgeo.2003.08.003

Alsop GI, Weinberger R. 2020. Are slump folds reliable indicators of downslope flow in recent mass transport deposits? Journal of Structural Geology. 135:104037. https://doi.org/10.1016/j.jsg.2020.104037

Alsop GI, Weinberger R, Marco S, Levi T. 2019. Identifying soft-sediment deformation in rocks. Journal of Structural Geology. 125:248–255. https://doi.org/10.1016/j.jsg.2017.09.001

Armitage DA, Romans BW, Covault JA, Graham SA. 2009. The Influence of Mass-Transport-Deposit Surface Topography on the Evolution of Turbidite Architecture: The Sierra Contreras, Tres Pasos Formation (Cretaceous), Southern Chile. Journal of Sedimentary Research. 79(5):287–301. https://doi.org/10.2110/jsr.2009.035

Bailleul J, Caron V, Chanier F, Mahieux G, Malié P, Gagnaison C, Potel S, Ferrière J. 2015. Modalités de la sédimentation de plate-forme sur la pente d'un prisme d'accrétion: l'exemple du Miocène Moyen du prisme Hikurangi (Nouvelle-Zélande). In: Proceedings of the Congrès Français de Sédimentologie 15. Chambéry, France; p. 47.

Bailleul J, Chanier F, Ferrière J, Robin C, Nicol A, Mahieux G, Gorini C, Caron V. 2013. Neogene evolution of lower trench-slope basins and wedge development in the central Hikurangi subduction margin, New Zealand. Tectonophysics. 591:152–174. https://doi.org/10.1016/j.tecto.2013.01.003

Bailleul J, Robin C, Chanier F, Guillocheau F, Field B, Ferrière J. 2007. Turbidite Systems in the Inner Forearc Domain of the Hikurangi Convergent Margin (New Zealand): New Constraints on the Development of Trench-Slope Basins. Journal of Sedimentary Research. 77(4):263–283. https://doi.org/10.2110/jsr.2007.028

Ballance PF. 1976. Evolution of the Upper Cenozoic Magmatic Arc and plate boundary in northern New Zealand. Earth and Planetary Science Letters. 28(3):356–370. https://doi.org/10.1016/0012-821X(76)90197-7

Beaubouef RT. 2004. Deep-water leveed-channel complexes of the Cerro Toro Formation, Upper Cretaceous, southern Chile. AAPG Bulletin. 88(11):1471–1500. https://doi.org/10.1306/06210403130

Beavan J, Tregoning P, Bevis M, Kato T, Meertens C. 2002. Motion and rigidity of the Pacific Plate and implications for plate boundary deformation. Journal of Geophysical Research: Solid Earth. 107(B10):ETG 19-1-ETG 19-15. https://doi.org/10.1029/2001JB000282

Best MMR, Kidwell SM. 2000. Bivalve taphonomy in tropical mixed siliciclastic-carbonate settings. I. Environmental variation in shell condition. pbio. 26(1):80–102. https://doi.org/10.1666/0094-8373(2000)026<0080:BTITMS>2.0.CO;2

Best MMR, Ku TCW, Kidwell SM, Walter LM. 2007. Carbonate Preservation in Shallow Marine Environments: Unexpected Role of Tropical Siliciclastics. The Journal of Geology. 115(4):437–456. https://doi.org/10.1086/518051

Bland KJ, Uruski CI, Isaac MJ. 2015. Pegasus Basin, eastern New Zealand: A stratigraphic record of subsidence and subduction, ancient and modern. New Zealand Journal of Geology and Geophysics. 58(4):319–343. https://doi.org/10.1080/00288306.2015.1076862

Bouma AH. 1962. Sedimentology of some Flysch deposits: a graphic approach to facies interpretation [PhD Thesis]. Amsterdam, Netherlands: Elsevier.

Bradshaw JD. 1989. Cretaceous geotectonic patterns in the New Zealand Region. Tectonics. 8(4):803–820. https://doi.org/10.1029/TC008i004p00803

Browne GH, Bull S, Arnot M, Boyes AF, King PR, Helle K. 2020. The role of mass transport deposits contributing to fluid escape: Neogene outcrop and seismic examples from north Taranaki, New Zealand. Geo-Marine Letters. 40:789–807. https://doi.org/10.1007/s00367-020-00641-z

Brunt RL, Hodgson DM, Flint SS, Pringle JK, Di Celma C, Prélat A, Grecula M. 2013. Confined to unconfined: Anatomy of a base of slope succession, Karoo Basin, South Africa. Marine and Petroleum Geology. 41:206–221. https://doi.org/10.1016/j.marpetgeo.2012.02.007

Bull S, Cartwright J, Huuse M. 2009. A review of kinematic indicators from mass-transport complexes using 3D seismic data. Marine and Petroleum Geology. 26:1132–1151.

Burgreen B, Graham S. 2014. Evolution of a deep-water lobe system in the Neogene trench-slope setting of the East Coast Basin, New Zealand: Lobe stratigraphy and architecture in a weakly confined basin configuration. Marine and Petroleum Geology. 54:1–22. https://doi.org/10.1016/j.marpetgeo.2014.02.011

Calhoun NC, Clague JJ. 2018. Distinguishing between debris flows and hyperconcentrated flows: an example from the eastern Swiss Alps. Earth Surface Processes and Landforms. 43(6):1280–1294. https://doi.org/10.1002/esp.4313

Campion KM, Sprague AR, Mohrig D, Lovell RW, Drzewiecki PA, Sullivan MD, Ardill JA, Jensen GN, Sickafoose DK. 2000. Outcrop Expression of Confined Channel Complexes. In: Deep-Water Reservoirs of the World: 20th Annual. Vol. 44. Oklahoma, America: SEPM (Society for Sedimentary Geology); p. 127–150.

Caron V. 2011. Contrasted textural and taphonomic properties of high-energy wave deposits cemented in beachrocks (St. Bartholomew Island, French West Indies). Sedimentary Geology. 237(3):189–208. https://doi.org/10.1016/j.sedgeo.2011.03.002

Caron V, Bailleul J, Chanier F, Mahieux G. 2021. Episodes of seabed rise and rapid drowning as primary controls for the development of regressive and transgressive heterozoan carbonates and rhodolithic limestones in a tectonically-active setting (Early Miocene, Wairarapa region, New Zealand). New Zealand Journal of Geology and Geophysics.

Caron V, Bailleul J, Chanier F, Mahieux G, Joanny F-X. 2019. A new analytical procedure to graphically characterize the taphonomic properties of skeletal carbonates. An example from Miocene limestones of new zealand. PALAIOS. 34(8):364–381. https://doi.org/10.2110/palo.2018.101

Caron V, Nelson CS. 2009. Diversity of Neomorphic Fabrics in New Zealand Plio-Pleistocene Cool-Water Limestones: Insights into Aragonite Alteration Pathways and Controls. Journal of Sedimentary Research. 79(4):226–246. https://doi.org/10.2110/jsr.2009.029

Caron V, Nelson CS, Kamp PJJ. 2004. Contrasting carbonate depositional systems for Pliocene cool-water limestones cropping out in central Hawke's Bay, New Zealand. New Zealand Journal of Geology and Geophysics. 47(4):697–717. https://doi.org/10.1080/00288306.2004.9515084

Chanier F. 1991. Le prisme d'accrétion Hikurangi: un témoin de l'évolution géodynamique d'une marge active pacifique (Nouvelle-Zélande) [PhD Thesis]. France: Université de Lille 1.

Chanier F, Bellier J-P, Bignot G, Ferrière J. 1990. Discovery of Pithonellids in the Upper Cretaceous of New Zealand; biogeographic, stratigraphic and tectonic consequences. Comptes Rendus de l'Académie des Sciences - Séries II - Earth and Planetary Science. 310(2):1095–1100.

Chanier F, Ferrière J. 1991. From a passive to an active margin: Tectonic and sedimentary processes linked to the birth of an accretionary prism (Hikurangi Margin, New Zealand). Société Géologique de France. 162(4):649–660. https://doi.org/10.2113/gssgfbull.162.4.649

Chanier F, Ferrière J, Angelier J. 1999. Extensional deformation across an active margin, relations with subsidence, uplift, and rotations: The Hikurangi subduction, New Zealand. Tectonics. 18(5):862–876. https://doi.org/10.1029/1999TC900028

Chiarella D, Longhitano SG. 2012. Distinguishing Depositional Environments In Shallow-Water Mixed, Bio-Siliciclastic Deposits On the Basis Of The Degree Of Heterolithic Segregation (Gelasian, Southern Italy)DEGREE OF HETEROLITHIC SEGREGATION IN MIXED DEPOSITS. Journal of Sedimentary Research. 82(12):969–990. https://doi.org/10.2110/jsr.2012.78

Chiarella D, Longhitano SG, Sabato L, Tropeano M. 2012. Sedimentology and hydrodynamics of mixed (siliciclastic-bioclastic) shallow-marine deposits of Acerenza (Pliocene, Southern Apennines, Italy). Italian Journal of Geosciences. 131(1):136–151. https://doi.org/10.3301/IJG.2011.36

Chiarella D, Longhitano SG, Tropeano M. 2017. Types of mixing and heterogeneities in siliciclastic-carbonate sediments. Marine and Petroleum Geology. 88:617–627. https://doi.org/10.1016/j.marpetgeo.2017.09.010

Chiarella D, Longhitano SG, Tropeano M. 2019. Different stacking patterns along an active fold-and-thrust belt—Acerenza Bay, Southern Apennines (Italy). Geology. 47(2):139–142. https://doi.org/10.1130/G45628.1

Claussmann B, Bailleul J, Chanier F, Mahieux G, Caron V, McArthur AD, Chaptal C, Morgans HEG, Vendeville BC. 2021. Shelf-derived mass-transport deposits: origin and significance in the stratigraphic development of trench-slope basins. New Zealand Journal of Geology and Geophysics. 1:1–36. https://doi.org/10.1080/00288306.2021.1918729

Ćosović V, Mrinjek E, Nemec W, Španiček J, Terzić K. 2018. Development of transient carbonate ramps in an evolving foreland basin. Basin Research. 30(4):746–765. https://doi.org/10.1111/bre.12274

Crisóstomo-Figueroa A, McArthur AD, Dorrell RM, Amy L, McCaffrey WD. 2020. A new modelling approach to sediment bypass prediction applied to the East Coast Basin, New Zealand. GSA Bulletin. https://doi.org/10.1130/B35687.1

Crundwell M. 1987. Neogene stratigraphy and geological history of the Wainuioru Valley, Eastern Wairarapa, New Zealand. [BSc Thesis]. Wellington, New Zealand: Victoria University.

Cumberpatch ZA, Soutter EL, Kane IA, Casson M, Vincent SJ. 2021. Evolution of a mixed siliciclastic-carbonate deep-marine system on an unstable margin: The Cretaceous of the Eastern Greater Caucasus, Azerbaijan. Basin Research. 33(1):612–647. https://doi.org/10.1111/bre.12488

Daly RA. 1936. Origin of submarine canyons. American Journal of Science. s5-31(186):401–420. https://doi.org/10.2475/ajs.s5-31.186.401

Davies DJ, Powell EN, Stanton RJ. 1989. Relative rates of shell dissolution and net sediment accumulation - a commentary: can shell beds form by the gradual accumulation of biogenic debris on the sea floor? Lethaia. 22(2):207–212. https://doi.org/10.1111/j.1502-3931.1989.tb01683.x

Deptuck ME, Steffens GS, Barton M, Pirmez C. 2003. Architecture and evolution of upper fan channel-belts on the Niger Delta slope and in the Arabian Sea. Marine and Petroleum Geology. 20(6):649–676. https://doi.org/10.1016/j.marpetgeo.2003.01.004

Di Celma C, Cantalamessa G, Didaskalou P, Lori P. 2010. Sedimentology, architecture, and sequence stratigraphy of coarse-grained, submarine canyon fills from the Pleistocene (Gelasian-Calabrian) of the Peri-Adriatic basin, central Italy. Marine and Petroleum Geology. 27(7):1340–1365. https://doi.org/10.1016/j.marpetgeo.2010.05.011

Festa A, Pini GA, Dilek Y, Codegone G. 2010. Mélanges and mélange-forming processes: a historical overview and new concepts. International Geology Review. 52(10–12):1040–1105. https://doi.org/10.1080/00206810903557704

Field B, Uruski CI, Institute of Geological & Nuclear Sciences. 1997. Cretaceous-Cenozoic geology and petroleum systems of the East Coast region, New Zealand. New Zealand.

Fisher RV. 1983. Flow transformations in sediment gravity flows. Geology. 11(5):273–274.

Fonnesu M, Patacci M, Haughton PDW, Felletti F, McCaffrey WD. 2016. Hybrid Event Beds Generated By Local Substrate Delamination On A Confined-Basin Floor. Journal of Sedimentary Research. 86(8):929–943. https://doi.org/10.2110/jsr.2016.58

Galloway WE. 1998. Siliciclastic Slope and Base-of-Slope Depositional Systems: Component Facies, Stratigraphic Architecture, and Classification. AAPG Bulletin. 824:569–595. https://doi.org/10.1306/1D9BC5BB-172D-11D7-8645000102C1865D

Gamberi F, Rovere M, Dykstra M, Kane IA, Kneller BC. 2013. Integrating modern seafloor and outcrop data in the analysis of slope channel architecture and fill. Marine and Petroleum Geology. 41:83–103. https://doi.org/10.1016/j.marpetgeo.2012.04.002

Gong C, Steel RJ, Wang Y, Lin C, Olariu C. 2016. Shelf-margin architecture variability and its role in sediment-budget partitioning into deep-water areas. Earth-Science Reviews. 154:72–101. https://doi.org/10.1016/j.earscirev.2015.12.003

Haak AB, Schlager W. 1989. Compositional variations in calciturbidites due to sea-level fluctuations, late Quaternary, Bahamas. Geol Rundsch. 78(2):477–486. https://doi.org/10.1007/BF01776186

Harris PT, Whiteway T. 2011. Global distribution of large submarine canyons: Geomorphic differences between active and passive continental margins. Marine Geology. 285(1):69–86. https://doi.org/10.1016/j.margeo.2011.05.008

Hayton S, Nelson CS, Hood SD. 1995. A skeletal assemblage classification system for non-tropical carbonate deposits based on New Zealand Cenozoic limestones. Sedimentary Geology. 100(1):123–141. https://doi.org/10.1016/0037-0738(95)00071-2

Haywick DW. 2004. Diagenesis of polymineralic temperate limestones in a cyclothemic sedimentary succession, eastern North Island, New Zealand. New Zealand Journal of Geology and Geophysics. 47(4):839–855. https://doi.org/10.1080/00288306.2004.9515092

Hein FJ, Gorsline DS. 1981. Geotechnical aspects of fine-grained mass flow deposits: California Continental Borderland. Geo-Marine Letters. 1(1):1–5. https://doi.org/10.1007/BF02463293

Hubbard SM, Covault JA, Fildani A, Romans BW. 2014. Sediment transfer and deposition in slope channels: Deciphering the record of enigmatic deep-sea processes from outcrop.

GSA Bulletin. 126(5–6):857–871. https://doi.org/10.1130/B30996.1

Iverson RM. 1997. The physics of debris flows. Reviews of Geophysics. 35(3):245–296. https://doi.org/10.1029/97RG00426

Janocko J, Basilici G. 2021. Architecture of coarse-grained gravity flow deposits in a structurally confined submarine canyon (late Eocene Tokaren Conglomerate, Slovakia). Sedimentary Geology. 417:105880. https://doi.org/10.1016/j.sedgeo.2021.105880

Janocko M, Nemec W, Henriksen S, Warchoł M. 2013. The diversity of deep-water sinuous channel belts and slope valley-fill complexes. Marine and Petroleum Geology. 41:7–34. https://doi.org/10.1016/j.marpetgeo.2012.06.012

Jiao R, Seward D, Little TA, Kohn BP. 2014. Thermal history and exhumation of basement rocks from Mesozoic to Cenozoic subduction cycles, central North Island, New Zealand. Tectonics. 33(10):1920–1935. https://doi.org/10.1002/2014TC003653

Johnson AM. 1984. Debris flow. In: Brunsden D, Prior DB, editors. Slope Instability. New York, America: Wiley and Sons; p. 257–361.

Johnston MR. 1980. Geology of the Tinui-Awatoitoi district. Wellington, New Zealand: New Zealand Dept of Scientific and Industrial Research.

Kneller B. 1995. Beyond the turbidite paradigm: physical models for deposition of turbidites and their implications for reservoir prediction. Geological Society, London, Special Publications. 94(1):31–49. https://doi.org/10.1144/GSL.SP.1995.094.01.04

Kneller B, Bozetti G, Callow R, Dykstra M, Hansen L, Kane I, Li P, McArthur A, Catharina AS, Santos TD, Thompson P. 2020. Architecture, process, and environmental diversity in a late cretaceous slope channel system. JSedimentRes. 90(1):1–26. https://doi.org/10.2110/jsr.2020.1

Kowalewski M. 1996. Time-Averaging, Overcompleteness, and the Geological Record. The Journal of Geology. 104(3):317–326. https://doi.org/10.1086/629827

Kuenen PhH. 1964. Deep-Sea Sands and Ancient Turbidites. In: Bouma AH, Brouwer A, editors. Developments in Sedimentology. Vol. 3. Netherlands: Elsevier; p. 3–33. https://doi.org/10.1016/S0070-4571(08)70953-1

Lackey JK, Regalla CA, Moore GF. 2020. Tectonic Influences on Trench Slope Basin Development via Structural Restoration Along the Outer Nankai Accretionary Prism, Southwest Japan. Geochemistry, Geophysics, Geosystems. 21(8):1–17.

Lee J, Begg J. 2002. Geology of the Wairarapa area. Institute of Geological & Nuclear Sciences 1:250 000 geological map: Institute of Geological & Nuclear Sciences Limited.

Lewis KB, Pettinga JR. 1993. The emerging, imbricate frontal wedge of the Hikurangi margin. In: Ballance PF, editor. South Pacific sedimentary basins. Amsterdam, Netherlands: Elsevier Science; p. 225–250.

Li P, Kneller B, Thompson P, Bozetti G, dos Santos T. 2018. Architectural and facies organisation of slope channel fills: Upper Cretaceous Rosario Formation, Baja California, Mexico. Marine and Petroleum Geology. 92:632–649. https://doi.org/10.1016/j.marpetgeo.2017.11.026

Lowe DR. 1982. Sediment gravity flows; II, Depositional models with special reference to the deposits of high-density turbidity currents. Journal of Sedimentary Research. 52(1):279–297. https://doi.org/10.1306/212F7F31-2B24-11D7-8648000102C1865D

Malie P, Bailleul J, Chanier F, Toullec R, Mahieux G, Caron V, Field B, Mählmann RF, Potel S. 2017. Spatial distribution and tectonic framework of fossil tubular concretions as onshore analogues of cold seep plumbing systems, North Island of New Zealand. Bulletin de la Société géologique de France. 188(4):25. https://doi.org/10.1051/bsgf/2017192

Maltman A, editor. 1994. The Geological Deformation of Sediments. Netherlands: Springer Netherlands. https://doi.org/10.1007/978-94-011-0731-0

McArthur AD, Bailleul J, Mahieux G, Claussmann B, Wunderlich A, McCaffrey WD. 2021. Deformation-sedimentation feedback and the development of anomalously thick aggradational turbidite lobes: subsurface and outcrop examples from the Hikurangi Margin, New Zealand. Journal of Sedimentary Research. 91(4):362–389. https://doi.org/10.2110/jsr.2020.013

McArthur AD, Claussmann B, Bailleul J, McCaffrey W, Clare A. 2019. Variation in syn-subduction sedimentation patterns from inner to outer portions of deep-water fold and thrust belts: examples from the Hikurangi subduction margin of New Zealand. Geological Society, London, Special Publications. 490:285–310. https://doi.org/10.1144/SP490-2018-95

McArthur Adam D., Jolley DW, Hartley AJ, Archer SG, Lawrence HM. 2016a. Palaeoecology of syn-rift topography: A Late Jurassic footwall island on the Josephine Ridge, Central Graben, North Sea. Palaeogeogr Palaeoclimatol Palaeoecol. 459:63–75. https://doi.org/10.1016/j.palaeo.2016.06.033

McArthur A. D., Kneller BC, Souza PA, Kuchle J. 2016b. Characterization of deep-marine channel-levee complex architecture with palynofacies: An outcrop example from the Rosario Formation, Baja California, Mexico. Marine and Petroleum Geology. 73:157–173. https://doi.org/10.1016/j.marpetgeo.2016.02.030

McArthur AD, McCaffrey WD. 2019. Sedimentary architecture of detached deep-marine canyons: Examples from the East Coast Basin of New Zealand. Sedimentology. 66(3):1067–1101. https://doi.org/10.1111/sed.12536

McHargue T, Pyrcz MJ, Sullivan MD, Clark JD, Fildani A, Romans BW, Covault JA, Levy M, Posamentier HW, Drinkwater NJ. 2011. Architecture of turbidite channel systems on the continental slope: Patterns and predictions. Marine and Petroleum Geology. 28(3):728–743. https://doi.org/10.1016/j.marpetgeo.2010.07.008

Mohrig D, Ellis C, Parker G, Whipple KX, Hondzo M. 1998. Hydroplaning of subaqueous debris flows. GSA Bulletin. 110(3):387–394. https://doi.org/10.1130/0016-7606(1998)110<0387:HOSDF>2.3.CO;2

Mohrig D, Marr JD. 2003. Constraining the efficiency of turbidity current generation from submarine debris flows and slides using laboratory experiments. Marine & Petroleum Ecology. 20(6–8):883–899. https://doi.org/10.1016/j.marpetgeo.2003.03.002

Moore GF, Karig DE. 1976. Development of sedimentary basins on the lower trench slope. Geology. 4(11):693–697. https://doi.org/10.1130/0091-7613(1976)4<693:DOSBOT>2.0.CO;2

Moscardelli L, Ochoa J, Lunt I, Zahm L. 2019. Mixed siliciclastic–carbonate systems and their impact for the development of deep-water turbidites in continental margins: A case study from the Late Jurassic to Early Cretaceous Shelburne subbasin in offshore Nova Scotia. AAPG Bulletin. 103(10):2487–2520. https://doi.org/10.1306/02151917318

Moscardelli L, Wood L. 2008. New classification system for mass transport complexes in offshore Trinidad. Basin Research. 20(1):73–98. https://doi.org/10.1111/j.1365-2117.2007.00340.x

Moscardelli L, Wood L. 2015. Morphometry of mass-transport deposits as a predictive tool. GSA Bulletin. 128(1–2):47–80.

Mountjoy JJ, Barnes PM, Pettinga JR. 2009. Morphostructure and evolution of submarine canyons across an active margin: Cook Strait sector of the Hikurangi Margin, New Zealand. Marine Geology. 260(1):45–68. https://doi.org/10.1016/j.margeo.2009.01.006

Mountjoy JJ, Howarth JD, Orpin AR, Barnes PM, Bowden DA, Rowden AA, Schimel ACG, Holden C, Horgan HJ, Nodder SD, et al. 2018. Earthquakes drive large-scale submarine canyon development and sediment supply to deep-ocean basins. Science Advances. 4(3):1–9. https://doi.org/10.1126/sciadv.aar3748

Mulder T, Alexander J. 2001. The physical character of subaqueous sedimentary density flows and their deposits. Sedimentology. 48(2):269–299. https://doi.org/10.1046/j.1365-3091.2001.00360.x

Mulder T, Cochonat P. 1996. Classification of offshore mass movements. Journal of Sedimentary Research. 66(1):43–57. https://doi.org/10.1306/D42682AC-2B26-11D7-8648000102C1865D

Mulder T, Ducassou E, Gillet H, Hanquiez V, Tournadour E, Combes J, Eberli GP, Kindler P, Gonthier E, Conesa G, et al. 2012. Canyon morphology on a modern carbonate slope of the Bahamas: Evidence of regional tectonic tilting. Geology. 40(9):771–774. https://doi.org/10.1130/G33327.1

Mulder T, Joumes M, Hanquiez V, Gillet H, Reijmer JJG, Tournadour E, Chabaud L, Principaud M, Schnyder JSD, Borgomano J, et al. 2017. Carbonate slope morphology revealing sediment transfer from bank-to-slope (Little Bahama Bank, Bahamas). MAR PETROL GEOL. 83:26–34. https://doi.org/10.1016/j.marpetgeo.2017.03.002

Mutti E. 1985. Turbidite Systems and Their Relations to Depositional Sequences. In: Zuffa GG, editor. Provenance of Arenites. Dordrecht, Netherlands: Springer Netherlands; p. 65–93. https://doi.org/10.1007/978-94-017-2809-6_4

Naranjo-Vesga J, Ortiz-Karpf A, Wood L, Jobe Z, Paniagua-Arroyave JF, Shumaker L, Mateus-Tarazona D, Galindo P. 2020. Regional controls in the distribution and morphometry of deep-water gravitational deposits along a convergent tectonic margin. Southern Caribbean of Colombia. Marine and Petroleum Geology. 121:104639. https://doi.org/10.1016/j.marpetgeo.2020.104639

Nardin TR, Hein FJ, Gorsline DS, Edwards BD. 1979. A review of mass movement processes, sediment and acoustic characteristics, and contrasts in slope and base-of-slope systems versus canyon-fan-basin floor systems. SEPM Special Publication. 27:61–73.

Nebelsick JH, Rasser MW, Bassi D. 2005. Facies dynamics in Eocene to Oligocene circumalpine carbonates. Facies. 51(1):197–217. https://doi.org/10.1007/s10347-005-0069-2

Neef G. 1992. Geology of the Akitio area (1:50 000 metric sheet U25BD, east), northeastern Wairarapa, New Zealand. New Zealand Journal of Geology and Geophysics. 35(4):533–548. https://doi.org/10.1080/00288306.1992.9514546

Neef G. 1999. Neogene development of the onland part of the forearc in northern Wairarapa, North Island, New Zealand: A synthesis. New Zealand Journal of Geology and Geophysics. 42(1):113–135. https://doi.org/10.1080/00288306.1999.9514835

Nemec W, Steel RJ. 1984. Alluvial and Coastal Conglomerates: Their Significant Features and Some Comments on Gravelly Mass-Flow Deposits. In: Koster EH, Steel RJ, editors. Sedimentology of Gravels and Conglomerates, Memoir 10. Canada: Canadian Society of Petroleum Geologists; p. 1–31.

Nicol A, Mazengarb C, Chanier F, Rait G, Uruski C, Wallace L. 2007. Tectonic evolution of the active Hikurangi subduction margin, New Zealand, since the Oligocene. Tectonics. 26(4):1–24. https://doi.org/10.1029/2006TC002090

Nicol A, VanDissen R, Vella P, Alloway B, Melhuish A. 2002. Growth of contractional structures during the last 10 m.y. at the southern end of the emergent Hikurangi forearc basin, New Zealand. New Zealand Journal of Geology and Geophysics. 45(3):365–385. https://doi.org/10.1080/00288306.2002.9514979

Nicolaides S. 1995. Cementation in Oligo-Miocene non-tropical shelf limestones, Otway Basin, Australia. Sedimentary Geology. 95:97–121. https://doi.org/10.1016/0037-0738(94)00102-Z

Ogata K, Festa A, Pini GA, Pogačnik Ž, Lucente CC. 2019. Substrate deformation and incorporation in sedimentary mélanges (olistostromes): Examples from the northern Apennines (Italy) and northwestern Dinarides (Slovenia). Gondwana Research. 74:101–125. https://doi.org/10.1016/j.gr.2019.03.001

Ortiz-Karpf A, Hodgson DM, Jackson CA-L, McCaffrey WD. 2017. Influence of Seabed Morphology and Substrate Composition On Mass-Transport Flow Processes and Pathways: Insights From the Magdalena Fan, Offshore Colombia. Journal of Sedimentary Research. 87(3):189–209. https://doi.org/10.2110/jsr.2017.10

Ortiz-Karpf A, Hodgson DM, Jackson CA-L, McCaffrey WD. 2018. Mass-transport complexes as markers of deep-water fold-and-thrust belt evolution: insights from the southern Magdalena fan, offshore Colombia. Basin Research. 30(S1):65–88. https://doi.org/10.1111/bre.12208

Paumard V, Bourget J, Payenberg T, George AD, Ainsworth RB, Lang S, Posamentier HW. 2020. Controls On Deep-Water Sand Delivery Beyond the Shelf Edge: Accommodation, Sediment Supply, and Deltaic Process Regime. Journal of Sedimentary Research. 90(1):104–130. https://doi.org/10.2110/jsr.2020.2

Peakall J, Sumner EJ. 2015. Submarine channel flow processes and deposits: A process-product perspective. Geomorphology. 244:95–120. https://doi.org/10.1016/j.geomorph.2015.03.005

Perry CT. 1998. Grain susceptibility to the effects of microboring: implications for the preservation of skeletal carbonates. Sedimentology. 45(1):39–51. https://doi.org/10.1046/j.1365-3091.1998.00134.x

Pettinga JR. 1982. Upper Cenozoic structural history, coastal Southern Hawke's Bay, New Zealand. New Zealand Journal of Geology and Geophysics. 25(2):149–191. https://doi.org/10.1080/00288306.1982.10421407

Pirmez C, Beaubouef RT, Friedmann SJ, Mohrig DC. 2000. Equilibrium Profile and Baselevel in Submarine Channels: Examples from Late Pleistocene Systems and Implications for the Architecture of Deepwater Reservoirs. In: Deep-Water Reservoirs of the World. Vol. 20. Oklahoma, America: SEPM (Society for Sedimentary Geology); p. 792–805.

Pomar L. 2001. Ecological control of sedimentary accommodation: evolution from a carbonate ramp to rimmed shelf, Upper Miocene, Balearic Islands. Palaeogeography, Palaeoclimatology, Palaeoecology. 175(1):249–272. https://doi.org/10.1016/S0031-0182(01)00375-3

Posamentier HW, Kolla V. 2003. Seismic geomorphology and stratigraphy of depositional elements in deep-water settings. Journal of Sedimentary Research. 73(3):367–388.

Posamentier HW, Martinsen OJ. 2011. The Character and Genesis of Submarine Mass-Transport Deposits: Insights from Outcrop and 3D Seismic Data. In: Shipp RC, Weimer P, Posamentier HW, editors. Mass-Transport Deposits in Deepwater Settings. Oklahoma, America: SEPM; p. 7–38.

Posamentier HW, Vail PR. 1988. Eustatic Controls on Clastic Deposition II—Sequence and Systems Tract Models. In: Sea-Level Changes: An Integrated Approach. Vol. 42.

Oklahoma, America: SEPM (Society for Sedimentary Geology); p. 125–154.

Posamentier HW, Walker RG. 2006. Deep-Water Turbidites and Submarine Fans. In: Posamentier HW, Walker RG, editors. Facies Models Revisited. Oklahoma, America: SEPM Special Publication 84; p. 397–520. https://doi.org/10.2110/pec.06.84

Postma G. 1986. Classification for sediment gravity-flow deposits based on flow conditions during sedimentation. Geology. 14:291. https://doi.org/10.1130/0091-7613(1986)14<291:CFSGDB>2.0.CO;2

Postma G, Nemec W, Kleinspehn KL. 1988. Large floating clasts in turbidites: a mechanism for their emplacement. Sedimentary Geology. 58(1):47–61. https://doi.org/10.1016/0037-0738(88)90005-X

Powers MC. 1953. A new roundness scale for sedimentary particles. Journal of Sedimentary Research. 23(2):117–119. https://doi.org/10.1306/D4269567-2B26-11D7-8648000102C1865D

Prather BE. 2003. Controls on reservoir distribution, architecture and stratigraphic trapping in slope settings. Marine and Petroleum Geology. 20(6):529–545. https://doi.org/10.1016/j.marpetgeo.2003.03.009

Prélat A, Hodgson DM, Flint SS. 2009. Evolution, architecture and hierarchy of distributary deep-water deposits: a high-resolution outcrop investigation from the Permian Karoo Basin, South Africa. Sedimentology. 56(7):2132–2154. https://doi.org/10.1111/j.1365-3091.2009.01073.x

Puigdefàbregas C, Muñoz JA, Marzo M. 1986. Thrust Belt Development in the Eastern Pyrenees and Related Depositional Sequences in the Southern Foreland Basin. In: Foreland Basins. United Kingdom: John Wiley & Sons, Ltd; p. 229–246.

Raine JI, Beu A, Boyes A, Campbell H, Cooper R, Crampton J, Crundwell M, Hollis C, Morgans H, Mortimer N. 2015. New Zealand Geological Timescale NZGT 2015/1. New Zealand Journal of Geology and Geophysics. 58(4):398–403. https://doi.org/10.1080/00288306.2015.1086391

Reijmer JJG, Palmieri P, Groen R, Floquet M. 2015. Calciturbidites and calcidebrites: Sea-level variations or tectonic processes? Sedimentary Geology. 317:53–70. https://doi.org/10.1016/j.sedgeo.2014.10.013

Richards M, Bowman M, Reading H. 1998. Submarine-fan systems i: characterization and stratigraphic prediction. Marine and Petroleum Geology. 15(7):689–717. https://doi.org/10.1016/S0264-8172(98)00036-1

Romero-Otero GA, Slatt RM, Pirmez C. 2010. Detached and Shelf-Attached Mass Transport Complexes on the Magdalena Deepwater Fan. In: Mosher DC, Shipp RC, Moscardelli L, Chaytor JD, Baxter CDP, Lee HJ, Urgeles R, editors. Submarine Mass Movements and Their Consequences. Dordrecht, Netherlands: Springer Netherlands; p. 593–606. https://doi.org/10.1007/978-90-481-3071-9_48

Sobiesiak MS, Kneller B, Alsop GI, Milana JP. 2018. Styles of basal interaction beneath mass transport deposits. Marine and Petroleum Geology. 98:629–639. https://doi.org/10.1016/j.marpetgeo.2018.08.028

Sohn YK, Choe MY, Jo HR. 2002. Transition from debris flow to hyperconcentrated flow in a submarine channel (the Cretaceous Cerro Toro Formation, southern Chile). Terra Nova. 14(5):405–415.

Sømme TO, Helland-Hansen W, Martinsen OJ, Thurmond JB. 2009. Relationships between morphological and sedimentological parameters in source-to-sink systems: a basis for predicting semi-quantitative characteristics in subsurface systems. Basin Research. 21(4):361–387. https://doi.org/10.1111/j.1365-2117.2009.00397.x

Spörli KB. 1980. New Zealand and Oblique-Slip Margins: Tectonic Development up to and during the Cainozoic. In: Ballance PF, Reading HG, editors. Sedimentation in Oblique-Slip Mobile Zones. United Kingdom: John Wiley & Sons, Ltd; p. 147–170. https://doi.org/10.1002/9781444303735.ch9

Sprague AR, Garfield TR, Goulding FJ, Beaubouef RT. 2005. Integrated slope channel depositional models: the key to successful prediction of reservoir presence and quality in Offshore West Africa. In: Proceedings of the CIPM conference. Vol. 5. Veracruz, Mexico; p. 1–13.

Stanley DJ. 1986. Turbidity current transport of organic-rich sediments: Alpine and Mediterranean examples. Marine Geology. 70(1):85–101. https://doi.org/10.1016/0025-3227(86)90090-3

Stevens SH, Moore GF. 1985. Deformational and sedimentary processes in trench slope basins of the western Sunda Arc, Indonesia. Marine Geology. 69(1):93–112. https://doi.org/10.1016/0025-3227(85)90135-5

Strachan LJ. 2008. Flow transformations in slumps: a case study from the Waitemata Basin, New Zealand. Sedimentology. 55(5):1311–1332. https://doi.org/10.1111/j.1365-3091.2007.00947.x

Sylvester Z, Pirmez C, Cantelli A. 2011. A model of submarine channel-levee evolution based on channel trajectories: Implications for stratigraphic architecture. Marine and Petroleum Geology. 28(3):716–727. https://doi.org/10.1016/j.marpetgeo.2010.05.012

Talling PJ, Amy LA, Wynn RB, Peakall J, Robinson M. 2004. Beds comprising debrite sandwiched within co-genetic turbidite: origin and widespread occurrence in distal depositional environments. Sedimentology. 51(1):163–194. https://doi.org/10.1111/j.1365-3091.2004.00617.x

Van den Heuvel HB. 1960. The geology of the flat point area, eastern Wairarapa. New Zealand Journal of Geology and Geophysics. 3(2):309–320. https://doi.org/10.1080/00288306.1960.10423603

Watson SJ, Mountjoy JJ, Crutchley GJ. 2020. Tectonic and geomorphic controls on the distribution of submarine landslides across active and passive margins, eastern New Zealand. Geological Society, London, Special Publications. 500:477–494. https://doi.org/10.1144/SP500-2019-165

Zuschin M, Stachowitsch M, Stanton RJ. 2003. Patterns and processes of shell fragmentation in modern and ancient marine environments. Earth-Science Reviews. 63(1):33–82. https://doi.org/10.1016/S0012-8252(03)00014-X

11. SUPPLEMENTARY MATERIAL

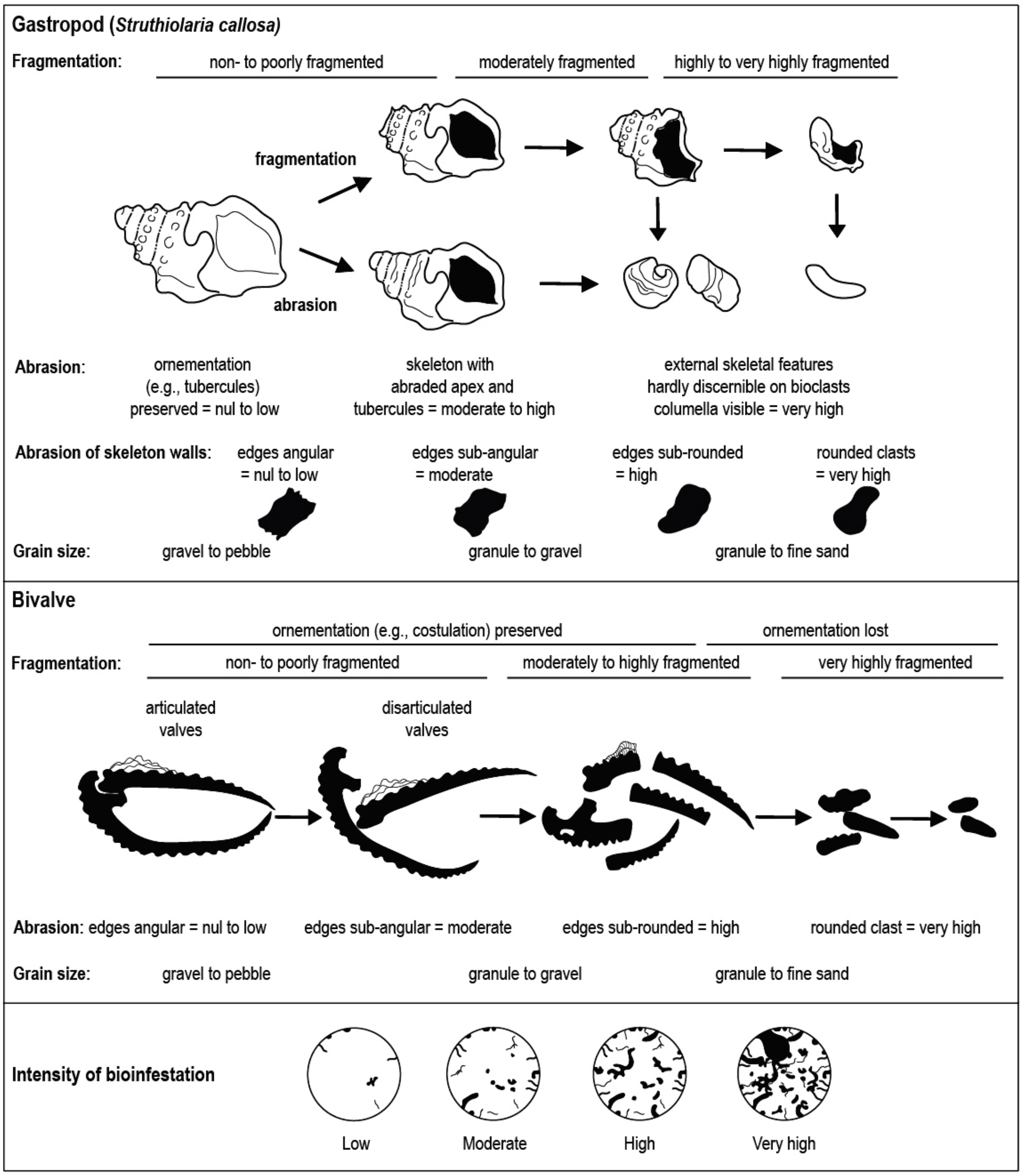

Appendix 1: Taphonomic methodology used on the macrofossils observed in the Waikaraka and Homewood localities. Qualitative taphonomic grading system established for the two dominant categories of fossil remains found in the studied deposits, namely Gastropods and Bivalves. The scales of alteration features were established to help characterize poorly to very highly damaged grains at outcrop. The particle contours displayed derive from field observations. The degree of abrasion was determined using the visual chart of (Powers 1953). The scale of skeleton bio-infestation is modified from (Perry 1998). The photographs provide field examples.

Accepted Manuscript version. Published Journal Article version available online, published by Elsevier in Marine and Petroleum Geology Journal: https://doi.org/10.1016/j.marpetgeo.2021.105252

Sections	Fossil record Nb. & Field Nb.	LF code	Collector	Identifier	Date	Age	Age comment	Paleoecology & Paleobathymetry	Longitude	Latitude
Homewood-1 section	T27/f0631 18_05_01	MDST	Claussmann, B.	Morgans, H.E.G. Gard, H.J.L.	02/2018	Upper Sc Lower Sl	Planktic fauna suggests Late Clifdenian to Early Lillburnian (Middle Miocene; ca. 15.5 – ca. 14 Ma). No age diagnostic molluscs were present. Stratigraphically located above sample 18_05_06 and below T27/f0493.	Deep middle bathyal (>800 m) or deeper. Planktic abundance >90% indicates a fully oceanic water mass overlay the site of deposition.	175,99153300	-41,19158700
	T27/f634 18_05_06	DF	Claussmann, B.	Morgans, H.E.G. Gard, H.J.L.	02/2018	Sl - Tt	Broadest age is Lillburnian to Early Tongaporutuan (Middle to Late Miocene; Late Langhien - Tortonian; 15.1 - 7.2 Ma). The absence of *Paragloborotalia mayeri* could indicate Early Tongaporutuan. Stratigraphically located below sample 18_05_01.	Middle bathyal paleodepth (>700 m). Although not abundant, the planktic fauna is 95% of the total foraminiferal fauna and indicates a fully oceanic water mass.	175,99254500	-41,18961700
	T27/f0493	DF	Crundwell, M.P. Watson J.	Crundwell, M.P.	01/1992	Sl	Restricted to Lillburnian age (Middle Miocene; Late Langhien - Serravalian; 15.1 - 13.05 Ma). Stratigraphically located above sample 18_05_01 and 18_05_06.	Upper bathyal. Planktic abundance is 20%. Marginal oceanic slightly anoxic bottom conditions. Abundant Thalmannammina-like taxa (turbidite fauna?).	175.99248°E	41.1905°S
Waikaraka section	T27/f0625 18_03_02a	DF/CF	Claussmann, B. Mahieux, G.	Morgans, H.E.G. Gard, H.J.L.	02/2018	Sl - Tt	No planktics were recovered. The benthics indicate an age from Runangan to Waipipian (Late Eocene to Pliocene; 34.6 - 3.00 Ma). Associated molluscs (*Struthiolaria callosa*) give a Lillburnian to Tongaporutuan age (Middle to Late Miocene; Late Langhien - Tortonian; 15.1 - 7.2 Ma).	The presence of *Cibicides molestus* indicates deep outer bathyal paleodepth (>150 m). The presence of molluscs indicates shallow waters.	176,03276700	-41,15014600
	T27/f0626 18_03_02b	DF/CF	Claussmann, B. Mahieux, G.	Morgans, H.E.G. Gard, H.J.L.	02/2018	Lw - Sw	Only benthic recovered has a range of Waitakian to Waiauan (Late Oligocene to Middle Miocene; Late Chattian - Serravalian; 25.2 - 11.04 Ma). No age diagnostic molluscs were present.	No real data. The molluscs indicate shallow waters and originate from mid to inner shelf environment.	176,03276700	-41,15014600
	T27/f0627 18_03_02c	DF/CF	Claussmann, B. Mahieux, G.	Morgans, H.E.G. Gard, H.J.L.	02/2018	Sl - Tt	A very poor foraminiferal fauna suggests Runangan to Recent (Late Eocene - Recent; 36.7 - 0 Ma). Molluscs give a Lillburnian to Tongaporutuan age (Middle to Late Miocene; Late Langhien - Tortonian; 15.1 - 7.2 Ma).	No real data. The molluscs indicate shallow waters and originate from mid to inner shelf environment.	176,03276700	-41,15014600
	T27/f0628 18_03_02e	DF/CF	Claussmann, B. Mahieux, G.	Morgans, H.E.G. Gard, H.J.L.	02/2018	NA	Only some possible agglutinated taxa and a nodosariid were observed.	Marine.	176,03276700	-41,15014600
	T27/0644 20_16_17	LDTC	Claussmann, B. Mahieux, G.	Morgans, H.E.G.	12/2020	Sw	A good planktic fauna was recovered including a sinistrally coiled population of *Globorotalia miotumida, Globoquadrina dehiscens* and *Paragloborotalia mayeri*. The age is Waiauan (Middle Miocene; Serravallian. 13.05 - 11.63).	The presence of *Tritaxilina zealandica, Sigmoilopsis schlumbergeri, Karreriella cylindrica* indicates paleodepths at 1500 metres or deeper (lower bathyal). Abundant *Amphistegina,* and less common *Zeaflorilus, Florilus, Ehrenbergina,* and *Cibicides* perforatus indicate shallow to middle shelf reworking across the shelf into deeper water. Planktic abundance is about 40% indicating a middle neritic watermass.	176,02902333	-41,15342233

Appendix 3: [next page] Sample list used for the Whareama Basin outcrops of Homewood and Waikaraka. The Fossil Record numbers including "T27" relate to the T27 New Zealand Map Grid 1:50,000 series and are captured in the Fossil Record Electronic Database (https://fred.org.nz/). See Table 1 for the description of the associated lithofacies code. The age of the sedimentary units and the paleobathymetries were defined using micro- and macropaleontological analyses conducted by GNS Science New Zealand.

Appendix 2: [next page] List of the macroorganisms & microorganisms observed in each sample during the analyses conducted by GNS New Zealand. This information is captured in the Fossil Record Electronic Database (https://fred.org.nz/).

(A) Macropaleontology list

		T27/f0631	T27/f0634	General observations throughout entire outcrop deposits	T27/f0625	T27/f0626	T27/f0627	General observations throughout entire outcrop deposits
Fossil record Nb.		T27/f0631	T27/f0634		T27/f0625	T27/f0626	T27/f0627	
Field Nb.		18_05_01	18_05_06		18_03_02a	18_03_02b	18_03_02c	
Identifier		Gard, H.J.L.	Gard, H.J.L.		Gard, H.J.L.	Gard, H.J.L.	Gard, H.J.L.	
Identification data		11/2018	11/2018		11/2018	11/2018	11/2018	
Stage - Start (older)		Sc	Sl		Sl	Lw	Sl	
Stage - Start (younger)		Sl	Tt		Tt	Sw	Tt	
Lithofacies code		MDST	DF		DF/CF	DF/CF	DF/CF	
Locality		Homewood	Homewood		Waikaraka	Waikaraka	Waikaraka	
Trench-slope basin		Whareama	Whareama		Whareama	Whareama	Whareama	
Laboratory		GNS Science	GNS Science		GNS Science	GNS Science	GNS Science	
Macrofauna								
Molluscs (gastropod)	*Austrofusus* sp. (?)		x					
Molluscs (gastropod)	*Naticidae*						x	
Molluscs (gastropod)	*Policines* sp.			x	x			x
Molluscs (gastropod)	*Struthiolaria (Callusaria) callosa*			x	common		x	x
Molluscs (gastropod)	*Struthiolaria aff. spinosa*					x		
Molluscs (gastropod)	*Struthiolaria* sp.			x				x
Molluscs (gastropod)	*Turritella* sp.		x	x				x
Molluscs (gastropod)	*Volutidae*					x		
Molluscs (bivalvia)	*Cardium* sp.			x				x
Molluscs (bivalvia)	*Glycymerididae*				x	x		
Molluscs (bivalvia)	*Glycymeris* sp.			x	x			x
Molluscs (bivalvia)	*Glycymerita* sp. (?)		x					
Molluscs (bivalvia)	*Ostrea* sp.			x				x
Corals	*Oculina* sp. (?)	x		x				
Corals	*Colonial corals*	x		x				
Corals	*Solitary corals*							x
Marine mammals	*Undifferentiated (bones)*			x				
Rhodolith	/			x				x

(B) Micropaleontology list

Fossil record Nb.		T27/f0631	T27/f0634	T27/0493	T27/f0625	T27/f0626	T27/f0627	T27/f0628	T27/0644
Field Nb.		18_05_01	18_05_06	/	18_03_02a	18_03_02b	18_03_02c	18_03_02e	20_16_17
Identifier		Morgans, H.E.G.	Morgans, H.E.G.	Crundwell, M.P.	Morgans, H.E.G.	Morgans, H.E.G.	Morgans, H.E.G.	Morgans, H.E.G.	Morgans, H.E.G.
Identification data		11/2018	11/2018	01/1992	11/2018	11/2018	11/2018	11/2018	12/2020
Stage - Start (older)		Sc	Sl	Sl	Sl	Lw	Sl	NA	Sw
Stage - Start (younger)		Sl	Tt	Sl	Tt	Sw	Tt	NA	Sw
Lithofacies code		MDST	DF	DF	DF/CF	DF/CF	DF/CF	DF/CF	LDTC
Locality		Homewood	Homewood	Homewood	Waikaraka	Waikaraka	Waikaraka	Waikaraka	Waikaraka
Trench-slope basin		Whareama	Whareama	Whareama	Whareama	Whareama	Whareama	Whareama	Whareama
Laboratory		GNS Science	GNS Science	GNS Science	GNS Science	GNS Science	GNS Science	GNS Science	GNS Science
Microfauna									
Foraminifera	*Amphistegina* sp.		x						x
Foraminifera	*Anomalinoides orbiculus*	x							
Foraminifera	*Anomalinoides* sp.		x						
Foraminifera	*Baggina ampla*	x							
Foraminifera	*Biloculina* sp.	x							
Foraminifera	*Bolivinia* sp.								x
Foraminifera	*Bulimina* sp.								x
Foraminifera	*Bulimina striata*	x							x
Foraminifera	*Chilostomella ovoidea*		x						x
Foraminifera	*Chilostomella* sp.	x							x
Foraminifera	*Chrysalogonium striatissimum*	x							
Foraminifera	*Cibicides molestus*		x		x				x
Foraminifera	*Cibicides novozelandicus*	x							x
Foraminifera	*Cibicides perforatus*				x				x
Foraminifera	*Cibicides truncanus*								reworked
Foraminifera	*Cibicides* spp.	x	x						x
Foraminifera	*Discorbinella sp.*				x		x		
Foraminifera	*Discorotalia tenuissima*								x
Foraminifera	*Dorothia* sp.								x
Foraminifera	*Ehrenbergina sp.*								x
Foraminifera	*Euuvigerina miozea*	group							x
Foraminifera	*Euuvigerina* sp.		x						x
Foraminifera	*Evolvocassidulina orientalis*		x						
Foraminifera	*Florilus stachei*					x			
Foraminifera	*Florilus* sp.								x
Foraminifera	*Fohsella peripheronda*	x							
Foraminifera	*Globigerina praebulloides*		x						
Foraminifera	*Globigerina* spp.		x						x
Foraminifera	*Globigerina woodi*		x						x
Foraminifera	*Globobulimina pacifica*		x						x
Foraminifera	*Globocassidulina subglobosa*								x
Foraminifera	*Globoquadrina dehiscens*		x						x
Foraminifera	*Globorotalia miotumida*	sinistral	x						sinistral
Foraminifera	*Globorotalia miozea*	x							
Foraminifera	*Globorotalia panda*			x					
Foraminifera	*Globorotalia praemenardii*			x					
Foraminifera	*Gyroidina zelandica*								x
Foraminifera	*Gyroidinoides neosoldanii*	x	x						x
Foraminifera	*Haeuslerella pukeuriensis*								x
Foraminifera	*Haplophragmoides* sp.						x		
Foraminifera	*Hoeglundina elegans*	x	x						
Foraminifera	*Karreriella cylindrica*	x							x
Foraminifera	*Karreriella* sp.	x							
Foraminifera	*Laticarinina pauperata*	x							
Foraminifera	*Lenticulina echinatus*								x
Foraminifera	*Lenticulina gyroscalprus*								x
Foraminifera	*Lenticulina* sp.	x	x						
Foraminifera	*Lingulina avellanoides*	x							
Foraminifera	*Marinottiella communis*	x							
Foraminifera	*Melonis zeabesus*								x
Foraminifera	*Nodosaria callosa*								x
Foraminifera	*Nodosaria longiscata*	x							x
Foraminifera	*Nodosaria* sp.	x	x		x			x	x
Foraminifera	*Notorotalia taranakia*								x
Foraminifera	*Notorotalia spp.*								x
Foraminifera	*Orbulina* sp.		x						
Foraminifera	*Orbulina suturalis*	x		x					
Foraminifera	*Orbulina universa*								x
Foraminifera	*Oridorsalis umbonatus*		x						x
Foraminifera	*Osangularia culter*								x
Foraminifera	*Parafissurina* sp.	x							
Foraminifera	*Paragloborotalia mayeri*	x							x
Foraminifera	*Pararotalia mackayi*								x
Foraminifera	*Parvicarinina altocamerata*	x							
Foraminifera	*Pleurostomella* sp.		x						x
Foraminifera	*Praeorbulina* sp.	x							
Foraminifera	*Pullenia bulloides*	x	x						
Foraminifera	*Quinqueloculina* spp.	x	x						x
Foraminifera	*Sigmoilopsis schlumbergeri*	x	x						x
Foraminifera	*Siphouvigerina plebeja*	x	x						x
Foraminifera	*Sphaeroidina bulloides*				x		x		x
Foraminifera	*Sphaeroidina dehiscens*								x
Foraminifera	*Stilostomella pomuligera*	x							
Foraminifera	*Textularia gladizea*								x
Foraminifera	*Textularia miozea*								x
Foraminifera	*Tritaxilina zealandica*								x
Foraminifera	*Trochamminoides* sp.	x							
Foraminifera	*Vaginulina* sp.								x
Foraminifera	*Vaginulinopsis* spp.	x							
Foraminifera	*Zeaflorilus* sp.								x

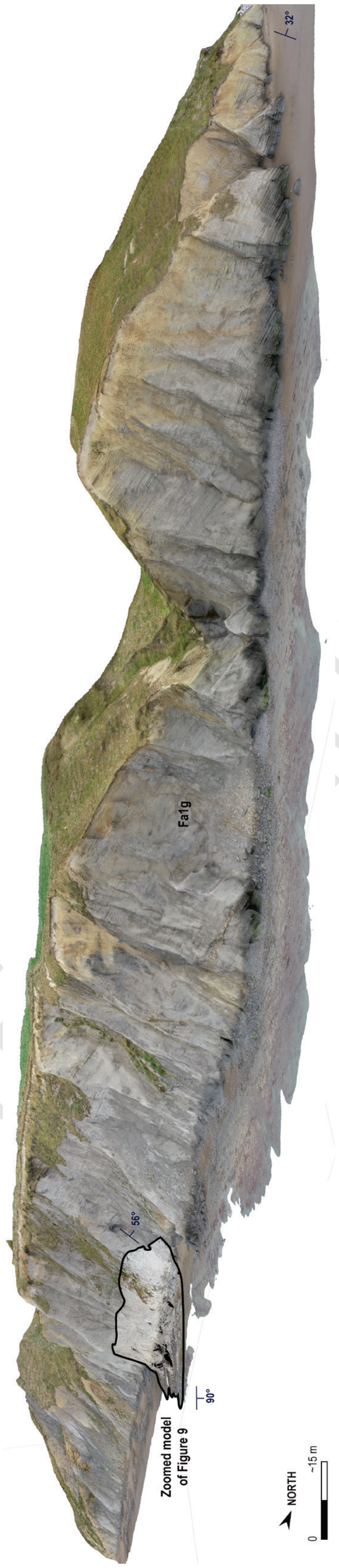

Appendix 4: Enlarged view of the Homewood outcrop, mostly comprising a several hundreds of meter-thick distal depositional lobe system (Fa1g). This study particularly focuses on the gravity-driven systems present at the base of this series and which are presented in the detailed view of the outcrop model in Figure 9.

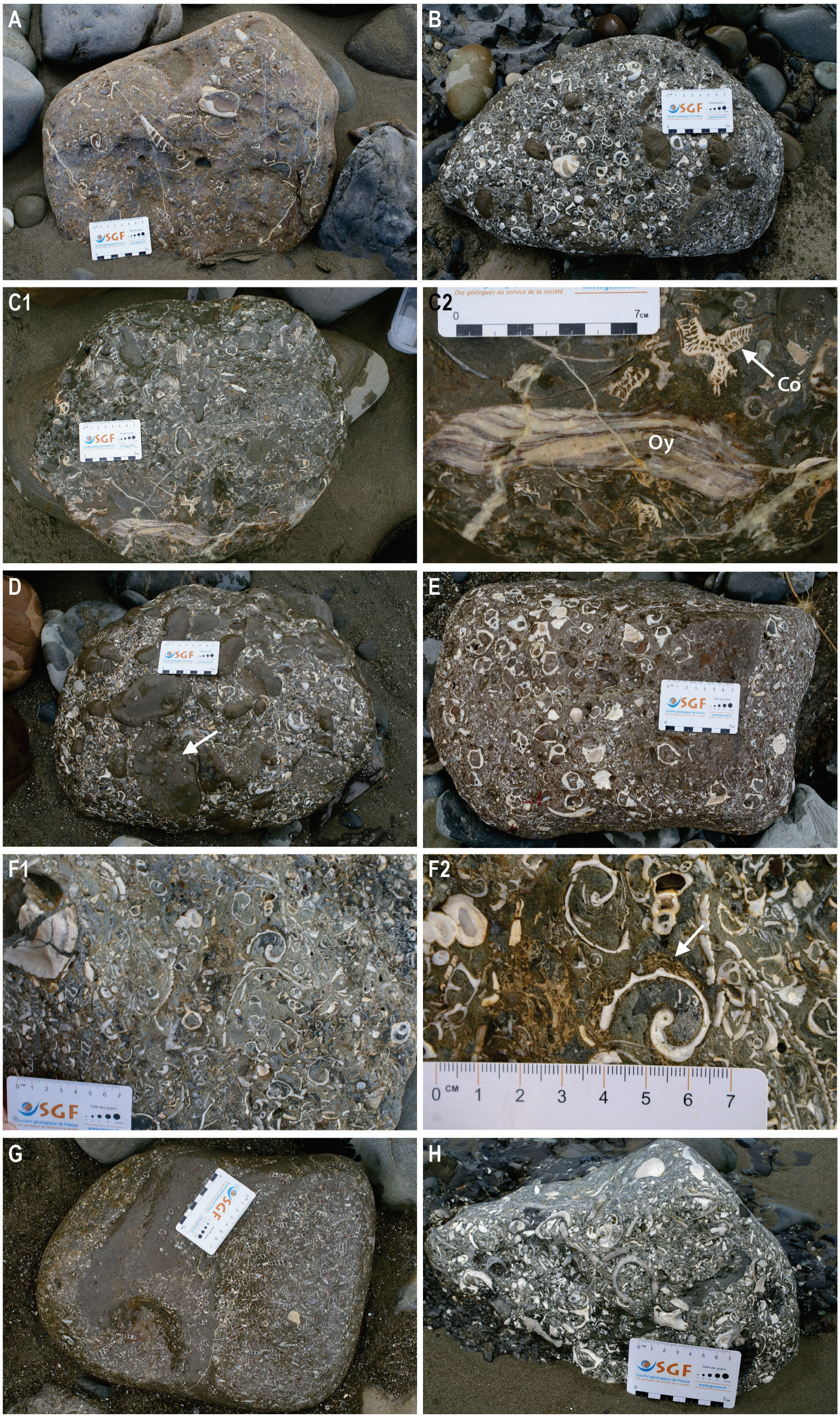

Appendix 5: Clasts of the inner- to mid-shelf shell beds clasts encountered at Waikaraka. (A): Siliciclastic floatstone dominated by gastropods (Struthiolaria sp. and turritellids) and thick-shelled bivalves in a sandstone matrix. (B): Pebbly molluscan rudstone. Sandstone clasts include sub-rounded to rounded gravels and pebbles. (C1-2): High-diversity clast-supported

Accepted Manuscript version. Published Journal Article version available online, published by Elsevier in Marine and Petroleum Geology Journal: https://doi.org/10.1016/j.marpetgeo.2021.105252

rudstone containing thick-shelled oysters (Oy, C2), zooxanthellate branching corals (Co, C2), brachiopods, turritellids, serpulids and subsidiary bryozoans. (D): Poorly-sorted pebbly rudstone containing abundant bored, well-rounded, sandy pebbles, and highly fragmented and abraded molluscan remains. (E): Molluscan floatstone-rudstone rich in thick-shelled gastropods and bivalves. (F1-2): Molluscan rudstone includes both thin- and thick-shelled molluscs commonly encrusted by coralline red algae (arrow, F2). (G): Turritellid floatstone. (H): Densely packed, thick-shelled molluscan rudstone.

Calculations using Moscardelli & Wood 2015

GENERAL
Equation (1): L = 1.5051 * (A ^(0.4977))
Equation (4): V = 0.0008 * (T ^(2.1998))
Equation (12): V = 0.0281 * (A ^(1.1123))
Rearranged Equation (12): A = ((V) * (1/0.0281))^(1/1.1123)

DETACHED
Equation (2): Ld = 1.2477 * (Ad ^(0.5415))
Equation (6): Vd = 0.0014 * (Td ^(1.6223))
Equation (14): Vd = 0.0261 * (Ad ^(1.1507))
Rearranged Equation (14): Ad = ((Vd) * (1/0.0261))^(1/1.1507)

USING OUTCROP THICKNESS

		Thickness T (m)		Volume V (km3)	Area A (km2)	Length L (km)	Equations
		Sefton Hills-1					
WHAREAMA	*INPUT*	15	*RESULT*	Equation (4) 0,31	Rearranged Equation (12) 9	Equation (1) 4	*General*
				Equation (6) 0,11	Rearranged Equation (14) 4	Equation (2) 2	*Detached s.l.*

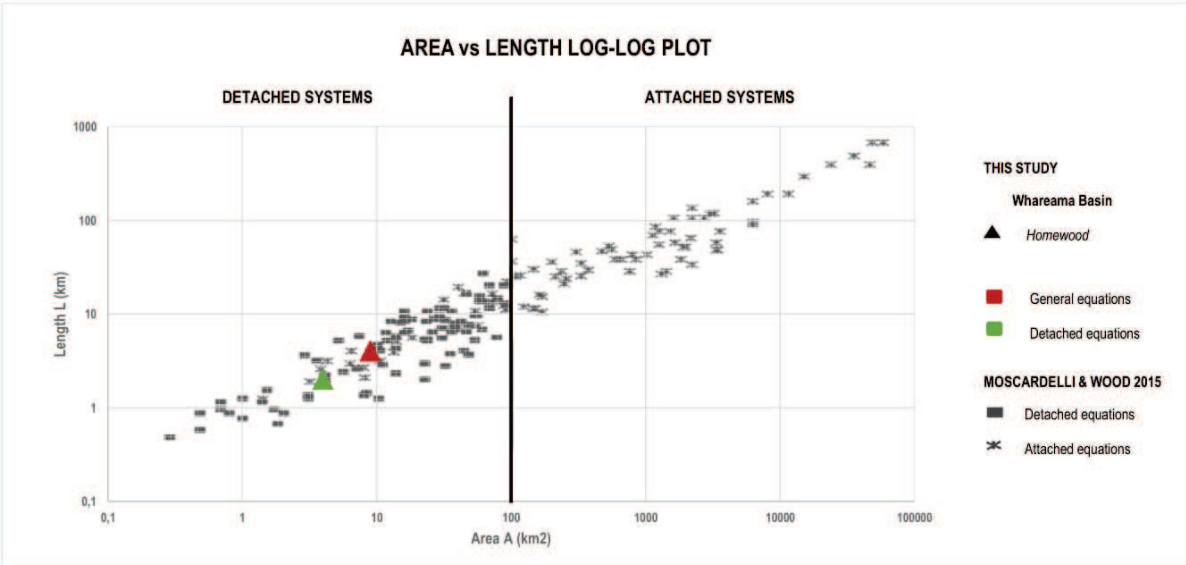

Appendix 6: Morphometric parameter calculations using the equations from (Moscardelli and Wood 2015) for the Homewood mass-transport deposits. The outcrop conditions prevented the recognition of most of the morphometric parameters and therefore the calculations were estimated using the assumption of a relative uniform thickness of 15 meters. The calculations were done using the general set of equations as well as the dedicated set for “detached systems”.